STRUCTURAL AND FUNCTIONAL CHARACTERIZATION OF A-KINASE ANCHORING PROTEIN 18

Dissertation zur Erlangung des akademischen Grades des Doktors der Naturwissenschaften (Dr. rer. nat.)

eingereicht im Fachbereich Biologie, Chemie, Pharmazie der Freien Universität Berlin

vorgelegt von

Verena Kathrin Ezerski

aus Wuppertal

April 2011

Die vorliegende Arbeit wurde von Oktober 2007 bis Januar 2008 in der Arbeitsgruppe von Prof. Dr. Bernd Reif am Leibniz-Institut für Molekulare Pharmakologie (FMP) und von Februar 2008 bis April 2011 in der Arbeitsgruppe von Prof. Dr. Oliver Daumke am Max-Delbrück-Centrum für Molekulare Medizin (MDC) unter der Leitung von PD Dr. Enno Klussmann durchgeführt.

1. Gutachter: Prof. Dr. Udo Heinemann
2. Gutachter: PD Dr. Enno Klussmann

Disputation am 11. Juli 2011

CONTENTS

1 Introduction

Every organism and, indeed, every cell has to respond to environmental stimuli and must be able to communicate and adapt to new conditions. In this context, signal transduction from the cell surface to the nucleus is essential for translating an external signal into an internal response, i.e. a change in gene expression. Coordination and regulation of such signaling events is of major importance for nearly every physiological reaction: coordination of metabolite fluxes, regulation of cell division, differentiation, and development as well as processing of sensory information. Understanding how signal transduction is organized is the key to understanding communication between cells and their environment.

A broad variety of signaling pathways is known today, e.g. G protein-coupled signal transmission pathways, mitogen-activated protein kinase (MAPK) signaling, as well as signaling events associated with serine/threonine-, or tyrosine-specific protein kinases and phosphatases [1]. Of these signaling enzymes, protein kinases play a major role in cellular signaling events. By reversibly phosphorylating their target molecules, they can alter enzyme activities, change affinities for ligands and binding partners and change the localization of a protein in the cell. There are various ways of regulating these phosphorylation events. The protein kinase itself can be “switched” on and off by phosphorylation and dephosphorylation, respectively, catalyzed by higher order kinases or phosphatases [2]. Allosteric regulation of kinase activity by effector molecules adds another level of control. Phosphatases terminate signaling events by dephosphorylating kinase substrates. Additionally, scaffolding of kinases, substrate proteins, and/or phosphatases as well as targeting to specific subcellular locations is used to orchestrate protein kinase signaling [2].

1.1 Cyclic 3´,5´-adenosine monophosphate (cAMP)-dependent kinase

The cyclic 3´,5´-adenosine monophosphate (cAMP)-dependent kinase, also called protein kinase A (PKA), is a broad spectrum serine/threonine-specific kinase [3]. It belongs to the family of AGC kinases that are related to PKA, cyclic 3´,5´-guanosine monophosphate (cGMP)-dependent kinase (PKG) and protein kinase C (PKC) based on sequence alignments of their catalytic domains. This protein family comprises about 60 members that are highly conserved among eukaryotes. PKA is the best investigated and best understood member of this family [3, 4] and serves as the prototype for the protein kinase superfamily [3].

1.1.1 cAMP/PKA signaling pathway

In the canonical cAMP/PKA signaling pathway, an extracellular ligand binds to its cognate G-protein-coupled receptor (GPCR) on the cell surface. The family of GPCRs comprises a large number of seven-transmembrane-helix receptors (about 800 different members in humans [5])

that are activated in response to a variety of physiological and environmental stimuli like hormones (e.g. adrenaline or glucagon), neurotransmitters, chemoattractants, calcium ions, light, odorants and many more [6]. Active GPCRs can bind their cognate heterotrimeric G proteins at the cytoplasmic membrane surface. Heterotrimeric G proteins consist of α, β, and γ subunits (Gα, Gβ, and Gγ) and guanosine-diphosphate, GDP, is bound to Gα in the inactive state. Binding of extracellular "ligands" to the specific binding site of the receptor induces a conformational change in the ligand binding site, which extends via the transmembrane helices into the intracellular domain and switches the receptor from an inactive to an active state conformation. This increases the rate of GDP-GTP (guanosine triphosphate) exchange in Gα which activates the Gα subunit by a conformational change and leads to its dissociation from the receptor and from the Gβγ subunit [7]. Gα and Gβγ can then bind to their target protein and initiate or suppress their effectors' activity. Hydrolysis of GTP leads to the reassociation of Gα and Gβγ subunits and terminates signal transduction. There are various types of Gα proteins, amongst them is the stimulating G protein $G\alpha_s$, which activates adenylyl cyclases (ACs) in the membrane. These convert adenosine-triphosphate (ATP) to cAMP. There are at least nine closely related isoforms of ACs in mammals. ACs are not only activated by $G\alpha_s$ but also by the diterpene forskolin (FSK) from the plant *Coleus forskohlii* [8].

cAMP, as an intracellular second messenger, is involved in many cellular processes such as gene transcription, cell growth and differentiation, ion channel conductivity, and synaptic release of neurotransmitters. It binds to and activates cyclic nucleotide-gated ion channels [9], guanine nucleotide-exchange proteins activated by cAMP (EPACs) [10], and phosphodiesterases (PDEs), the latter degrading cAMP to 5´adenosine monophosphate (5´AMP) thereby terminating the signal. The most important effector molecule of cAMP in mammalian cells is the cAMP-dependent protein kinase (PKA) [11]. PKA signaling is involved in a vast array of cellular processes ranging from control of metabolic enzymes to regulation of the cell cycle, proliferation and differentiation, microtubule dynamics, chromatin condensation and decondensation, intracellular transport mechanisms and ion channel conductivity. Additionally, cAMP participates in β-adrenergic signaling in the cardiovascular system and in adipose tissue. It further modulates immune and hormone responses [12]. Regarding this diversity, the major question is how one single second messenger causes tissue- and organ-specific effects and, more generally speaking, how specificity is maintained in cAMP/PKA signaling.

1.1.2 Compartmentalization

One important aspect of conferring specificity to cAMP/PKA signaling is differential expression and regulation of GPCRs and specific isoforms of adenylyl cyclases, phosphodiesterases, and PKA subtypes [12]. Additionally, cAMP action is limited temporally by regulation of its synthesis and

degradation. However, cAMP levels are not only controlled in time, but also in space. This so-called compartmentalization of cAMP/PKA signaling creates local pools of the second messenger (**Fig. 1**). A-kinase anchoring proteins (AKAPs) spatially regulate cAMP signaling by associating with PKA, PDEs, and other signaling molecules into multiprotein signaling complexes targeting them to certain subcellular compartments. In this way, cAMP microdomains, or gradients, are shaped by tightly regulated and specifically located phosphodiesterases. Binding of cAMP to the regulatory subunit dimer leads to a conformational change in these proteins. The formerly bound catalytic subunits are released from inhibition by the regulatory subunits and are activated to phosphorylate target molecules in specific compartments of the cell [13, 14].

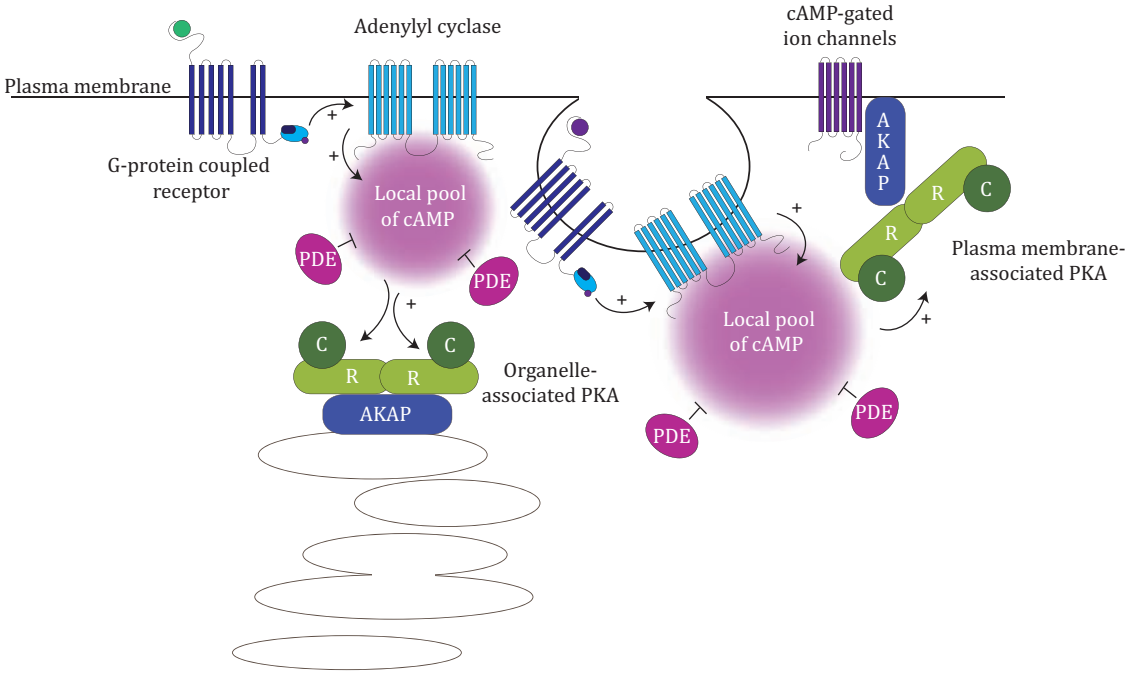

Fig. 1 Compartmentalization of cAMP-dependent protein kinase signaling. Binding of an extracellular ligand to its cognate G-protein coupled receptor leads to the activation of adenylyl cyclases, which synthesize cAMP from ATP. Local pools of cAMP are shaped by the action of phosphodiesterases (PDEs) that degrade cAMP to 5´AMP and are localized in different subcellular compartments. Targeting of PKA to organelles or the plasma membrane by AKAPs leads to focal activation of PKA by cAMP. *C, PKA catalytic subunit; R, PKA regulatory subunit* (Figure adapted from **[12]**)

1.1.3 Structure of protein kinase A

The cAMP-dependent kinase or protein kinase A (PKA) was discovered and partly purified from rabbit skeletal muscle by Krebs *et al.* in 1968 [15]. The amino acid sequence of the catalytic (C) subunit was determined in 1981 [16] and the gene coding for the mouse PKA catalytic subunit was cloned five years later [17]. The structure of the murine catalytic subunit co-crystallized with a 20 amino acids peptide from the protein kinase inhibitor (PKI) was solved by Knighton and co-workers [18] and was the first protein kinase structure to be determined.

PKA, especially its catalytic subunit, has been purified from different tissues and was intensely investigated during the 1970s [19-21]. Two types of PKA holoenzymes (type I and type II) were discovered that contain different regulatory (R) subunits (RI and RII) named after the order in which they elute from anion exchange resins [20, 22]. Both R and C subunits exist as multiple isoforms that are expressed in a tissue-specific manner and are differentially localized in the cell. In humans, there are RIα, RIβ, RIIα, RIIβ, Cα, Cβ, Cγ, PrKX (human X chromosome encoded catalytic subunit, [23]), and PrKY (human Y-homolog of protein kinase PrKX [24]). While RII subunits are mostly found in the so-called "particulate fraction" after centrifugation, RI isoforms can be found predominantly in the cytosol [25-27]. RIα and RIIα are the predominant isoforms and are expressed in most tissues [28, 29], whereas RIβ and RIIβ represent the main isoforms in the central nervous system and in reproductive tissue [30, 31]. Of both Cα and Cβ, there are different splice variants known, isolated from different species [11, 23].

In the absence of cAMP, PKA forms an inactive holoenzyme complex consisting of two catalytic subunits bound to a regulatory subunit dimer, R_2C_2. Cooperative binding of two cAMP molecules to each R subunit monomer causes the C subunits to dissociate from the R subunit dimer. The free and active C monomers can then phosphorylate specific serine or threonine residues on target proteins [11] at their preferred consensus sequence Arg-Arg/Lys-X-Ser/Thr [32]. In general, the mechanism whereby cAMP translates an extracellular signal into an intracellular response is defined by the R subunit and mediated by the C subunit.

1.1.4 Structure of the PKA holoenzyme

In the holoenzyme complex, i.e. in the absence of cAMP, the C subunits are locked in an inactive state by binding of the R subunit dimer. In contrast to RI, RII subunits are not only inhibitors of the PKA C subunit catalytic activity but substrates as well. To understand how the C subunit is inhibited by R subunits, how cAMP induces PKA activation, and what differences there are between different isoforms, high-resolution structures of the holoenzyme complex were solved.

A detailed description of PKA holoenzyme structure is beyond the scope of this work. For completeness, a short overview of crystal structures of PKA holoenzyme complexes solved will

be provided. All of them were published by the group of Susan Taylor. Even though these structures were designated “holoenzymes”, they rather constitute heterodimers of one R and one C subunit than tetrameric holoenzymes. First, the structure of bovine RIα(91-244) in complex with an oxidation resistant murine Cα(C199A) subunit, the non-hydrolysable ATP analog adenylyl-imidodiphosphate and Mn^{2+} (AMP-PNP:Mn^{2+}) was solved to a resolution of 2.0 Å [33]. In this case, the RIα subunit only contains one of the two cAMP binding sites (cAMP-binding domain (CBD) A) and, therefore, does not provide any clues as to the allosteric activation of PKA. Still, the structure showed for the first time the dramatic conformational change that the R subunit must undergo when binding cAMP and releasing the C subunit. Second, the 2.3 Å structure of murine Cα bound to bovine RIα(91-379) with AMP-PNP:Mn^{2+} was solved by Kim and colleagues [34]. This time, RIα contained the mutation of an essential arginine residue (R333K) in the cAMP binding site of CBD B, but both cAMP binding sites are present. The structure reveals the uncoupling of the two cAMP-binding domains of RIα upon C subunit binding and shows the importance of a holoenzyme-specific conserved salt bridge in the R subunit for PKA activation. Third, the structure of murine RIIα(90-400) in complex with nucleotide-free murine Cα was solved (2.5 Å) [35]. It revealed a differential role of ATP in regulation of type I and type II holoenzymes: ATP promotes dissociation of the type II holoenzyme by being essential for autophosphorylation of the P-site, whereas in type I holoenzymes, ATP is needed to form the tetrameric complex. Fourth, the 1.6 Å structure of murine $C\alpha_1$(2-351) bound to rat RIIβ(108-268) and AMP-PNP:Mn^{2+} was solved [36]. There are remarkable differences in RIIα and RIIβ containing holoenzymes, e.g. RIIα and RIIβ both have a rod-like shape in the free form [37] but upon binding to the C subunit, RIIα remains extended whereas RIIβ forms a more or less globular complex. Additionally, upon binding to the C subunit, the cAMP binding sites are completely restructured.

Recently, the structure of bovine RIα(73-244) in complex with murine Cα and AMP-PNP:Mn^{2+} was published [38]. For the first time, nine additional residues of the flexible linker region of RIα were visible in this structure. They were ordered by interaction with the symmetry-related heterodimer. This created a tetrameric configuration of the two heterodimers that was consistent with models of the full-length tetrameric RIα holoenzyme based on small angle light scattering (SAXS) [39]. Boettcher and co-workers created a model of the full-length tetramer on the basis of the SAXS data and the two symmetry-related heterodimers including the structure of Cα bound to RIα(91-379) by Kim and colleagues mentioned above. In the model (**Fig. 2**) the R subunits form a compact dimer separating the two C subunits from each other. The structure of the dimerization and docking (D/D) domain of the RIα subunit [40] was also included in the model (see chapter 1.1.4.2) [38].

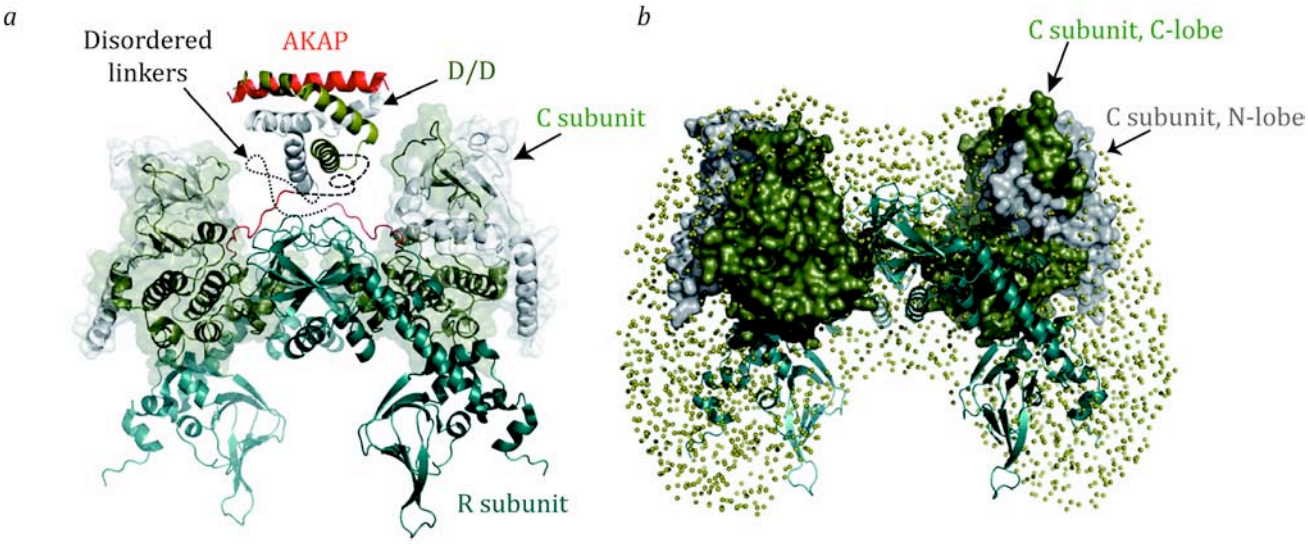

Fig. 2 Model of the tetrameric PKA RIα holoenzyme**. *a***, Cartoon representation of the two heterodimers consisting of the C subunit (green) and the R subunit (blue) as observed in crystal packing. The proposed position of the D/D domain dimer is illustrated bound to an A-kinase anchoring protein (AKAP) helix (red) and is connected to the R subunit by the linker (red). Still unknown linker sections are depicted as dashed lines. *b*, Comparison of the SAXS data [39] shown as space-filling model and the proposed model from *a*. R subunits are shown as cartoon, C subunits are shown in the surface representation in green (C-lobe) and white (N-lobe). (Figure adapted from [38])

1.1.4.1 General structural features of PKA catalytic subunits

The C subunit of PKA contains the catalytic core motif, which is typical for all protein kinases. It folds into a globular domain consisting of two lobes, the small and the large lobe. In the cleft between the two lobes, the binding site for adenosine 5´triphosphate (ATP) and substrates is located. Opening and closing of the active site cleft is an essential part of catalysis. It is mainly ATP that mediates the interaction between the two lobes [3].

The small lobe lies at the N-terminus and is highly dynamic. It serves as the binding site for ATP and consists mostly of β-strands. The glycine-rich loop between β-strands 1 and 2 is a highly conserved motif that is part of the ATP-binding site and essential for catalysis. Gly^{52} proved to be the most essential residue in this loop [41, 42]. Several other conserved residues in the small lobe contribute to ATP binding and catalysis [43].

The large lobe is located C-terminally and is mostly α-helical. It contains much of the catalytic machinery and has an exposed docking surface for binding of peptide and protein substrates. Conserved structural features include the catalytic loop, the magnesium positioning loop, the activation loop, and the peptide positioning loop. All of these loops contain highly conserved residues, e.g. the catalytic loop contains Asp^{166}, which serves as catalytic base, and Asn^{171}, which binds the essential magnesium ions. The magnesium positioning loop contains Asp^{184} that forms

the catalytic triad together with residues Lys[72] and Glu[91] from the small lobe. The catalytic triad is important for binding the phosphates of ATP and for positioning the γ-phosphate for transfer. The activation loop contains residue Thr[197], which is phosphorylated in the activated kinase and is connected to the catalytic loop and the magnesium positioning loop via a network of interactions. The peptide positioning loop is needed for positioning of the consensus site substrate peptide [43].

The kinase core is flanked by an N- and a C-terminal tail that are of regulatory importance. Among other things, the N-tail seems to play a role in targeting the catalytic subunit to certain subcellular locations: its interaction with A kinase interacting protein 1 (AKIP1) leads to translocation of the C subunit to the nucleus [44]. The C-tail seems to be an integral part of the active enzyme as well, with residue Phe[327] being an essential part of the ATP binding site and Tyr[330] being necessary for the closed conformation of PKA C subunit [45, 46].

Taken together, the catalytic subunit is much more than its name implies: besides phosphoryl transfer it also has a scaffolding function and provides docking surfaces to mediate different protein – protein interactions. First and foremost it serves as an extended stable scaffold for the binding of R subunits, thereby closing the active site cleft [3].

1.1.4.2 Structure of PKA regulatory subunits

The regulatory (R) subunit exists in at least four isoforms termed RIα, RIβ, RIIα, and RIIβ that all possess the same domain structure as shown in **Fig. 3**.

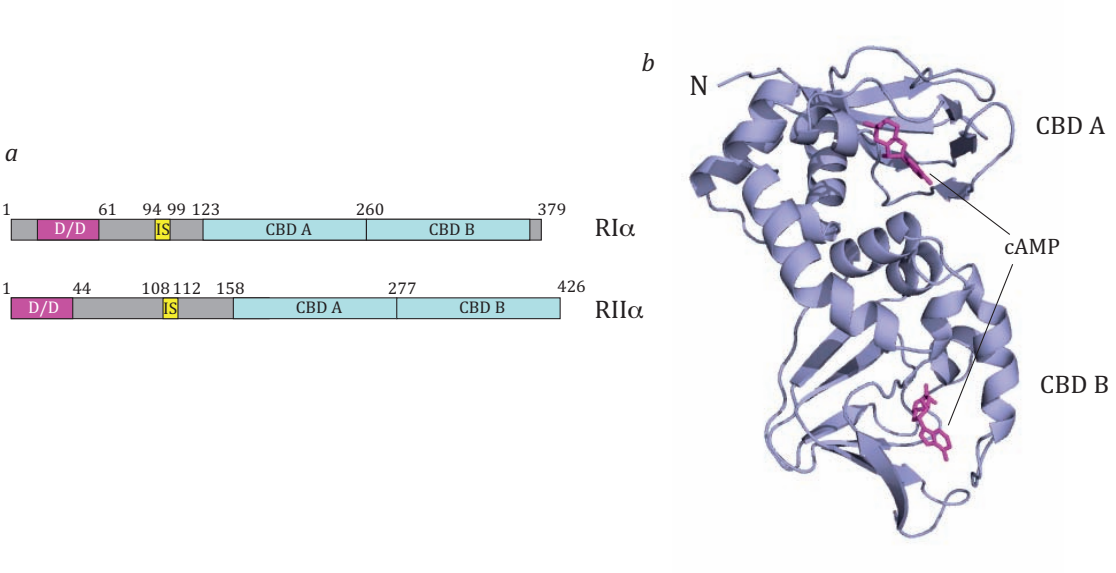

Fig. 3 Domain organization of PKA regulatory subunits. ***a***, Schematic representation of RIα and RIIα domain structure. D/D stands for dimerization and docking domain. IS is the inhibitor sequence that is a pseudo-substrate in RI and a substrate site in RII domains. CBDs A and B are the tandem cAMP-binding domains. ***b***, The crystal structure of bovine RIα(91-379) (pdb file 1rgs) is shown with cAMP bound to each of the two cAMP binding domains. (Figure adapted from **[3]**)

At the N-terminus there is a dimerization and docking domain (D/D domain) important not only for dimerization but also for interaction with A-kinase anchoring proteins (AKAPs). Downstream of the D/D domain is the hinge region, a flexible linker region that contains an inhibitor sequence (IS) which is auto-phosphorylated in RII subunits. In contrast, in RI subunits it is only a pseudo-substrate [3]. The hinge region is important for the interaction between R and C subunits, because it binds to the active-site cleft of the C subunit. Additionally, it contains multiple phosphorylation sites [47, 48]. The C-terminus is comprised of two tandem and homologous but not equivalent cAMP-binding domains (CBDs), A and B [49]. These show extensive sequence similarities with the *Escherichia coli* catabolite gene activator protein (CAP), the primary receptor for cAMP in prokaryotes [50]. Site A is not accessible for cAMP in the holoenzyme. Binding of cAMP to site B triggers a conformational change that renders site A accessible for ligand binding [51]. Interestingly, a deletion mutant of the R subunit lacking domain B (Δ260-379) and also a mutant consisting only of domain A (aa 91-259) are able to bind to the C subunit tightly [52, 53]. Finally, binding of cAMP to site A leads to the dissociation of the holoenzyme.

The domain structure of the regulatory subunit was characterized by limited proteolysis that yielded soluble protein [54] but impeded dimerization [19]. The first structure of the PKA R subunit was the 2.8 Å resolution structure of bovine PKA RIα(91-379), one of the most stable truncated constructs that can be purified in high yields, with two cAMP molecules bound [55]. Each cAMP-binding domain consists of three major α-helices and eight β-strands. The β-strands are arranged in two anti-parallel β-sheets consisting of four strands each. The two β-sheets form a flattened β-barrel that accounts for the major part of the cAMP binding site with the α-helices connected to the ends of the β barrel. The so-called Phosphate Binding Cassette (PBC) is located between β6 and β7 and is the key feature of the CBD, as it anchors the ribose phosphate of cAMP. Two important conserved residues lie in this region, Glu^{200} and Arg^{209} in domain A, and Glu^{324} and Arg^{333} in domain B, respectively, which participate directly in cAMP binding [3, 55]. These residues were already predicted to be important for binding of cAMP by computational analysis [56]. In addition, cAMP-binding involves hydrophobic interactions with several side chains, most importantly stacking of the aromatic rings of Trp^{260} and Tyr^{371} with the adenine base of cAMP in domain A and B, respectively [55].

The first structure of a type II regulatory subunit was determined by Diller and co-workers to a resolution of 2.45 Å [57]. It is a deletion mutant of rat RIIβ missing the first 111 amino acids. The structure contains one cAMP molecule bound per CBD. The structure was solved using the structure of CBD A of RIα for molecular replacement, demonstrating its close homology. Superposition of RIIβ(112-416) and RIα(91-379) reveals significant differences in the orientation of the CBDs. The two cAMP molecules bound to site A and B, respectively, are much

closer together in the RIIβ model than in the RIα model (19.3 Å in comparison to 29.5 Å). The interface surfaces between the two CBDs are different between the two models and are defined by variability in the amino acid sequence of the interdomain linker [57].

There is no structure of the RIIα subunit alone. The only structure known of RIIα is the complex structure of murine RIIα(90-400) bound to Cα mentioned above [35]. Crystallization of the full-length R subunit dimer has never been achieved. Most likely, this is because the linker region between the D/D domain and CBD A is highly flexible [58] and the full-length protein is prone to degradation [59]. But similar to the CBDs, the N-terminal D/D domain is relatively stable and several structures of this part of the R subunits have been solved.

1.1.5 Structure of PKA dimerization and docking domain and interaction with A-kinase anchoring proteins

The N-terminal dimerization and docking (D/D) domain of the PKA regulatory subunit primarily mediates dimerization of R subunits. It comprises the first 61 amino acid residues of RI subunits and the first 44 residues of RII subunits (**Fig. 3**a) [3]. Notably, the dimeric structure is not necessary for interaction with the catalytic subunit [60], nor does it directly influence other functional properties of PKA [61]. Instead, it has been long recognized that the subcellular distribution of PKA depends on the R subtype [26] and an R subunit dimer is needed for targeting of the PKA holoenzyme in the cell [62] by binding to an amphipathic helix in A-kinase anchoring proteins (AKAPs) (see below) [63-65]. The D/D domain is responsible for AKAP binding (hence the word “docking” in the second part of its name) [66, 67].

In the bovine RIα D/D dimer, there are two interchain disulfide bridges between residues Cys^{16} and Cys^{37}, which are not required for dimerization as shown by analytical gel filtration of wild type and mutant RIα [68]. The RIα D/D dimer proved to be stable over a wide range of pH (2-12) and temperature (0-92°C). More than 50 mM DTT were needed to reduce the disulfide bridges [68]. Only double mutants of RIα (C37H and F47A or C37H and F52A) were found to be monomeric as these aromatic residues contribute to the dimer interface [69]. In RII subunits, the corresponding disulfide bridges do not exist, but RII subunits can still form stable dimers [70].

A short helical peptide from AKAP-lbc (lymphoid blast crisis), also known as AKAP13 and originally called human thyroid anchoring protein Ht31, comprising amino acid residues 493-515, binds to both the RIIα and the type II PKA holoenzyme [71] with nanomolar affinity [72]. It became the prototype of the amphipathic helix model, which states that an amphipathic helix in each AKAP is responsible for binding to PKA regulatory subunits. Interestingly, short peptides mimicking the amphipathic helix of AKAPs can be used as competitors of PKA anchoring as first established for Ht31(493-515) (see chapter **1.3**) [71].

Disruption of secondary structure formation by site-directed mutagenesis of certain residues within the helix (I502P, I507P) or upstream and downstream of the helix (K490P, L494P, A512P, and L517P) abolished interaction with RIIα (see **Fig. 4**) [63, 71]. Similar results from other mutation studies have been reported for other AKAPs and their specific PKA-binding helix, for example human AKAP79 binding to RIIα [73], bovine AKAP75 binding to RIIβ [74], and rat mAKAP binding to RIIα [75]. On the other hand, mutational analysis of RIIα revealed the importance of its first 5 amino acid residues. An RIIα mutant lacking these residues was unable to bind AKAPs even though it could dimerize [66]. Substitution of Ile^{3} and Ile^{5} with leucines strongly decreased Ht31 binding showing the importance of β-branched side chains in positions 3 and 5 of RIIα. Mutation of these amino acids to hydrophilic residues (serine and asparagine) practically abolished binding of Ht31 [76]. In RIIβ, mutation of Val^{20} and Leu^{21} to alanine disrupts AKAP75 binding but not dimerization [77].

Taken together, these studies have shown that binding between RII D/D and AKAPs is promoted by hydrophobic interactions of the D/D domain dimer with an amphipathic helix in the specific AKAP. In addition, they indicated key residues and key differences between RII subtypes and different AKAPs.

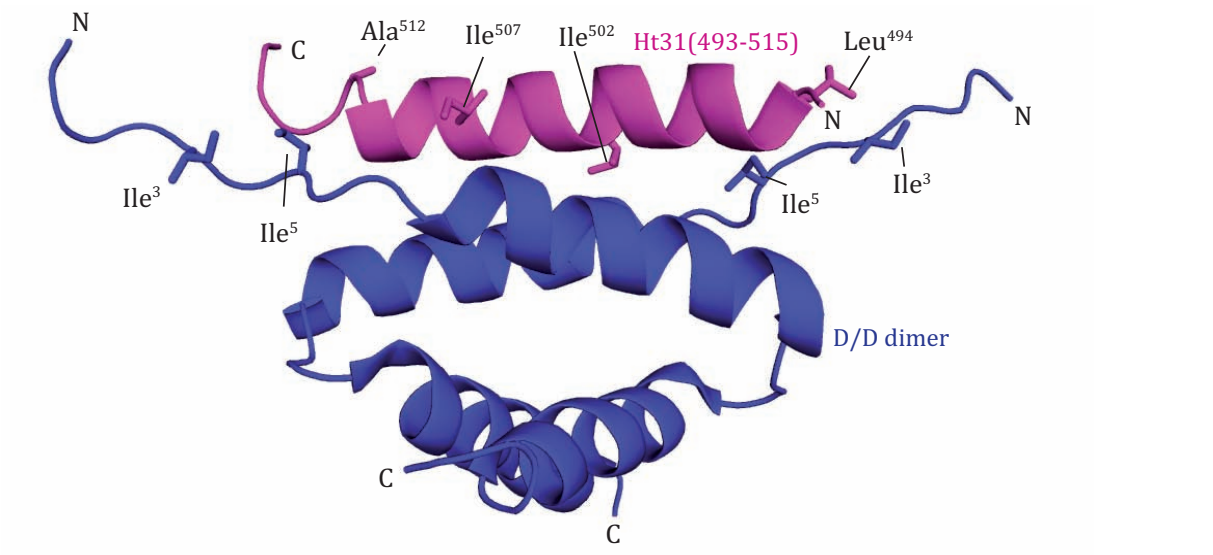

Fig. 4 NMR model of RIIα-D/D (blue) in complex with Ht31(493-515) (magenta). Critical residues for Ht31(493-515) – D/D interaction are shown as sticks (pdb file 2drn).

The first structural insights of the D/D domain were obtained by Newlon and co-workers, who investigated RIIα(1-44) by nuclear magnetic resonance (NMR) techniques [70]. A helical structure was proposed with two α-helices forming a helix-turn-helix motif and one short β-

strand in each monomer of a symmetric dimer. In this way, the dimer forms an anti-parallel four-helix bundle. The X-type four-helix bundle dimerization motif was later shown to contain an extended hydrophobic surface [78]. Upon addition of Ht31(493-515) to ^{15}N-labeled RIIα(1-44), chemical shift changes were observed in heteronuclear single quantum coherence (HSQC) spectra that mapped to the same hydrophobic surface and proved it to be the AKAP binding site. A model of the RIIα(1-44)-Ht31(493-515) complex was calculated where hydrophobic side chains of the first 21 residues of RIIα(1-44) make extensive hydrophobic contacts to similar residues in Ht31(493-515) [78]. As mentioned above, mutations of these residues in the R subunit had already been shown to impair AKAP binding [76, 77].

Finally, the structures of two RIIα D/D-AKAP peptide complexes, D/D-Ht31(493-515) and D/D-AKAP79(392-413), were solved at pH 4.0 using NMR [79]. The model of D/D-Ht31(493-515) is shown in **Fig. 4**. The amino acid sequences of the two AKAP peptides contain little homology but still bind to RIIα D/D domain in the same way and with hydrophobic interactions being the major binding forces. The structures both show the X-type four-helix bundle of RIIα D/D with the AKAP peptide bound to it at an angle of 45° with regard to helices I and I´ in the D/D dimer. For the first time, direct structural data of the helical nature of the AKAP peptides was obtained. In both structures, 18 residues of each AKAP peptide form a well-defined α-helix and constitute the D/D binding region. With the hydrophobic face of its amphipathic helix, the AKAP binds to the surface-exposed hydrophobic groove preformed by the D/D domain dimer. There are only subtle changes in the conformation of the hydrophobic residues of D/D observed when the AKAP peptide is bound to it. The stoichiometry of binding in these AKAP-D/D complexes is one AKAP peptide per RIIα dimer. Accordingly, binding of AKAP peptides results in an asymmetric molecular complex, whereas the free D/D dimer has an intrinsic symmetry [79].

The crystal structures of the complex between human RIIα D/D(1-45) and AKAP-IS (AKAP-*in silico*, an engineered high-affinity AKAP peptide of 18 amino acids [80]) and of murine RIIα D/D(1-43) in the apo state was solved to a resolution of 1.3 Å and 2.2 Å, respectively [81]. At the same time, the complex structure of rat RIIα D/D(1-44) with the 22 amino acid residue peptide from D-AKAP2 at a resolution of 1.6 Å was solved [82]. D-AKAP2 was shown before to be a dual-specific AKAP, binding to both RI and RII isoforms with high affinity [83]. The crystal structures of bovine RIα D/D and rat RIIα D/D domains in the absence and in complex with D-AKAP2 peptide are shown in **Fig. 5**.

All D/D crystal structures are in agreement with the NMR structures of D/D with the peptides Ht31(493-515) or AKAP79(392-413) [79]. Again, the D/D dimer forms an X-type four helix bundle with an antiparallel arrangement of helices I and II of one protomer with their counterparts, helices I´ and II´, of the other protomer. The protomers in the symmetric dimer of D/D in the D/D-D-AKAP2 complex are nearly identical and align with an rmsd (root-mean-

square deviation) value of 0.17 Å for the 96 equivalent Cα atoms (0.2 Å for D/D protomers in apo-D/D and 0.5 Å in D/D-AKAP-*IS* complex). Only the N-termini are very flexible, and in the apo-structure residues Ser[1] and His[2] are disordered.

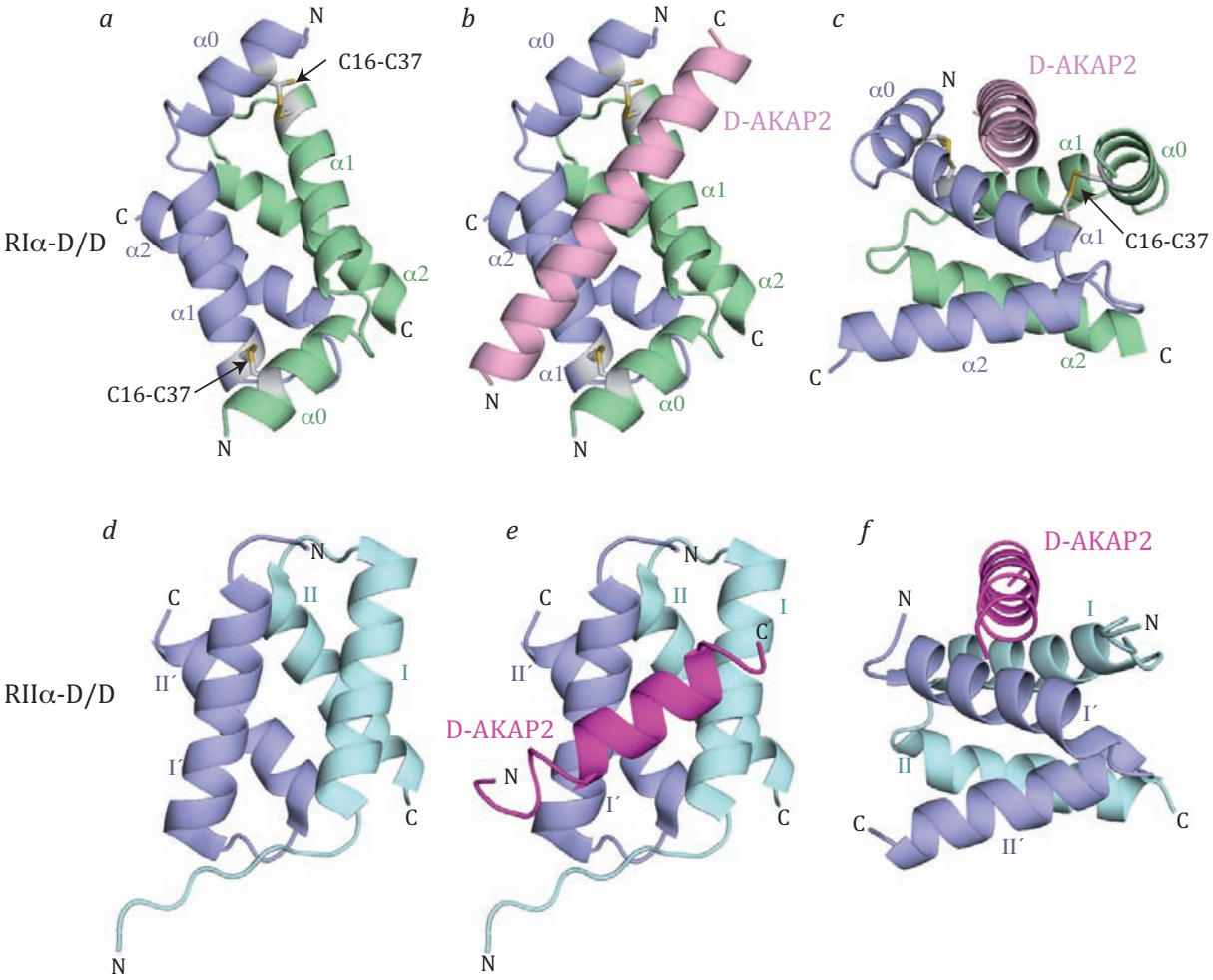

Fig. 5 Crystal structures of the dimerization and docking (D/D) domains of PKA RIα (*a-c*) and RIIα (*d-f*) in the absence or in the presence of D-AKAP2 peptide. The RIα D/D protomers are displayed in blue and green, respectively, and the D-AKAP2 peptide in pink (pdb file 3im4). The RIIα D/D protomers are shown in blue and cyan and D-AKAP2 is shown in magenta (pdb file 2hwn). ***a***, The RIα D/D domain in the absence of D-AKAP2 showing the anti-parallel four helix bundle and the intermolecular disulfide bond between residues Cys[16] and Cys[37] represented as sticks and indicated by arrows. ***b***, The RIα D/D domain in complex with D-AKAP2. The peptide binds diagonally across the surface formed by the two monomers. ***c***, Side view of b. Only residues from α-helices 0 and 1 interact with D-AKAP2. ***d***, The RIIα D/D domain in the absence of D-AKAP2. The N-terminus of only one of the protomers is ordered. ***e***, The RIIα D/D domain in complex with D-AKAP2. ***f***, Side view of e. Only residues α-helices I and I´ interact with D-AKAP2.

In the complexes, the AKAP helix binds diagonally to one face of the symmetrical D/D dimer formed by the N-terminal helices, I and I`, of each protomer. For the AKAP helix, Gold and co-workers describe a symmetrical pattern of hydrophilic and hydrophobic residues in the helix of

AKAP-*IS* creating a pseudo 2-fold symmetry of the complex [81]. But as the N-terminal residues from one D/D protomer become ordered upon AKAP binding, asymmetry is introduced into each of the D/D-AKAP complexes, as explained below.

Two elements in the D/D domain are critical for creating an asymmetric binding surface for AKAPs: first, the dynamic N-terminus of the D/D domain and, second, the formerly described [79] solvent-excluded hydrophobic docking surface (~1400 Å^2 in D/D-AKAP-*IS*) that is more or less preformed. The latter is relatively featureless and shallow without prominent binding pockets or protrusions. Accordingly, AKAP-*IS* contains four short-chain hydrophobic residues (Ala^9, Val^{13}, Ala^{16}, and Ala^{20}) that project towards the centre of the hydrophobic face on RIIα and longer aliphatic residues protrude from the sides of the helix. This hydrophobic ridge along the AKAP helix can interact tightly with the RIIα AKAP interface and is also found in D-AKAP2, Ht31, and AKAP79. It can be referred to as the recognition motif of AKAPs for regulatory subunits [82].

In contrast to the predominantly rigid docking surface, the N-terminal residues Ile^3 and Ile^5 in one D/D protomer shift by 2-3 Å upon complex formation. They contact Ile^5 and Leu^8 of AKAP-*IS*, respectively [81]. The same is true for the D/D-D-AKAP2 complex. In this case as well, the N-terminal residues Ile^3 and Ile^5 in one D/D protomer make contact to several residues in the AKAP peptide, whereas these residues in the other D/D protomer are disordered or have at least high temperature factors. Kinderman and colleagues even call this an “induced fit” mechanism which is stimulated by AKAP binding [82]. The flexible N-termini of the D/D domain convey plasticity and versatility to AKAP binding and enable the D/D domain to interact with various AKAP sequences.

Corresponding to the above mentioned two elements in the D/D dimer that are responsible for AKAP binding, the AKAP helix can also be divided into two segments. First, there is the helical segment in which side chains dock to the hydrophobic groove on RIIα and second, there is the helical segment recognizing the RIIα N-terminus. Many efforts were undertaken to find out which residues determine AKAP binding specificity towards the RI versus the RII isoform. To design isoform-specific inhibitor peptides in the absence of a high-resolution RIα D/D structure, peptide scanning assays were performed [80, 81, 84, 85]. Bulky residues like tryptophan replacing Val^{13} in D-AKAP2 do not fit into the hydrophobic groove of RIIα and disrupt peptide docking. In contrast, RIα is able to accommodate the V13W mutant peptide but cannot bind AKAPs with several mutations in the N-terminal part of the AKAP helix as RIIα can. Thus, RIIα subunits can tolerate various side chains at other positions in the AKAP helix except for the four required amino acids mentioned above.

The crystal structure of bovine RIα D/D(1-61) alone and in complex with D-AKAP2 (27 amino acid residues visible) was solved by Sarma and colleagues (**Fig. 5** a-c) and is very similar to

other D/D-AKAP structures [40]. Again, the typical anti-parallel four-helix bundle is observed with the D-AKAP2 peptide bound diagonally across the face of the hydrophobic groove formed by the D/D dimer. But, in comparison to RIIα D/D, RIα not only contains two intermolecular disulfide bridges but also possesses an additional small helix called the α0 or N-1 helix. The position of this helix is variable due to flexibility in the α0-α1 loop [86]. Cys^{16}, one of the cysteine residues involved in the disulfide bond, lies in the α0 helix and contributes to the dimer interface. In addition to extensive hydrophobic interactions, the AKAP helix makes polar interactions with the dimer [40]. The rmsd between the dimer of the complex structure and the free D/D domain structure is 1.4 Å for 98 equivalent Cα atoms. This rearrangement of the two monomers upon AKAP binding takes mainly place in the α0 and α1 helix region. In contrast, nothing similar is observed in the RIIα D/D structures.

Four pockets, I through IV, have been identified on the surface of the RIα D/D dimer that accommodate hydrophobic residues from the D-AKAP2 helix. They are formed by helices α0 and α1 of the D/D domain. Surprisingly, there is a shift in α-helical register when comparing the two complex structures of RIα D/D and RIIα D/D in complex with the D-AKAP2 peptide: the D-AKAP2 peptide is shifted towards the N-terminus by a complete turn. In the case of the complex with RIIα D/D, only two binding pockets are occupied instead of four in the RIα D/D dimer. Due to the additional contacts, RIα is not able to bind the wide variety of AKAPs that RIIα can, thus explaining the results from peptide array assays mentioned above. Certain requirements have been proposed that should be fulfilled by a (putative) AKAP to be RI, RII, or dual-specific, on the basis of the amino acid sequence and the identified binding pockets in RIIα and RIα. But additional interactions outside the core region can still influence binding specificity on an AKAP, as shown for the RI-specific RIAD peptide [40].

1.2 Scaffolding proteins

Scaffolding proteins represent a diverse family of large multi-domain proteins that are able to organize various intracellular signal transduction elements into large complexes [87]. By bringing them in close proximity to each other, scaffolding proteins simultaneously target and regulate other proteins. Thus, their general function is to organize and optimize signal transmission. As so-called “professional recruiter proteins” (PRPs), they can form large signaling modules when combining several recruited proteins in one complex [87, 88].

Importantly, this seems to be a mutual relationship: modification of the scaffold itself by its recruited partners can in turn facilitate the regulation of the activity of the recruited proteins [88]. Therefore, scaffolding proteins are responsible for the specific behavior of whole signaling

complexes [88] and can mostly be regarded as non-catalytic fine-tuning elements of pre-existing signaling pathways [89]. This demonstrates that a formerly attributed passive role of scaffolding proteins might rather be an active regulatory role that shapes the signaling outcome. The observed structural disorder of many scaffolding proteins (43 % on average) might be connected with this active role and enable these PRPs to dynamically adapt to different binding partners and functions [87].

As the family of scaffold proteins and proteins with similar molecular and/or cellular function is versatile, comprising docking, anchoring, scaffolding, as well as adaptor proteins, it is useful to differentiate between three main functional categories [87]:

- *Adaptor proteins* that simply bring two interacting proteins into close proximity
- *Scaffolding/anchor proteins* that recruit more proteins and regulate them (in the case of anchoring proteins the influence on cellular localization is stressed)
- *Docking proteins* that target their binding partners to the cell membrane by containing an N-terminal motif or domain for direct membrane association

There are, nevertheless, many ambiguities in this functional definition and whether a protein belongs to the one or the other category is not always clearly defined. For example, a docking protein performs an adaptor function by establishing a link between an activated tyrosine kinase and a Src homology 2 (SH2)-domain containing effector [90]. Throughout this work the above-mentioned definitions will be used.

1.3 A-kinase anchoring proteins (AKAPs)

A-kinase anchoring proteins, so-called AKAPs, belong to the family of scaffolding and anchoring proteins. They play a key role in the organization and regulation of cAMP-dependent kinase (PKA) signaling. Their main task is to provide a molecular framework for connecting PKA, phosphoprotein phosphatases, phosphodiesterases, and other proteins involved in signal transduction, like other kinases. As described in chapter **1.1.2**, compartmentalization is one important way to confer specificity to these enzymes and to optimize the cellular response to cAMP and other second messengers [91, 92].

AKAPs are classified by their characteristic co-purification with PKA catalytic activity from tissue. There are at least 50 different AKAPs known (including splice variants). Their common feature is the presence of a PKA-anchoring domain, an amphipathic helix, which is required for binding to PKA regulatory subunits (see chapter **1.1.5** and **Fig. 4**) [93]. In addition to PKA binding, common functional properties classifying a protein as an AKAP are a unique localization in the cell and the ability to form complexes with other signaling effectors [92]. In this way,

AKAPs target PKA to its specific substrates and assemble multi-protein signaling complexes controlling PKA signaling both in space and time [93].

AKAPs can be further classified by their specificity for binding different PKA subtypes as defined by the particular PKA regulatory subunit. Although the first AKAPs to be characterized were RII-binding proteins (microtubule-associated protein-2 (MAP-2) [94, 95] and rat brain AKAP150 [96], as well as its homolog bovine brain AKAP75 [97]), more and more type I specific AKAPs have been discovered, e.g. $AKAP_{CE}$ in *Caenorhabditis elegans* [98], myosin VIIA [99], and sperm fibrous sheath protein (FSC1)/AKAP82 [100]. Additionally, dual-specific AKAPs that can bind both the RI and the RII subunits have been found, first and foremost D-AKAP1 [101] and D-AKAP2 [102] identified by Huang and co-workers. FSC1 also contains an RII-specific binding site in addition to its RI-binding region [100]. A detailed summary of RI-, RII-, and dual-specific AKAPs can be found in the recent review by Skroblin and co-authors [103]. In general, RIα binding to AKAPs is much weaker than to RIIα, suggesting a more dynamic RI targeting in comparison to RII [72].

Several techniques have been developed to identify AKAPs and to investigate their function. The so-called RII-overlay method has been widely used to detect proteins that can bind to RII subunits. In general, it is a western blot analysis using ^{32}P-labeled RIIβ as a probe. It was established by Lohmann and co-workers who characterized RII-binding proteins from brain by this method [104]. On the other hand, intermolecular fluorescence resonance energy transfer (FRET) was used to study compartmentalization and dynamics of PKA signaling, e.g. a fusion protein consisting of cyan flourescent protein (CFP), a phosphorylation recognition domain, a consensus substrate site for PKA, and yellow fluorescent protein (YFP) was designed that upon phosphorylation in the linker between the two GFP variants changes its conformation [105]. This results in a change in FRET that can be detected *in vitro* and *in vivo*.

Apart from that, several peptides have been developed that disrupt the interaction between PKA and AKAPs, e.g. to assess involvement of PKA in specific signaling pathways. The prototype of these disruptor peptides is Ht31(493-515) described in chapter **1.1.4**. It was discovered and analyzed by Carr and co-workers [71]. Ht31(493-515) competes with full-length AKAPs for binding RII *in vitro* but also *in vivo* [106, 107] and associates with RIIα as well as RIα [72]. Via a combination of bioinformatics, peptide screening arrays, and the RII overlay procedure, several new peptides have been derived such as AKAP-*IS* that has a K_D for RII of 0.4 nM [80]. By using a two-dimensional peptide substitution array, RIα and RIIα isoform-specific peptides have been developed based on the amino acid sequence of the minimal PKA binding site of D-AKAP2 [85]. An optimized peptide was described by Carlson and co-workers that specifically disrupts RIα-dependent PKA signaling and was therefore called RI-anchoring disruptor (RIAD) [84]. It displays a three orders of magnitude higher selectivity of binding to RI over RII. Compared to the

Ht31 peptide, RIAD has a 1300-fold higher RIα affinity. Likewise, AKAP-*IS* was optimized to yield a peptide that has a four-fold higher apparent affinity for RIIα than the original peptide [81]. The so-called SuperAKAP-*IS* peptide exhibits a 12.5-fold lower affinity for RIα than AKAP-*IS*. At the same time, Hundsrücker and co-workers could show that a naturally occurring peptide derived from the PKA binding site of rat AKAP18δ can bind RIIα with similarly high affinity as AKAP-*IS* and that it can be used as an anchoring inhibitor peptide as well [108].

1.3.1 A-kinase anchoring protein 18 (AKAP18)

The A-kinase anchoring protein investigated in this study is AKAP18, also called AKAP7 or AKAP15. In general, it is regarded as RII-specific, but there are hints that it might as well bind RIα, making it a dual-specific AKAP [81, 109].

AKAP18 was originally discovered by Gray and co-workers who were able to co-purify PKA with L-type calcium channels from rabbit skeletal muscle cells [110]. They determined that these proteins were linked by an AKAP. They subsequently isolated AKAP18 from rabbit skeletal muscle cells and determined its sequence [111]. They found the protein to possess a theoretical molecular weight of ~9 kDa but as it migrates at ~15 kDa on SDS-PAGE they called it AKAP15 according to the nomenclature by Hirsch et al. [112]. In a study similar to that of Gray and co-workers, Fraser and colleagues cloned AKAP18 from a human fetal brain cDNA expression library and characterized it [113]. They as well found that the protein has a theoretical molecular weight of ~9 kDa but a significantly higher apparent molecular weight in SDS-PAGE and called it AKAP18.

AKAP15/18 was found to be a lipid-anchored protein of 81 amino acids that binds to PKA via a single amphipathic helix, co-localizing the kinase with L-type calcium channels in transverse tubules of skeletal muscle cells. The protein is myristoylated at an N-terminal glycine residue and palmitoylated at two cysteines in position 5 and 6, resulting in attachment to the membrane. Its solubilization requires the presence of detergent or mutation of the acylated residues. AKAP18 was found to be ubiquitously expressed in rat tissue but prominently in the heart and in the brain. A synthetic peptide called AP2 corresponding to the PKA anchoring site of AKAP18 blocks voltage-dependent potentiation of calcium channels in skeletal muscle cells [111]. Shortly afterwards, it was shown that AKAP18 also interacts with rat brain sodium channels, anchoring PKA in the vicinity of this substrate [114, 115]. AKAP18 can also bind to the C-terminus of the $Ca_v1.2$ channel, a voltage-gated L-type Ca^{2+} channel in rat cardiomyocytes. This interaction is mediated by a conserved leucine zipper-like motif in the $Ca_v1.2$ channel [116].

An increase in L-type calcium channel activity and therefore in cAMP-responsive Ca^{2+} current upon AKAP18 overexpression in HEK293 cells was observed by Fraser and colleagues [113].

They also found an increase in insulin secretion upon stimulation with glucagon-like peptide 1 when overexpressing AKAP18 in the rat β-cell line RINm5F. These studies support the PKA targeting hypothesis in general, and, in particular, showed for the first time a clear example of an AKAP possessing a membrane targeting domain, i.e. having lipid modifications by which it functionally couples PKA and ion channels, thereby influencing physiological events.

Two additional AKAP18 splice variants were identified in human lung and pancreas, and called AKAP18β and AKAP18γ, thereby re-naming the original AKAP18 AKAP18α [117]. **Fig. 6** shows the domain organisation of AKAP18 isoforms.

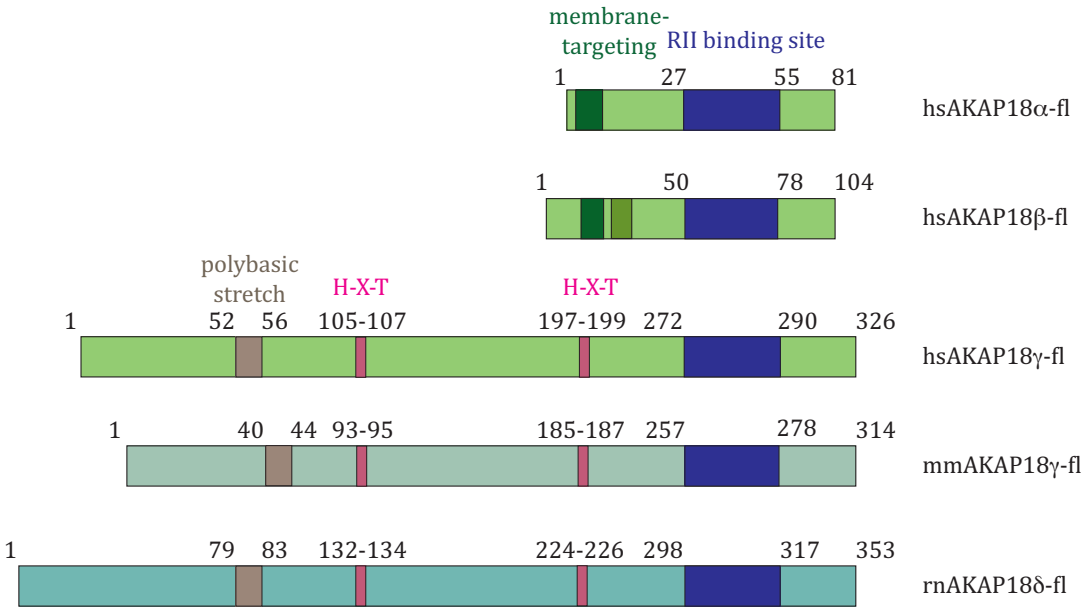

Fig. 6 Schematic representation of the domain organization of human (hs), mouse (mm), and rat (rn) AKAP18 isoforms. AKAP18α and β isoforms contain a membrane targeting domain that is similar but the β isoform has an additional membrane targeting region. The γ and δ isoforms have a polybasic stretch in their N-terminal region and all of them contain the conserved His-X-Thr motif. The RII binding site is shown in blue and is highly conserved in all isoforms.

All of the three isoforms α, β, and γ have been detected in human, mouse, and rat tissue. They arise from differential splicing of exons in a single gene and all of them contain the same RII binding determinant encoded by one exon. Another exon codes for the N-terminal membrane targeting domain and is common to AKAP18α and β. In comparison to AKAP18α, the β isoform contains an additional 69 bp exon coding for 23 unique amino acids that follow the N-terminal targeting domain. AKAP18γ is different from AKAP18α and β, in that it does not have a domain for lipid modification. In humans, it consists of 326 amino acids of which the N-terminal 262 residues are unique. Accordingly, AKAP18α and β localize to the plasma membrane when overexpressed in HEK293 cells while AKAP18γ is cytosolic [117].

Upon overexpression of GFP-tagged AKAP18α and β in Madin-Darby canine kidney (MDCK) cells, a polarized kidney epithelial cell line, AKAP18α localized to the lateral membrane while AKAP18β was found in the apical membrane parts. Interestingly, the 23-amino acid insert contained in AKAP18β alone was not sufficient for membrane targeting but facilitates targeting to the apical membrane. An association of AKAP18β with lipid rafts was excluded because 0.2 % Triton X-100 was already enough to extract it from membranes, an observation that does not correlate with localization in detergent-resistant membrane fractions [117].

Nuclear targeting of human AKAP18γ in human embryonic kidney (HEK) 293 cells due to a predicted nuclear localization sequence (NLS) between residues 37 to 54 was not detectable by immunoflourescence (IF) microscopy [117]. In contrast to these results, overexpressed mouse AKAP18γ fused to GFP was shown to translocate to the nucleus of HEK293 cells [109]. The mouse variant of AKAP18γ contains only 314 amino acids but the putative NLS is conserved in human, mouse, and also in rat AKAP18γ. Even though sharing 79 % sequence identity with the human orthologue, it has a much higher pI value (7.7 for mouse in comparison to 5.7 for human AKAP18γ). It is not clear, whether these differences account for the different localization of AKAP18γ in HEK293 cells.

A fourth isoform of AKAP18, AKAP18δ, was identified when screening a rat kidney cDNA expression library for AKAPs involved in the shuttling of the water channel aquaporin-2 (AQP2) from intracellular vesicles to the cell membrane [118]. The mechanism of AQP2 shuttling is fundamental for water re-uptake in the kidney. In brief, it is regulated by binding of the anti-diuretic hormone arginine/vasopressin (AVP) to its cognate vasopressin 2 (V_2)-receptor in the membrane of renal collecting duct principal cells. Through activation of the heterotrimeric G protein G_s and adenylyl cyclases, PKA is activated and phosphorylates AQP2 at Ser^{256}. AQP2, which is located in intracellular vesicles under resting conditions, translocates to the apical cell membrane upon phosphorylation by PKA [119]. Fusion of AQP2 containing vesicles with the apical cell membrane increases the water permeability of the cell and facilitates water reabsorption from the collecting duct. It was previously shown that incubation of rat inner medullary collecting duct (IMCD) cells with the disruptor peptide Ht31(493-515) inhibits AQP2 shuttling [120] suggesting that PKA anchoring might be important for the redistribution of AQP2. AKAP18δ was then found to be involved in this process [118]. It shares an identical RII binding sequence with the other splice variants of AKAP18 but is the longest of the four isoforms (353 amino acids) and contains a unique N-terminus. AKAP18δ was shown to bind RII subunits with nanomolar affinity in biacore experiments [108]. AKAP18δ was detected mainly in the soluble fraction of rat renal inner medullary tissue homogenates rather than in the particulate fraction [118, 121], but could nevertheless pull down RIIβ and AQP2 from the same homogenates using beads coupled to an antibody raised against rat AKAP18δ. These findings

suggest that RIIβ, AQP2, and AKAP18δ co-localize on intracellular vesicles [118]. Further experiments showed that cAMP-specific phosphodiesterase (PDE) 4D resides on the same vesicles [122]. Like AQP2, PDE4D translocates to the cell membrane (and also to the nucleus) upon stimulation with AVP in IMCD cells. Inhibition of PDE activity in IMCD cells with the PDE4D-selective inhibitor rolipram leads to an increase in cAMP levels, in water permeability, and in AQP2 shuttling if AVP is present. In the absence of AVP, the inhibition of PDE4D alone does not trigger these events. Interestingly, PDE4D3 is phosphorylated by PKA at Ser^{54} causing an increase in its activity [123]. Phosphorylated PDE4 was found to shuttle to the plasma membrane as observed before for PDE4D in IF microscopy. Its function there might be to decrease PKA activity by enhanced degradation of local cAMP to AMP, thereby decreasing water permeability and thus constituting a negative feedback loop.

PDE4D is anchored to AQP2 vesicles by AKAP18δ [122], which is the only AKAP detectable on these vesicles [118]. The interaction was shown by co-immunoprecipitation of PDE4D3/9 from rat renal inner medulla lysates using an antibody that predominantly recognizes the δ isoform of AKAP18. To confirm that the interaction is a direct one and to map the interaction sites, peptide spot arrays were performed using recombinant GST-AKAP18δ or PDE4D3-GST and GST alone as control. Two binding sites for AKAP18δ in PDE4D3 were found, comprising amino acids 341-365 and 586-600. Substitution of residues Asp^{535} and Glu^{355} with arginine or alanine, respectively, or of both residues Phe^{598} and Phe^{600} with alanine, reduces or even inhibits the interaction with recombinant GST-AKAP18δ. Four different binding sites for PDE4D3 were found in AKAP18δ covering the regions of residues 51-80 (binding site 1), 96-135 (2), 196-230 (3), and 291-315 (4). In order to confirm these results, deletion constructs of AKAP18δ were designed containing an N-terminal YFP-tag, and were co-expressed with vesicular stomatitis virus (VSV)-tagged PDE4D3. A pulldown using an anti-GFP antibody confirmed the interaction and showed that only the deletion of all four binding sites abolished the interaction between AKAP18δ and PDE4D3. Full-length AKAP18δ seemed to co-precipitate PDE4D3 less efficiently than the deletion constructs, which was attributed to a negative regulatory role of the N-terminal residues in the interaction [122]. On the other hand, the full-length construct was the only one having the YFP-tag at the C-terminus. This might as well have interfered with the interaction with PDE4D3.

Taken together, a signaling module was discovered that consists of PKA, AKAP18δ, and PDE4D3. It resides on the same vesicle as AQP2 channels and thereby regulates AQP2 distribution throughout the inner medullary collecting duct cell. Still, it remains unclear how AKAP18δ is tethered to the AQP2-bearing vesicle.

Another function of AKAP18δ was found in cardiac myocytes. In these cells, a supramolecular complex consisting of AKAP18δ and PKA as well as phospholamban (PLN) and the sarcoplasmic

reticulum Ca^{2+}-ATPase (SERCA) 2 was detected [124]. SERCA2 is important for the re-uptake of Ca^{2+} into the sarcoplasmic reticulum (SR) after the contraction phase of the heart [125]. It is regulated by phospholamban, a 52-amino acid protein consisting of a transmembrane helix (residues 23-52) and a cytoplasmic helix (residues 1-16) that are connected by a linker region (residues 17-22) [126, 127]. PLN is reversibly phosphorylated by PKA on residues Ser^{16} and Thr^{17}. In the dephosphorylated state, it binds to SERCA2 and inhibits its Ca^{2+} pump activity. Phosphorylation of PLN by PKA leads to the dissociation of PLN from SERCA2 and releases the ATPase from inhibition which in turn promotes re-uptake of Ca^{2+} into the SR and relaxation of cardiac myocytes [128].

AKAP18δ was found to regulate PKA-mediated phosphorylation of PLN, thereby influencing SERCA2 activity [124]. AKAP18δ co-localized with PLN and SERCA in rat heart tissue and interaction of AKAP18δ with PLN was shown by immunoprecipitation. In pulldown experiments from rat heart SR fractions using the PKA antagonist Rp-8-AHA-cAMP, AKAP18δ and SERCA2 were detected in addition to RIIα and the catalytic PKA subunit. The core interaction site with full length AKAP18δ containing an N-terminal GST-tag was mapped to PLN residues 13-20 using peptide spot arrays. These residues predominantly lie in the linker region of PLN, which comprises amino acids 17-21, and contain the PKA phosphorylation site. Phosphorylation of Ser^{16} abolished AKAP18δ binding. The same was true for substitution of Arg^{13}, Arg^{14}, and Pro^{21}. The binding sites for PLN in AKAP18δ were also determined by co-immunoprecipitation and peptide spot arrays and were mapped to amino acids 124-138 (binding site 1) and 201-220 (binding site 2). These regions also exist in AKAP18γ but IF microscopy studies showed that, in contrast to AKAP18δ, the distribution of AKAP18γ only partially overlapped with that of PLN or SERCA2 [124].

In general, it can be said that AKAP18 isoforms are involved in a variety of cellular processes: interaction with and (possible) regulation of Ca^{2+} channels in skeletal muscle cells [111] and cardiac muscle cells [116], of brain Na^{+}-channels [114, 115] and L-type Ca^{2+} channels [113], and regulation of AQP2 shuttling in renal principal cells [118] in addition to regulation of Ca^{2+} re-uptake into the SR in cardiomyocytes [124]. As important scaffolding proteins, AKAP18 isoforms constitute the core of protein-protein interactions in different signaling modules at specific locations inside the cell, bringing together PKA and other enzymes with their substrates, thereby controlling various cellular events.

1.3.2 Structure of A-kinase anchoring proteins and AKAP18

One characteristic of A-kinase anchoring proteins, besides containing a PKA binding site, is their ability to bind to multiple effector proteins. Therefore, AKAPs often are very flexible in structure,

which enables them to contact a variety of binding partners. Nevertheless, AKAPs can possess specialized domains for protein-protein interactions. For example, AKAP13 contains a Dbl homology (DH) domain followed by a pleckstrin homology (PH) domain. The DH domain is important for the nucleotide exchange activity of AKAP13-activating GTPases of the Rho family, whereas the role of the PH domain is more complex as it can target the protein to different sub-cellular compartments but as well can regulate nucleotide exchange efficiency [129, 130]. Several three-dimensional structures of DH/PH-domains have been solved (e.g. [131, 132]). Other examples of AKAPs containing subdomains with known folds are the brefeldin A-inhibited guanine nucleotide-exchange proteins BIG1 and BIG2 that are involved in the regulation of membrane trafficking. In addition to their PKA-binding domain [133], they possess a Sec7 domain, which activates members of the Ras superfamily of GTPases, so-called ADP-ribosylation factors (ARFs) [134]. Moreover, BIG2 was predicted to contain an armadillo repeat [135], a structural motif that takes part in various processes including signaling and cytoskeletal regulation [136], but its actual binding partner has not yet been identified. Several structures of Sec7 domains [137, 138] and armadillo repeat motifs [139] are currently known.

The structural features of the short PKA-binding α-helix, the defining characteristic of most AKAPs, have been described in chapter **1.1.4**, summarizing the known structures of the dimerization and docking (D/D) domain of PKA regulatory subunit. Most of these structures are complexes of D/D with short amphipathic peptides originating from the PKA binding site of different AKAPs like Ht31 [79] or D-AKAP2 [82]. Up to now, no structure of an AKAP has been solved that is longer than these approximately 20 amino acid residue peptides. The only AKAP structures that are known are those of the different subdomains mentioned above, and they do not contain the PKA-binding site.

In an attempt to solve the structure of an AKAP, Gold and co-workers used a bioinformatics approach to define putative globular domains in AKAPs amenable to structural analysis [135]. They solved the crystal structure of rat AKAP18δ(76-292) domain that is common to the γ isoform as well, the so-called “core domain” (CD) (**Fig. 7**). As this truncation construct does not contain the PKA-binding helix, it cannot be considered as an AKAP but rather as the structure of another functional subdomain of a protein known for its AKAP function. Nevertheless, this study revealed fundamental structural insights concerning AKAP18γ and δ.

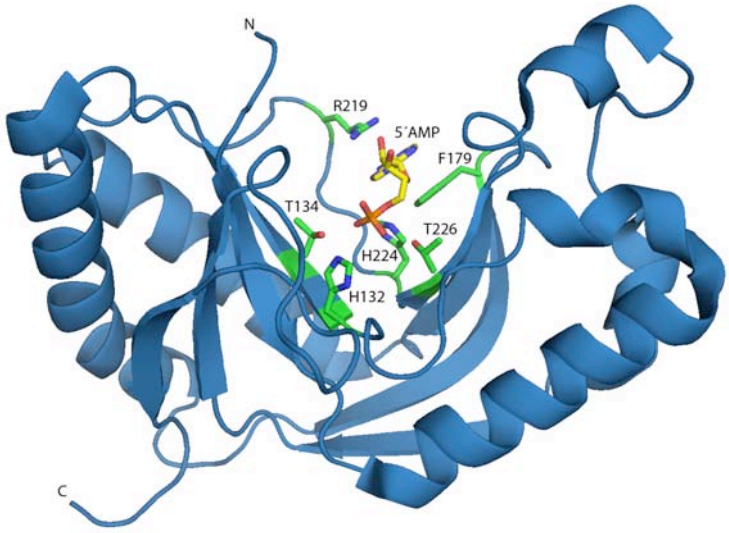

Fig. 7 Crystal structure of rat AKAP18δ(76-292) with 5´AMP bound in the groove between the two lobes. The residues most important for 5´AMP binding are shown as sticks.

AKAP18δ-CD is a globular protein. It shows striking structural similarities to members of the 2H phosphoesterase family despite the low sequence identity of only 17 % [140]. AKAP18δ-CD adopts a bilobal fold and consists of four α-helices and eight β-strands that form two four-stranded anti-parallel β-sheets. Between the two lobes lies a deep water-filled groove containing a pair of conserved motifs that define the 2H phosphoesterase family, the His-X-(Ser/)Thr motif [135]. In this protein family, the two highly conserved His residues (hence the name of the enzymes) and, to a lesser extent, the Ser/Thr residues play a critical role in the catalytic activity of the respective enzyme [140].

As 2H phosphoesterases catalyze reactions in which the ends of two tRNA half molecules are joined together, AKAP18δ-CD was co-crystallized in the presence of various nucleotides. Besides the apo-structure of AKAP18δ-CD solved at 1.8 Å, the structures of the core domain with 5´AMP or 5´CMP bound were solved to 1.5 and 2.25 Å resolution, respectively. Co-crystallization with several other nucleotides, e.g. 3´AMP, guanosine 5´-monophosphate (5´GMP), and cAMP did not yield complex structures. Only 5´AMP and 5´CMP can form the specific hydrogen bonds with the backbone carbonyl of Thr^{220} needed for nucleotide binding. Furthermore, analysis of the crystal structure revealed that there is no space in the binding groove to accommodate additional phosphate groups.

To determine the dissociation constant (K_D) for 5´AMP binding apart from estimating it from the co-crystallization conditions, equilibrium fluorescence measurements were performed using a fluorescently labeled 5´AMP analogue, 2´-O-(N-methylantraniloyl) adenosine 5´-monophosphate (MANT-AMP). These measurements yielded a K_D of 194 ± 30 µM for 5´AMP binding.

The affinities for nucleotide binding to AKAP18δ-CD are relatively similar for 5´AMP and 5´CMP. The nucleotides bind in the cleft between the two lobes and the phosphate moiety is coordinated by the two His-X-Thr motifs at the base of the groove. The only interaction to the ribose moiety of the nucleotides is a van der Waals contact with Val^{183}. The side chains of residues Phe^{179} and Arg^{219} sandwich the base moieties of either 5´AMP or 5´CMP, forming π-stacking interactions from both sides of the base. Nucleotide binding stabilizes the flexible loops containing residues Phe^{179} and Arg^{219}.

The structural homology of AKAP18γ to 2H phosphoesterases had been detected before by Mazumder and co-workers who performed a bioinformatics approach to identify new members of this superfamily and to evolutionarily classify them. In addition, they performed a structure-function analysis [140]. They classified human AKAP18γ as belonging to a subgroup of the 2H phosphoesterase family of proteins, namely the eukaryotic-viral LigT-like proteins, and speculated about a possible function of AKAP18γ in targeting PKA to cytoplasmic RNA processing complexes to regulate these through phosphorylation.

Gold et al. found that bacterial 2´-5´RNA ligases from *Pyrococcus horikoshii* [141] and *Thermus thermophilus* [142] have the highest structural similarity with AKAP18δ-CD (from superposition of the structures). In general, members of this ligase family catalyze the following reaction: a 5´ and a 3´ half-tRNA molecule with a 2´,3´-cyclic phosphate at the 5´ fragment and a free 5´OH at the 3´ fragment are joined together by the ligase. In order to find out whether AKAP18δ would be able to catalyze this kind of reaction, they tried to co-crystallize AKAP18δ(76-292) with 3´AMP (mimicking the 3´ half-tRNA molecule) and 2´-3´cCMP (mimicking the 5´ half-tRNA molecule), which was not successful. The authors also tested for cAMP or cGMP phosphodiesterase activity by transiently overexpressing and afterwards immunoprecipitating AKAP18δ with radioactively labeled cAMP. They did not detect any PDE activity of AKAP18δ. Thus, it can only be speculated what might be the function of the conserved His-X-Thr motif in AKAP18γ/δ.

The position of critical residues in the catalytic site of *T. thermophilus* 2´-5´RNA ligase was compared to the equivalent residues in AKAP18δ. One of the conserved histidine residues, His^{130} in *T. thermophilus*, which corresponds to His^{224} in AKAP18δ, is proposed to activate the 5´OH at the 3´ fragment. The second conserved histidine, His^{39} in *T. thermophilus* corresponding to His^{132} in AKAP18δ, is important for opening the cyclic phosphate by protonating its 2´´-oxygen. The activated hydroxyl group performs a nucleophilic attack at the 2´,3´-cyclic phosphate of the 5´ fragment leading to a 2´-5´phosphodiester linkage between the two tRNA half-molecules [142]. Several additional residues in AKAP18δ would be correctly positioned to perform this reaction even though there are differences as well [135]. Co-crystallization of AKAP18δ with molecules

mimicking the 3´ and 5´ fragments of tRNA half-molecules, i.e. 3´AMP and 2´-3´CMP, respectively, did not yield complex structures. The authors state that this may indicate that AKAP18δ does not play a role in RNA processing [135].

Binding of 5´AMP does not lead to large structural rearrangements but still changes the shape and charge of the protein surface which could in turn result in new binding sites for interaction with other proteins. As the amount of 5´AMP in the cell is an indicator for energy balance, AKAP18γ/δ could also be imagined as an energy sensor. Upon 5´AMP binding, AKAP18γ/δ could interact with proteins involved in regulating intermediary metabolism, like AMP-activated protein kinase (AMPK) or glycogen phosphorylase, positioning PKA in their close vicinity. On the other hand, AMP binding could as well influence the cellular localization of AKAP18γ/δ by changing its surface properties [135].

As there is no structure known of the full-length AKAP18γ or δ isoforms nor of a complex with a PKA regulatory subunit or dimerization and docking (D/D) domain, it is not possible to elucidate the influence the remaining amino acids, which are not present in the construct crystallized by Gold et al., could have on possible nucleotide binding or even on enzymatic activity. Neither is it possible to determine the influence of 5´AMP binding on the AKAP18γ/δ structure in complex with an R subunit or D/D. Determination of the structure of AKAP18 containing the PKA binding site and/or a complex of AKAP18 and RIIα or D/D with or without 5´AMP would enable a better understanding of the function of AKAPs in general. It would provide insights into how other parts of an AKAP could interact with PKA and maybe detect (mutual) influences of both proteins on each other. Additionally, a high-resolution structure of the AKAP-PKA complex in the apo-state and in the nucleotide-bound state could reveal a function of 5´AMP binding by AKAP18γ/δ, if there 5´AMP binds to a full-length AKAP18 construct/complex at all. Last but not least, in order to elucidate further structural features of AKAP18 as a scaffold, it would also be very interesting to solve the structure of AKAP18 in complex with its binding partners PDE4D3 and phospholamban, which could as well be influenced by 5´AMP binding.

1.4 Scope of the work

The present doctoral thesis aimed at the functional and structural characterization of the interaction of AKAP18 with its binding partners PDE4D3, phospholamban, and RIIα. The structure of such a complex would be the basis to determine the molecular mechanisms of signaling events these proteins are involved in. Furthermore, this knowledge would enable us to better understand the function of AKAP18δ in a physiological context, i.e. in regulating water reabsorption through aquaporin shuttling in the kidney and in regulating the contraction – relaxation cycle in the heart *via* influencing Ca^{2+} re-uptake into the sarcoplasmic reticulum.

Moreover, it is of importance to gain knowledge of the biochemical and biophysical properties of AKAP18 isoforms. This would provide deeper insights into conformation, oligomerization, and ligand binding properties of AKAP18. On the other hand, based on these findings, optimal conditions for *in vitro* assays using purified AKAP18 isoforms can be established. This could be for example an ELISA or a surface plasmon resonance assay for screening approaches.

In addition, the structure of AKAP18 in complex with the RIIα D/D domain should be solved by X-ray crystallography, as no structural information is available on longer AKAPs bound to D/D. On the basis of this structure, molecular modeling could be used to screen for small molecules as specific inhibitors of the AKAP18δ - RIIα interaction in a rational drug design approach. These drugs might alter the outcome of cAMP-dependent signaling events and may lead to the development of new treatments for renal and cardiovascular disease.

2 Materials and Methods

2.1 Materials

2.1.1 Chemicals

Chemicals were purchased from the following companies: Karl Roth GmbH & Co. KG (Karlsruhe, Germany), Merck KGaA (Darmstadt, Germany), Jena Bioscience (Jena, Germany), Sigma-Aldrich GmbH (Hannover, Germany), Biolog (Bremen, Germany), Serva Electrophoresis GmbH (Heidelberg, Germany), GE Healthcare (Munich, Germany), Pierce Biotechnology Incorporation (Rockland, IL, USA).

2.1.2 Enzymes

Enzymes	**Manufacturer**
DNase I	Roche (Mannheim, Germany)
Benzonase ® Nuclease	Novagen (Merck KGaA, Darmstadt, Germany)
Restriction Endonucleases (BamHI, XhoI, DpnI)	New England Biolabs (Frankfurt a.M., Germany)
Pfu DNA Polymerase	Stratagene (Amsterdam, Netherlands)
KOD DNA Polymerase	Novagen (Merck KGaA, Darmstadt, Germany)
T4 DNA Polymerase	New England Biolabs (Frankfurt a.M., Germany)
PreScission Protease	GE Healthcare (Piscataway, NJ, USA)
Thrombin Protease	Serva (Heidelberg, Germany)
Tag-off™ High Affinity Enterokinase Protease	Novagen (Merck KGaA, Darmstadt, Germany)
Trypsin, Chymotrypsin	Sigma-Aldrich (Hannover, Germany)

2.1.3 Kits and Standards

Kit	Manufacturer
pET30 Ek/LIC Vector Kit	Novagen (Merck KGaA, Darmstadt, Germany)
Qiagen Plasmid Purification Kit (Mini, Midi)	Qiagen (Hilden, Germany)
Ultrafree-DA Centrifugal Filter (gel extraction)	Millipore Corp. (Billerica, MA, USA)
QuikChange®Site-Directed Mutagenesis Kit	Stratagene (Amsterdam, Netherlands)
2-log, 1 kb, and 100 bp DNA ladder	New England Biolabs (Frankfurt a.M., Germany)
GeneRuler ™ 1kb DNA ladder	Fermentas GmbH (St. Leon-Rot, Germany)
Bradford Protein Assay	Biorad (Munich, Germany)
Unstained Protein Molecular Weight Marker	Fermentas GmbH (St. Leon-Rot, Germany)
Mark12 Unstained Standard	Invitrogen Corporation (Carlsbad, CA, USA)
NuPAGE® Novex® Bis-Tris precast gel system	Invitrogen Corporation (Carlsbad, CA, USA)
Rotifect Transfection Reagent	Karl Roth GmbH & Co. KG (Karlsruhe, Germany)
Lipofectamine™ 2000 Transfection Reagent	Invitrogen Corporation (Carlsbad, CA, USA)

2.1.4 Bacteria strains

strain	genotype	Manufacturer
E.coli TG1 K12	*supE, hsdΔ 5, thi, Δ(lac-proAB), F'[traD36, proA⁺B⁺, lacq, lacZΔ M15]*	Promega (Mannheim, Germany)
E.coli Rosetta 2 DE3	*F⁻ ompT hsdSB (rB⁻ mB⁻) gal dcm (DE3) pRARE (CamR)*	Novagen (Merck KGaA, Darmstadt, Germany)
E.coli BL21 DE3	*B, F-, hsdSB (rB-, mB-), gal, dcm, ompT, (DE3)*	Novagen (Merck KGaA, Darmstadt, Germany)

2.1.5 Cell lines

HeLa cells

Human cervix carcinoma cell line, adherent, epithelial

HEK293 cells

Human embryonic kidney cell line, adherent, epithelial

CHO cells

Chinese hamster ovary cell line, adherent, epithelial

HeLa, HEK293, and CHO cells were a generous gift from Marion Papst (MDC)

MCD4 cells

M1 cells (mouse renal collecting duct cells) stably expressing human aquaporin 2 (AQP2) (made by G. Proccino from the laboratory of G.Valentis in Bari, Italy), adherent, epithelial

2.1.6 Media and antibiotics

Medium	**Composition**
Luria-Bertani (LB)	5 g/l yeast extract, 10 g/l bacto-trypton, 5 g/l NaCl
Terrific Broth (TB)	purchased from Karl Roth GmbH & Co. KG (Karlsruhe, Germany) (HP61.1)
Overnight Express™ Instant TB Medium (autoinduction medium (AIM))	purchased from Novagen (Merck KGaA, Darmstadt, Germany)
M9 Minimal Medium	10 ml/l M9 trace elements, 1 mM $MgSO_4$, 0.3 mM $CaCl_2$, 100 ml/l M9 salt, 2 g/l Glucose, 1.5 mg/l Thiamine, 1.5 mg/l Biotin, 0.5 g/l NH_4Cl (pH 7.2-7.3!)
M9 salt (10x)	64 g/l Na_2HPO_4, 20 g/l KH_2PO_4, 5 g/l NaCl
M9 trace elements	5 g/l EDTA, 500 mg/l $FeSO_4$, 50 mg/l $ZnCl_2$, 10 mg/l $CoSO_4$
Minimum Essential Medium (MEM) without L-glutamine	purchased from Invitrogen Corporation (Carlsbad, CA, USA) (Cat.no.10370-047)
OptiMem® Reduced-Serum Medium	purchased from Invitrogen Corporation (Carlsbad, CA, USA) (Cat.no.11058-021)

Antibiotics	Concentration	Manufacturer
Kanamycin	25 µg/ml	Karl Roth GmbH & Co. KG (Karlsruhe, Germany)
Chloramphenicol	34 µg/ml	
Carbenicillin	60 µg/ml	
Ampicillin	100 µg/ml	

2.1.7 Plasmids

Plasmid	Properties
pET28a	prokaryotic expression vector for expression of N-terminally His_6-tagged fusion proteins, thrombin cleavage site, Kan^R (Novagen, Merck KGaA, Darmstadt, Germany)
pET30 Ek/LIC	prokaryotic expression vector version of pET30b(+) for high-level expression of N-terminally His_6-tagged fusion proteins, thrombin and enterokinase cleavage sites, Kan^R (Novagen, Merck KGaA, Darmstadt, Germany), additional thrombin or TEV cleavage site added
pET46 Ek/LIC modified	prokaryotic expression vector modified from pET46 Ek/LIC (Novagen, Merck KGaA, Darmstadt, Germany) by Andi Mainz (FMP) for high-level expression of non-tagged fusion proteins, Amp^R
pSKB2LNB	prokaryotic expression vector for high-level expression of N-terminally His_6-tagged fusion proteins, PreScission cleavage site, Kan^R (Oliver Daumke, MDC)
pGEX4T3	prokaryotic expression vector for expression of N-terminally GST-tagged fusion proteins, Amp^R (GE Healthcare, Piscataway, USA)
pEGFP-N1	eukaryotic expression vector for expression of C-terminally EGFP-tagged fusion proteins, Kan^R (Clontech, Mountain View, USA)
mCherry in pEGFP-N3	eukaryotic expression vector for expression of C-terminally mCherry-tagged fusion proteins, based on pEGFP-N3 (Clontech, Mountain View, USA), Kan^R, EGFP gene exchanged against mCherry gene (AG Lewin, MDC Berlin)

mCherry in pEGFP-C1	eukaryotic expression vector for expression of N-terminally mCherry-tagged fusion proteins, based on pEGFP-C1 (Clontech, Mountain View, USA), Kan^R, EGFP gene exchanged against mCherry gene (AG Lewin, MDC Berlin)
pEYFP-N1	eukaryotic expression vector for expression of C-terminally EYFP-tagged fusion proteins, Kan^R (Clontech, Mountain View, USA)

2.1.8 Buffers

In the following, generally used buffers are listed. The composition can vary in certain experiments.

Buffer	**Composition**
Lysis buffer for test expression	Hepes/NaOH pH7.5 50 mM, NaCl 150-600 mM, $MgCl_2$ 2 mM, DNaseI 1 µg/ml, Pefabloc 0.1 mM, Lysozyme 1 mg/ml, (β-Mercaptoethanol 2.8 mM)
Lysis buffer	Hepes/NaOH pH7.5 50 mM, NaCl 150-600 mM, $MgCl_2$ 2 mM, DNaseI 1 µg/ml, Pefabloc 0.1 mM, (β-Mercaptoethanol 2.8 mM)
Equilibration buffer (Buffer A)	Hepes/NaOH pH7.5 50 mM, NaCl 150-600 mM, $MgCl_2$ 2 mM, (β-Mercaptoethanol 2.8 mM)
Elution buffer (Buffer B)	Hepes/NaOH pH7.5 50 mM, NaCl 150-600 mM, $MgCl_2$ 2 mM, Imidazole 300 mM, (β-Mercapto-ethanol 2.8 mM)
Gel filtration buffer	Hepes/NaOH pH7.5 20 mM, NaCl 150-600 mM, $MgCl_2$ 2 mM and/or $CaCl_2$ 2mM, (DTT 2 mM)
HPLC buffer	Potassium phosphate pH 6.5 100 mM, TBAB 10 mM, Acetonitril 7.5 % (v/v)
ITC and RALS buffer	Hepes/NaOH pH7.5 20 mM, NaCl 100-300 mM, $MgCl_2$ 2 mM
PBS	Na_2HPO_4 8 mM, KH_2PO_4 1.8 mM, NaCl 170 mM, KCl 1.8 mM (pH 7.4)

NMR buffer	NaH_2PO_4 20 mM, NaCl 50 mM (pH between 6.8 and 7.2)
2x SDS sample loading buffer	Tris/HCl pH 6.8 100 mM, Glycerol 20 % (v/v), SDS 4 % (w/v), DTT 200 mM, 0.04 % (w/v) Bromophenol Blue
Coomassie-staining: Fixation solution	Ethanol 50 %, Acetic acid 10%
Coomassie-staining: Staining solution	Acetic acid 10 %, Coomassie-G 0.025 % (alternatively for cooking protocol: Acetic acid 10 %, Ethanol 20 %, Coomassie-R 0.1 %)
Coomassie-staining: Destaining solution	Acetic acid 10 % (alternatively for cooking protocol: Acetic acid 10 %, Ethanol 30 %)

2.1.9 Constructs

Construct	**Vector**	**Remarks**
hsAKAP18α-full length	pGEX4T3	kindly provided by J. Tröger
hsAKAP18α(20-60)	pET30 Ek/LIC	no test expression
hsAKAP18β-full length	pCMV6-XL5	ordered from Origene (NM_138633)
hsAKAP18β(43-83)	pET30 Ek/LIC	protein expressed and purified in large amounts, crystallized
hsAKAP18β(48-83)	pET30 Ek/LIC	solubly expressed
hsAKAP18γ-full length	pCMV6-XL5	ordered from Origene (NM_016377)
hsAKAP18γ(49-265)	pSKB2LNB	expressed protein insoluble
hsAKAP18γ(49-299)	pSKB2LNB	co-expression with PKA RIIα and RIIα-D/D, weak expression, degradation during purification
rnAKAP18δ-full length	pET28a	weak expression, mostly insoluble, prone to aggregation
rnAKAP18δ-full length	pGEX4T3	weak expression, mostly insoluble, prone to aggregation especially when GST is cleaved off
rnAKAP18δ(1-292)	pET30 Ek/LIC	solubly expressed, purification and cleavage possible in small amounts

rnAKAP18δ(87-292)	pET30 Ek/LIC	solubly expressed
rnAKAP18δ(91-292)	pET30 Ek/LIC	no expression
rnAKAP18δ(76-292)	pET30 Ek/LIC	solubly expressed, purification and cleavage possible in large amounts
rnAKAP18δ(1-326)	pET30 Ek/LIC	expressed protein insoluble
rnAKAP18δ(87-326)	pET30 Ek/LIC	small amounts solubly expressed
rnAKAP18δ(87-326)	pSKB2LNB	co-expression with RIIα-D/D and co-purification yields sufficient amounts for crystallization trials
rnAKAP18δ(91-326)	pET30 Ek/LIC	insoluble expressed
rnAKAP18δ(76-326)	pET30 Ek/LIC	expressed protein insoluble
rnAKAP18δ(76-326)	pSKB2LNB	co-expression with RIIα-D/D and co-purification yields sufficient amounts for crystallization trials
rnAKAP18δ(87-353)	pET30 Ek/LIC	expressed protein insoluble
rnAKAP18δ(91-353)	pET30 Ek/LIC	test purification not successful
rnAKAP18δ(76-353)	pET30 Ek/LIC	expressed protein insoluble
rnAKAP18δ(76-317)	pSKB2LNB	co-expression with RIIα-D/D and co-purification yields sufficient amounts for crystallization trials
rnAKAP18δ(87-317)	pSKB2LNB	co-expression with RIIα-D/D and co-purification yields sufficient amounts for crystallization trials
rnAKAP18δ-full length	mCherry in pEGFP-N3	expressed in eukaryotic cell lines for confocal microscopy
rnAKAP18δ-full length	mCherry in pEGFP-C1	expressed in eukaryotic cell lines for confocal microscopy
mmAKAP18γ(37-253)	pSKB2LNB	solubly expressed, purified in large amounts
mmAKAP18γ(37-287)	pSKB2LNB	cloned from mouse brain total RNA kindly provided by A. Kozlenkov, co-expression with RIIα-D/D and co-purification yields sufficient amounts for crystallization trials

mmAKAP18γ(37-287)	mCherry in pEGFP-C1	expressed in eukaryotic cell lines for confocal microscopy
mmAKAP18γ(37-287)	mCherry in pEGFP-N3	expressed in eukaryotic cell lines for confocal microscopy
mmAKAP18γ(37-287) F140A	mCherry in pEGFP-N3	point mutant (nucleotide binding should be impaired)
mmAKAP18γ(37-287) H93A, T95A	mCherry in pEGFP-N3	point mutant (nucleotide binding should be impaired)
mmAKAP18γ(37-287) H185A, T187A	mCherry in pEGFP-N3	point mutant (nucleotide binding should be impaired)
mmAKAP18γ(37-278)	pSKB2LNB	co-expression with RIIα-D/D and co-purification yields sufficient amounts for crystallization trials
mmAKAP18γ(48-278)	pSKB2LNB	co-expression with RIIα-D/D and co-purification yields sufficient amounts for crystallization trials
mmAKAP18γ(48-287)	pSKB2LNB	co-expression with RIIα-D/D and co-purification yields sufficient amounts for crystallization trials
hsPDE4D3-full length	pGEX4T3	kindly provided by J. Tröger
hsPDE4D3(245-579)	pET30 Ek/LIC	solubly expressed, purified in large amounts, catalytically active
hsPDE4D3(245-604)	pET30 Ek/LIC	solubly expressed
hsPDE4D3(245-610)	pET30 Ek/LIC	solubly expressed
hsPDE4D3(245-673)	pET30 Ek/LIC	solubly expressed in large amounts, cleavage with enterokinase not complete, degradation
hsPKA RIIα-full length	pET28a, pGEX4T3	solubly expressed and purified in large amounts, degradation to some extend, kindly purified by F.Götz
hsPKA RIIα-full length	pET46 Ek/LIC modified	solubly expressed, degradation to some extend, tag-free construct for co-expression with AKAPs; plasmid kindly provided by F.Götz

hsPKA RIIα-full length	pEGFP-N1	kindly provided by P.Skroblin
hsPKA RIIα-full length	pEYFP-N1	kindly provided by J.Tröger
hsPKA RIIα D/D (1-44)	pET46 Ek/LIC	solubly expressed and purified in large amounts, kindly provided by K.Fälber and purified by F.Götz
hsPKA RIIα D/D (1-44)	pET46 Ek/LIC modified	solubly expressed, tag-free construct for co-expression with AKAPs; plasmid kindly provided by F.Götz

2.1.10 Synthetic peptides

Peptides were synthesized by Dagmar Krause or Angelika Ehrlich from the group of Michael Beyermann at the FMP.

Peptide name	**Sequence**	**Molecular Weight**
hsPDE4D3(341-365)	LLSTP ALEAV FTDLE ILAAI FASAI	2590 Da
hsPDE4D3(586-610)	DQEDG RQGQT EKFQF ELTLE EDGES	2916 Da
rnPLN(1-20)	MEKVQ YLTRS AIRRA STIEM	2384 Da
rnPLN(3-22)	KVQYLTRS AIRRASTIEM PQ	2349 Da
rnPLN(4-32)	VQYLT RSAIR RASTIEMPQQ ARQNL QNLF	3434 Da
hsAKAP18β(40-73)	GEKNG GEPDD AELVR LSKRL VENAV LKAVQ QYLE	3766 Da

2.2 Molecular biological and microbiological methods

2.2.1 Polymerase chain reaction (PCR)

Amplification of DNA fragments was carried out with KOD polymerase (Novagen) or *Pfu* polymerase (Stratagene) according to standard protocols (Sambrook et al., 1989) [143].

2.2.2 Restriction digest

Digest of amplified DNA fragments was performed with restriction enzymes from New England Biolabs according to manufacturer's protocol.

2.2.3 Agarose gel electrophoresis

Agarose gel electrophoresis using 1 % Agarose gels was performed according to standard procedures (Sambrook, 1989) [143]. DNA fragments or plasmids were visualized by UV light and DNA was extracted from the cut-out gel slices by using Ultrafree-DA Centrifugal Filter devices (Millipore) according to manufacturer's protocol.

2.2.4 Ligation

After gel extraction of digested DNA insert and vector DNA concentration was determined with a NanoDrop Spectrophotometer (Thermo Scientific) at a wavelength of 260 nm. 10 ng of vector was ligated with a three to six times molar excess of insert by applying T4 Ligase (New England Biolabs) at 4°C overnight.

2.2.5 Ligation independent cloning (LIC)

For ligation independent cloning (LIC) the pET30 Ek/LIC Vector Kit (Novagen) was used. After PCR and gel extraction of the DNA, 0.2 pmol of the insert were treated with the supplied T4 DNA polymerase. It creates 12- to 15-nucleotide single stranded overhangs at the insert through its 3´→5´exonuclease activity. These overhangs are annealed with the purchased Ek/LIC vector and directly transformed into *E. coli* without ligation.

2.2.6 Preparation of heat-competent E. coli *cells*

Heat-competent *E. coli* cells were prepared as described in Chung et al. (1989) [144].

2.2.7 Transformation

After ligation or T4 DNA polymerase treatment in ligation independent cloning with the LIC system, respectively, transformation of *E. coli* cells was carried out according to standard protocols [143]. For cloning and plasmid amplification *E. coli* strains NovaBlue GigaSingles®

Competent cells (Novagen) or TG1 cells (Promega) were used. For protein expression Rosetta 2 DE3 (Novagen) *E. coli* strain was used.

2.2.8 Plasmid purification

Plasmid purification from 5 ml of *E. coli* LB culture (mini-preparation) or 50 ml LB culture (midi-preparation) was performed with Qiagen Plasmid Purification Kit (Qiagen) according to the manual. Purified plasmids were sequence-verified by using the sequencing service at Eurofins MWG Operon (Ebersberg) or Invitek GmbH (Berlin).

2.2.9 Site-directed mutagenesis

Point mutants of mmAKAP18γ(37-287) were produced using the QuikChange®Site-Directed Mutagenesis Kit (Stratagene) according to the manual.

2.2.10 Preparation of cryo stocks

For long-term storage of transformed *E. coli* cells, cryo stocks were prepared. 300 µl of autoclaved 40 % glycerol in LB medium were added to 300 µl of *E. coli* LB culture in the logarithmic phase, mixed immediately, flash-frozen in liquid nitrogen and stored at -80 °C.

2.3 Protein chemical methods

2.3.1 Sodium dodecyl sulfate polyacrylamide gel electrophoresis (SDS-PAGE)

Separation of proteins according to their molecular weight by SDS polyacrylamide gel electrophoresis (SDS-PAGE) was performed as described by Laemmli et al. (1970) [145] using self-casted 10-15 % polyacrylamide gels. Additionally, NuPage®Novex®Bis-Tris (Invitrogen) gradient gels (4-12 %) were used according to the manual.

2.3.2 Coomassie-staining of protein gels

After SDS-PAGE proteins were prefixed in gel fixation solution (compare **2.1.8**) for 20 to 30 min. Afterwards, the gel was stained in Coomassie-G staining solution for 1h until the gel was uniformly blue colored. Destaining was accomplished by incubation of the gel in destaining solution or dH_20 until the background was clear. Alternatively, a faster cooking protocol was used. In this case, the gel was directly put into the staining solution for cooking protocol (containing Coomassie-R) and shortly heated up in a microwave. After 15 min of incubation on a shaker the gel was transferred to the destaining solution for cooking protocol and again heated up in a microwave. Again, the gel was left in the destainer until the background was clear.

2.3.3 Protein concentration determination

Protein concentration was determined using a NanoDrop® Spectrophotometer at a wavelength of 280 nm and the concentration was calculated with the help of the theoretical extinction coefficient [146]. Alternatively, the Bradford Protein Assay (Biorad) was used according to Bradford et al. (1976) [147].

2.3.4 Protein over-expression test and solubility test

Over-expression in small scale (test expression) was performed by transforming *E. coli* Rosetta 2 DE3 cells with the respective plasmid(s) and by growing at least four different clones in 1 ml Overnight Express™ Instant TB Medium (autoinduction medium, AIM, Novagen) in 24-well deep well plates. Cultures were grown at a temperature of 37 °C under constant shaking on a thermomixer (Eppendorf, Hamburg) at 900 rpm. After three hours 10 µl of the culture were used to inoculate small agarose plates in 24-well format which were transferred to 37 °C to make the respective clone grow overnight. After another three hours temperature was shifted to 18 °C and cells were grown to high density overnight while continuing shaking at 900 rpm. *E. coli* cell culture was transferred to 1.5 ml Eppendorf caps and centrifuged at 5000 rpm and 4 °C for 5 min in a table top centrifuge. The supernatant was removed and the pellets were frozen for at least 30 min at -80 °C. After thawing at room temperature the pellets were resuspended in 200 to 400 µl of lysis buffer for test expression (see **2.1.8**). The resuspended cells were lysed at 4 °C for at least 1 h while intermittently vortexing them. Next an aliquot was taken from each lysate and the lysates were centrifuged at 13.200 rpm and 4 °C for 15 min in a table top centrifuge. Aliquots of the supernatant were taken and these as well as the aliquots of the whole cell lysates were mixed with 2x SDS sample loading buffer (see **2.1.8**) and cooked at 95 °C for 3 min. Samples were analyzed by SDS-PAGE and subsequent coomassie-staining (see **2.3.2**).

The best clones with the highest over-expression of soluble protein were chosen for preparing cryo stocks and were used for large-scale expression.

2.3.5 Large-scale over-expression in **E. coli**

For large-scale expression the cryo stocks of the best clones from test expression were used to inoculate 50 ml LB pre-cultures containing the respective antibiotics. Pre-cultures were grown overnight at 25 or 37 °C (depending on at what time they were inoculated) at 190 rpm. The next day large cultures were inoculated using 5 ml of the pre-culture for 1 l of TB medium plus antibiotics. Cells were grown at 37 °C and 90 to 120 rpm until reaching an OD_{600} of ~0.6. Cultures were cooled down to 18 °C. Induction of protein expression was achieved by adding 40, 100 or 1000 µM isopropyl β-D-1-thiogalactopyranoside (IPTG) and cells were grown another 20 h

under constant shaking. Cells were harvested by centrifugation at 6000 rpm and 4 °C for 15 min and resuspended in ice-cold lysis buffer (see **2.1.8**). The resuspended cells were stored at -30 °C.

For nuclear magnetic resonance (NMR) studies cells were grown in M9 minimal medium containing $^{15}NH_4Cl$ for uniformly labeling the recombinant protein (see **2.1.8**). In general, the over-expression procedure was the same.

2.3.6 E. coli *cell lysis and preparation of soluble fraction*

Harvested *E. coli* cells with over-expressed proteins of interest were thawed at room temperature for 1 h and vigorously vortexed. Fresh DNase I was added before disrupting the cells by passing them through a fluidizer (Microfluidics, Newton, USA) at least two times to remove cell debris. An aliquot of the lysate was taken before spinning the lysate at 35.000 rpm and 4 °C for 45 min. The supernatant was transferred to another vessel and filtrated through a 0.45 µm filter. For analysis, another aliquot was taken from the supernatant and the pellet.

2.3.7 Affinity chromatography and cleavage

All steps of protein purification were performed at 4 °C. Cleared supernatant containing recombinant His_6-tagged proteins was applied on a Talon® Cobalt affinity column (Clontech, Saint-Germain-en-Laye, France) pre-equilibrated with equilibration buffer (see **2.1.8**). The column was then intensely washed with equilibration buffer (about 20 column volumes). Flow through and wash fractions were collected separately. Protein was eluted with elution buffer either by gradually or step-wise increasing imidazole concentration. The eluate was collected in several fractions. From each step of purification small aliquots were taken, mixed with 2x SDS sample loading buffer, and heated up to 95 °C for 3 min for subsequent analysis by SDS-PAGE and coomassie-staining.

The eluate fractions of the highest purity were pooled and an aliquot of the pool was taken. The specific protease was added (thrombin, enterokinase, or PreScission-GST according to manufacturer's protocol). As the PreScission protease requires reducing conditions for full activity, β-mercaptoethanol was added to the eluate pool. In general, cleavage was performed at 4 °C overnight. In the case of the rnAKAP18δ constructs in the pET30 Ek/LIC vector, cleavage required incubation with both thrombin and enterokinase for 3 h or overnight at room temperature.

In parallel, the eluate was dialyzed against equilibration buffer overnight. To remove unspecifically bound proteins and the cleaved tag a second Talon® affinity column was run. This time, the flow through was collected in several fractions because it contains the protein of interest. Again, aliquots of each step were taken and analyzed by SDS-PAGE followed by Coomassie-staining. The cleanest flow through fractions were pooled and concentrated to 2 or

5 ml with an Amicon Ultra Centrifugal Filter Unit (Millipore Corp.) according to the manual and using an appropriate molecular weight cut off.

If it was not possible to cleave the tag because of degradation problems, instability of the protein without tag, or generally insufficient cleavage, the protein was directly concentrated after the first Talon® column and transferred to the size exclusion column.

2.3.8 Size exclusion chromatography (gel filtration)

The pooled and concentrated fractions from the second affinity column were centrifuged at 4 °C and 13.200 rpm for 15 min to remove precipitated protein. The supernatant was applied on a pre-equilibrated size exclusion chromatography (SEC) column, either a Superdex75 or a Superdex200 (GE Healthcare, Piscataway, USA), 16/60 or 26/60 depending on the molecular weight of the protein or the complex and on the amount of protein. The buffer used for equilibration and elution is listed under **2.1.8**. The eluate was analyzed by UV absorption at 280 nm and subsequent SDS-PAGE of peak fractions. The cleanest fractions were pooled and concentrated in an Amicon filter device as described in **2.3.8**.

If it was not possible to remove the protease by SEC alone an additional 1 ml glutathione affinity column, GSTrap™ HP (GE Healthcare, Piscataway, USA), was connected in series behind the gel filtration column. In this way the GST-tagged PreScission protease could be removed.

Analytical size exclusion chromatography using a Superdex75 or Superdex200 10/300 column (as well from GE Healthcare) was used for roughly molecular weight and oligomerization state of purified proteins and complexes. The columns were calibrated using a molecular weight standard kit (Gel Filtration Calibration Kit LMW, GE). In general 200 to 400 µg of protein solution was applied on the column in a volume of 50 to 100 µl.

2.3.9 Protein storage

Purified and concentrated protein was split into several small aliquots, shock frozen in liquid nitrogen, and stored at -80 °C.

2.3.10 Detection of nucleotides by high pressure liquid chromatography (HPLC)

Protein-bound nucleotides can be detected by reversed-phase high pressure liquid chromatography (HPLC) [148]. Protein was diluted in ITC buffer (**2.1.8**) to a final concentration of 5 µM in a volume of 20 µl and applied on a Hypersil ODS-2 column (Thermo Scientific) pre-equilibrated with HPLC running buffer (**2.1.8**). To absorb denatured protein a pre-filter, Nucleosil 100 C18 pre-column, was used. The HPLC run was performed at room temperature and at a flow rate of 1.5 ml/min. Different nucleotide standards at a concentration of 30 µM in

ITC buffer were used to calibrate the column. The absorption at 254 nm was measured and bound nucleotides were analyzed by the different retention times.

2.3.11 Cyclic nucleotide hydrolysis assay

In a cyclic nucleotide hydrolysis assay based on the nucleotide detection by HPLC (see **2.3.10**) the activity of purified cyclic nucleotide phosphodiesterase PDE4D3 was tested. Purified PDE4D3 was diluted in ITC buffer to a concentration of 50 µM. cAMP stock solution contained 10 mM cAMP in ITC buffer. PDE4D3 as well as cAMP were diluted 1:10 in ITC buffer (reaction volume of 20 µl) and shortly mixed by pipetting up and down. After 30, 60, 120 and 300 s each 2 µl of the reaction volume were taken out, diluted in ITC buffer (1:20) and immediately shock frozen in liquid nitrogen to stop the conversion of cAMP to 5´AMP. One sample after the other was then thawed and 20 µl were directly analyzed by HPLC as described before.

As standards, cAMP, 5´AMP, adenosine diphosphate (ADP), and ATP were separated on the Hypersil column and retention times recorded.

2.4 Biophysical methods

2.4.1 Circular dichroism (CD) spectroscopy

To analyze if peptides are folded circular dichroism (CD) spectra were recorded on a Jasco J-720 spectropolarimeter (Jasco Corp., Hachioji, Japan) supplied with a 450 W lamp. Spectra were recorded from 260 to 190 nm with a resolution of 1 nm at room temperature using a 1 mm quartz cuvette. NaCl in the standard buffer was replaced by same amounts of NaF for CD spectrometry. CD signals were converted to mean molar ellipticity per residue using the Jasco software.

One characteristic of plane-polarized light is that it can be viewed as being made up of two circular components, named left-handed and right-handed polarized light. Circular dichroism can be defined as the unequal absorption of these two components [149]. A CD spectrometer measures this difference and reports it in terms of ellipticity (θ) in degrees. The CD spectrum shows the ellipticity as a function of wavelength. Folded proteins often have highly asymmetric secondary structural elements, α-helices and β-sheets, which have characteristic CD spectra. For example, α-helical proteins have negative bands at 222 nm and 208 nm wavelength and a positive band at 193 nm wavelength. In contrast, β-sheets have a negative band at 218 nm and a positive band at 195 nm. If a protein is unstructured it has very low ellipticity above 210 nm and negative bands near 195 nm [150].

2.4.2 Thermal shift assay (TSA)

In order to identify optimal buffer conditions for proteins prone to aggregation thermal shift assays (TSA), also called differential fluorescence scanning (DFC) assays, were conducted. The thermal stability of a protein was determined by slowly heating it up from 20 to 100°C in a real-time PCR cycler (MyiQ2 Two-color real-time PCR Detection System, Biorad) while detecting the increase of the fluorescence dye Sypro®Orange (Invitrogen) when binding to hydrophobic patches being exposed when the protein unfolds.

Different buffers and pH values were used containing 300 mM NaCl each in addition to the respective additive. 30 µg of protein was added in a volume of 1.5 µl giving a sample volume of 40 µl. Finally, 10 µl of a 5x stock solution of Sypro®Orange was added. Each condition was tested in duplicate. Temperature was raised in 0.5°C steps per minute, and fluorescence was measured at each interval. Fluorescence intensity in relative fluorescence units (RFUs) can be plotted as a function of temperature. This creates a sigmoidal curve, which reflects the transition between two states: folded and unfolded protein. At the inflection point of the transition curve lies the melting temperature T_m [151]. This can also be shown by plotting the first derivation of RFU of time -d(RFU)/dT against the temperature. For plotting the graphs Microsoft Office Excel program was used.

2.4.3 Isothermal titration calorimetry (ITC)

Isothermal titration calorimetry (ITC) experiments can be used to determine the complete binding thermodynamics of a ligand binding to a protein [152]. The heat evolved by binding of the ligand can be directly measured and the binding constant (K_a), the stoichiometry (n), and the enthalpy of binding (ΔH_b) are determined. In this work, ITC experiments were performed at 8 °C using a VP-ITC isothermal titration calorimeter (MicroCal, GE Healthcare). Protein concentration in the measuring cell varied between 20 and 70 µM, ligand concentration usually was 10 times higher. Standard ITC buffer (listed under **2.1.8**) as well as the samples were vacuum degassed. In general, the samples were dialyzed in the same buffer overnight before the experiment and centrifuged at 13.200 rpm and 4 °C for 10 min to remove aggregated protein. Afterwards, protein concentration was determined again (see **2.3.3**). For most experiments 8 µl injections and a waiting time between injections of 240 s were used. Binding isotherms were fitted and equilibrium dissociation constants, K_D, were calculated using the MicroCal ORIGIN software.

2.4.4 Right angle light scattering (RALS)

By static light scattering it is possible to determine the molecular weight of a protein or protein complex and its oligomerization status [153]. A light scattering detector, Viskotek 270 Dual Detector, and a refractive index (RI) detector, VE3580 RI Detector (both Malvern Instruments

Ltd., Worcestershire, UK), were connected in-line with an analytical size exclusion chromatography column described in **2.3.8**. The whole system was permanently located at 4 °C. Before the run, it was equilibrated for at least 3 h at a flow rate of 0.5 ml/min in gel filtration buffer (see **2.1.8**). Afterwards, the protein was injected without changing the flow rate and the detected RI, UV (280 nm), as well as RALS signal was visualized by using OmniSEC software. The same software was also used for analysis of the results.

2.4.5 Nuclear magnetic resonance (NMR) spectroscopy

Solution-state nuclear magnetic resonance (NMR) spectroscopy is a very diverse method to gain structural and functional information on molecules ranging from small chemical compounds to proteins of a molecular weight of about 35 kDa. In order to investigate the dynamics and structure of proteins, they have to be labeled with atoms having an unequal number of neutrons and protons in their nucleus, like ^{15}N or ^{13}C, to be visible in the NMR spectrum. In a ^{1}H-^{15}N heteronuclear single quantum coherence (HSQC) spectrum, resonances for ^{1}H and ^{15}N frequencies are correlated which leads to one signal in the NMR spectrum per N-H atom pair. For every amino acid in a protein, at least one signal should be detected originating from its backbone amide group, with proline as an exception. The side chains of amino acid residues containing amine groups (Asn, Gln, His, and Trp) give rise to additional signals.

One widely used application of NMR spectroscopy is the detection of binding of a ligand to a protein of interest. The signals observed in a ^{1}H-^{15}N HSQC spectrum shift in the case of an interaction due to a variation in the electron distribution of the affected atoms. This indicates structural rearrangements in the protein upon binding of the ligand. Additionally, it can give information at atomic resolution, i.e. which amino acid residues of the protein are involved in the interaction.

Uniformly ^{15}N-labeled proteins at a concentration of 75 to 100 µM in NMR buffer (see **2.1.8**) were transferred into NMR tubes (sample volume 500 µl). The protein solution was diluted with D_2O (lock signal). One-dimensional ^{1}H and two-dimensional HSQC spectra were recorded using either a DRX-600 or an AV900 spectrometer both equipped with cryo probe heads (Bruker, Karlsruhe). The temperature for each experiment was 300 K (~27 °C). For interaction studies with synthetic peptides (see **2.1.10**), peptides were dissolved in NMR buffer and added in 1.25, 2.5, 5, and 10 times molar excess over protein concentration. Recorded spectra were processed using the program TopSpin (Bruker) and analyzed with the program Sparky [154].

2.5 Crystallographic methods

A short summary of the theoretical background of macromolecular crystallography is found in the appendix (see **5.1**). In the following, the practical aspects are discussed.

2.5.1 Crystallization

For crystallization trials different protein concentrations were used depending on the precipitation behavior of each construct. As most of the AKAP constructs are prone to aggregation and precipitation, most of the crystallization trials were performed at 4°C and at relatively low concentrations below 15 mg/ml. In all cases, initial crystallization screening was performed using commercially available screens from Hampton Research, Qiagen, or later on from Jena Bioscience by sitting-drop vapor-diffusion method. For the high-throughput approach, a Hydra Plus One crystallization robot (Thermo Scientific) was used to set up crystal plates in 96well format (Crystal Quick™ 96well plates, Greiner BioOne). In general, 300 nl of protein solution and 300 nl of crystallization solution were used. The reservoir contained 75 µl of the crystallization buffer.

For crystallization trials with rnAKAP18δ(76-292) and PDE peptides a protein concentration of 1.6 mg/ml was sufficient to yield crystals from initial screening, but crystals grew as well from higher concentrations up to 10 mg/ml. All crystals were rod-shaped and of different size (from 10 µm x 10 µm x 80 µm to 10 µm x 10 µm x 500 µm) and grew both at 4 and 20 °C. Crystals were tested at BESSY, BL 14.1 and 14.2, equipped with a Rayonics MX 225 CCD detector, or a MAR165 CCD detector, respectively. Best diffracting crystals grew in 100 mM Hepes/NaOH pH 7.0, 30 % (v/v) Jeffamine ED-2001 (JCSG screen, well G1), and in 100 mM Tris/HCl pH 8.5, 20 % (w/v) PEG 2000 MME, 200 mM TMAO (Classic II screen, well F2). In general, protein crystals must be protected from radiation damage by shock-freezing them in liquid nitrogen after transferring them into cryo-protectant [155]. The rnAKAP18δ(76-292) crystal grown in the first condition was directly frozen in crystallization buffer. In the case of the second condition 30 % PEG 2000 MME (w/v) were used to reach a condition suitable for cryo-cooling.

For hsAKAP18ß(43-83) peptide co-expressed with the D/D domain much higher concentrations were used for initial crystallization screens (40 mg/ml). Crystals grew under the following conditions: 100 mM Hepes/NaOH pH 7.5, 25 % (v/v) isopropanol, 100 mM $MgCl_2$ (ComPas screen, well E12) and 100 mM sodium-acetate pH 4.6, 30 % (v/v) MPD, 20 mM $CaCl_2$ (JCSG screen, well A4). The first condition gave very fine needles, in the second condition single crystals of different shape and size grew which were mostly hexagonal and relatively large (up to 500 µm x 300 µm x 300 µm). The best cryo-condition contained 20 mM Hepes/NaOH pH 7.5, 75 mM NaCl, 50 mM $MgCl_2$, 20 % (v/v) isopropanol, 50 mM sodium-acetate pH 4.0, and 20 % (v/v) ethylene glycol. To improve diffraction quality, various fine screens were performed

varying isopropanol and MPD concentration between 10 and 30 % (v/v), $MgCl_2$ and $CaCl_2$ concentration between 0 and 120 mM. pH-value was varied between 3.5 and 5.0 for sodium-acetate and between 7.2 and 7.8 for Hepes/NaOH, and between 8.0 and 8.5 for Tris/HCl. 48 different salts were tested as additives at a concentration of 100 mM. Protein concentration was varied as well. In an attempt to slow down needle growth and to obtain fewer but larger needles, different glycerol concentrations from 1 to 5, and 8 % (v/v) were tested. Crystal growth could be reproduced and crystals were tested at the in-house generator (SuperNova single wavelength diffractometer, Agilent Technologies) or at BESSY. Similar crystallization trials were also performed using a synthetic hsAKAP18β(40-73) peptide.

In order to crystallize the co-expressed and co-purified mmAKAP18γ and rnAKAP18δ constructs in complex with the PKA RIIα D/D domain, commercially available initial screens describe above were performed but did not yield any protein crystals. Therefore, screening was performed with in-house screens in 24well format (SuperClear Pregreased 24 Well Plates, Crystalgen) and by sitting-drop vapor-diffusion. 1 µl of protein solution was mixed with 1 µl of reservoir solution with a total reservoir volume of 500 µl. First, a precipitation test was performed using standard precipitants: PEG3350 (5-20 % (v/v)), PEG10.000 (4-20% (v/v)), isopropanol (5-30 % (v/v)), MPD (5-25 % (v/v)), NaCl (500-3000 mM), and $(NH_4)SO_4$ (100-2000 mM). The mmAKAP18γ and rnAKAP18δ complexes with D/D precipitated very easily therefore low amounts of precipitating agent were required, e.g. 2-6 % (v/v) for PEGs. PEG6000 was tested at a concentration of 5 to 10 % (v/v). Different buffers and pH values were screened, using sodium acetate pH 4.0, citric acid pH 5.0, MES pH 6.0, Hepes/NaOH pH 7.0 and 7.5, and Tris/HCl pH 8.0. 48 different ions were tested at a concentration of 100 mM using 5 % (v/v) PEG3350 as precipitant, and 100 mM sodium-acetate pH 4.0, or Tris/HCl pH 8.5, with or without 5mM DTT. The 48 ions were also tested in a buffer containing 8 % (v/v) PEG8000, and 100 mM sodium-citrate pH 6.0. Published crystallization conditions of rnAKAP18δ(76-292) [135] (100 mM Tris/HCl pH 8.0, 10 % (v/v) PEG8000, 7 mM DTT) were tested for AKAP18γ or δ complexes with D/D as well. 5´AMP (Biolog, Bremen) was added to the trials at a concentration of 3 or 5 mM.

In an attempt to reconstitute the complex of rnAKAP18δ(76-326) with the D/D domain, co-purified proteins were separated by 1 M NaCl and separately purified D/D was added in a 1:2 molar ratio (personal communication). Crystals of the D/D domain grew in 100 mM Bicine pH 9.0, 2.4 M $(NH_4)_2SO_4$ (pHClear screen, well F6), in 100 mM tri-sodium citrate pH 5.6, 2.0 M $(NH_4)_2SO_4$, 200 mM K/Na tartrate (Classic screen, well C10), and in 100 mM MES pH 6.0, 2.4 M $(NH_4)_2SO_4$ (pHClear screen, well F3). The crystals had a size of 10 µm x 10 µm x 100 µm. As cryo-protectant, 20 % (v/v) glycerol was added to the crystallization buffer. Collection of X-ray data was carried out at BESSY BL14.1.

2.5.2 Data collection and processing

Cryo-cooled protein crystals were tested at 100 K at the in-house generator Xcalibur™Nova O diffractometer (Agilent Technologies; Copper single wavelength sealed tube source λ=1.5418 Å, 50 kV, 1 mA; ONYX™ detector) or at the Berliner Elektronenspeicherring-Gesellschaft für Synchrotronstrahlung, BESSY, beamline BL 14.1 equipped with a Rayonics MX 225 CCD detector using a micro-focus set up, or at BL14.2 equipped with a MAR165 CCD detector. The oscillation range was 1°. Initial indexing and determination of an optimal data collection strategy was done using the program Mosflm [156]. The data was processed using XDS [157].

Two datasets were collected at the BESSY for rnAKAP18δ(76-292) with PDE4D3(341-365) peptide. Another dataset was collected from a crystal grown from trials with rnAKAP18δ(76-326) with D/D domain added afterwards. Detector distance was 290.13 mm and 100 images were taken. Data was processed with HKL-2000 [158] and XDS. Molecular replacement was performed using the programs Amore [159] and Phaser [160] and the structure of AKAP18δ(76-292) (pdb file 2vfy) [135] was used as search model. Initial refinement was performed with the program Refmac [161] included in the CCP4 suite [162] but not pursued any further when no electron density for PDE4D3 peptide appeared.

Crystals of the D/D domain were tested at BESSY BL14.1 and three datasets were recorded. Data integration and scaling as well as molecular replacement was performed as described for rnAKAP18δ(76-292). For molecular replacement, the structure of the D/D domain (pdb file 2izx) was used as search model.

Many hsAKAP18β(43-83) crystals were tested until the final cryo-condition was found (see **2.5.1**). Several data sets were recorded but often indexing was impossible even by manually picking the reflections. One dataset from a crystal grown in 100 mM sodium-acetate pH 4.6, 30 % (v/v) isopropanol, 100 mM $CaCl_2$ was recorded at BESSY BL14.1. 110 images were taken and processed with XDS. Solving the structure by molecular replacement using the programs Molrep [163] and Phaser was not successful.

2.6 Cell biological methods

Cell culture and cellular biological experiments were in part performed at the FMP (Leibniz-Institut für Molekulare Pharmakologie) in co-operation with Antje Schmidt from the group of Ralph Schülein and with Vedrana Tabor and Elvira Rhode from the group of Enno Klussmann.

2.6.1 Cell culture

HeLa and CHO cells were cultivated in MEM containing 10 % fetal calf serum, 2 mM L-glutamine, 100 U/ml penicillin, and 100 U/ml streptomycin (Roth). Cells were incubated at 37 °C and 5 % CO_2. Ongoing adherent cell culture was done by detaching cells with 2x trypsin (Gibco) for 2-5 min at 37 °C; the enzymatic activity was stopped by the addition of FBS-containing medium. Generally, cells were passaged every 2-4 days and splitted 1:5- 1:10.

MCD4 cells stably expressing AQP2 were grown in Dulbecco´s Modified Eagle Medium (DMEM) Nutrient Mixure F-12 (Invitrogen) containing 5 % fetal calf serum, 100 U/ml penicillin, 100 U/ml streptomycin, and 5 µM dexamethasone. Cells were incubated at 37°C and 5 % CO_2.

2.6.2 Transfection

Cells were seeded into 6well plates equipped with circular cover slips at a cell density of about 2 x 10^5 for Hela, HEK293 and CHO cells, or 2 x 10^6 MCD4 cells per well, respectively, and grown overnight under cultivating conditions. For live cell imaging cover slips were coated with poly-L-lysine. For stable over-expression of rnAKAP18δ-fl-mCherry, mmAKAP18γ-mCherry and RIIα-GFP constructs cells were transfected using either Roti®-Fect (Roth) or Lipofectamine™ 2000 (Invitrogen) according to manufacturer's instructions. 1 to 2 µg of plasmid were used per well. For MCD4 cells chloroquine was added 20 min before transfection at an end concentration of 20 µM. MCD4 cells were either left untreated or were treated with forskolin (FSK) at a concentration of 30 µM for 30 min.

2.6.3 Confocal laser scanning microscopy (LSM)

In preparation for laser scanning microscopy (LSM) cells grown on a cover slip were either fixed or investigated by live cell imaging. For fixation cells were washed once with PBS (see **1.2.8**) and subsequently incubated with 4 % paraformaldehyde (PFA) for 5 min and washed again three times with PBS. Cells were embedded in ProLong®Gold Antifade Reagent (Invitrogen) or Mowiol®4-88 (Roth). Cells were analyzed using a Zeiss LSM 510 Meta microscope at the microscope core facility of the MDC managed by Anje Sporbert and Zoltan Cseresnyes. Objectives used were 40x water and 63x oil. Fixed specimen were stored in the dark at 4 °C.

For live cell imaging cells were directly mounted on a Zeiss LSM 510 microscope with the glass cover slip they had grown on and covered with PBS to prevent drying out. A 100x oil objective was used for magnification. To analyze data the program LSM image browser from Zeiss was used.

MCD4 cells were also washed in PBS (ice-cold, 2x) and fixed with 4 % PFA. Permeabilization of MCD4 cells was performed by applying 0.5 % Triton X-100 in PBS for 10 min. Afterwards, cells were blocked in PBS containing fish-skin-gelantine for 30 min at 37 °C. For

immunocytochemistry staining, first and second antibodies were diluted in the same blocking solution. Affinity purified rabbit anti-AQP2 antibody (H-27) [118] was used at a dilution of 1:300 for 1 h at 37 °C followed by washing with PBS (3 x 5 min). Cells were incubated with the secondary antibody, anti-rabbit and Cy2-labelled (1:1000), and DAPI nuclear staining for 1h and washed with PBS (3x 5 min). As a control, two out of four cover slips were not with the primary antibody. One of the cover slips was incubated only with secondary antibody. Cells were imaged using a Zeiss LSM 510 microscope.

3 Results

3.1 Purification of A-kinase anchoring protein 18 isoforms

3.1.1 Deletion constructs of rat AKAP18δ and test expression

The rat isoform of A-kinase anchoring protein 18, AKAP18δ, was found to interact with phosphodiesterase (PDE) 4D3 [122] and phospholamban (PLN) [124], which should be structurally and functionally characterized in this study. For structural studies, milligram amounts of protein are required. Expression and purification of full-length (fl) constructs of rat AKAP18δ fused to an N-terminal His_6 or glutathion-S-transferase (GST) tag was performed. However, these constructs were poorly expressed in *E. coli* Rosetta 2 DE3, degradation was observed during purification and yields were consequently low. It also proved impossible to separate AKAP18δ-fl from GST after cleavage, and the protein appeared to be misfolded, as native polyacrylamide gel electrophoresis (PAGE) of AKAP18δ-fl together with hsRIIα did not show complex formation (data not shown). For the His_6-tagged full-length AKAP18δ construct thrombin cleavage of the tag was never complete and this construct was even more prone to degradation than the GST-tagged variant. Thus, several truncated constructs of AKAP18δ were cloned for expression in *E. coli*.

On the basis of the existing AKAP18δ-core domain structure by Gold et al. [135] and the results of secondary structure and disorder prediction programs (jpred [164], and PONDR [165], respectively) truncated constructs of AKAP18δ were designed and afterwards cloned using the ligation-independent cloning (LIC) system (Novagen) described in **2.2.5**. Three different N-terminal truncations were chosen. The N-terminus of AKAP18δ is predicted to be completely disordered. Additionally, it contains many basic amino acids, rendering it highly charged and flexible (especially the putative nuclear localization signal comprising amino acids 79 through 83 with the sequence KKRKK). Certain amino acid residues with high intrinsic conformational entropy, e.g. lysine or glutamate, have been shown to reduce the likelihood of a protein to form crystals [166]. In addition, proline residues in the vicinity of the recognition site of the protease (like Pro^{90}) might interfere with the cleavage of a tag by reducing the accessibility of the cleavage site. The C-terminally located RIIα-binding site is expected to form an amphipathic helix as known from different structures of the D/D domain and the PKA binding site of other AKAPs (see chapter **1.1.4**). Two different C-terminal truncation constructs were therefore cloned, one containing the PKA-binding site and one without. Furthermore, constructs of AKAP18δ with the full N- or C-termini were created. **Fig. 8** depicts the truncated rat AKAP18δ constructs in the vector pET30 Ek/LIC. This vector contains a thrombin and an enterokinase

cleavage site. Cleavage with enterokinase does not result in additional amino acid residues remaining after cleavage of the tag. But as this protease is expensive, additional thrombin or tobacco etch virus (TEV) protease cleavage sites were introduced.

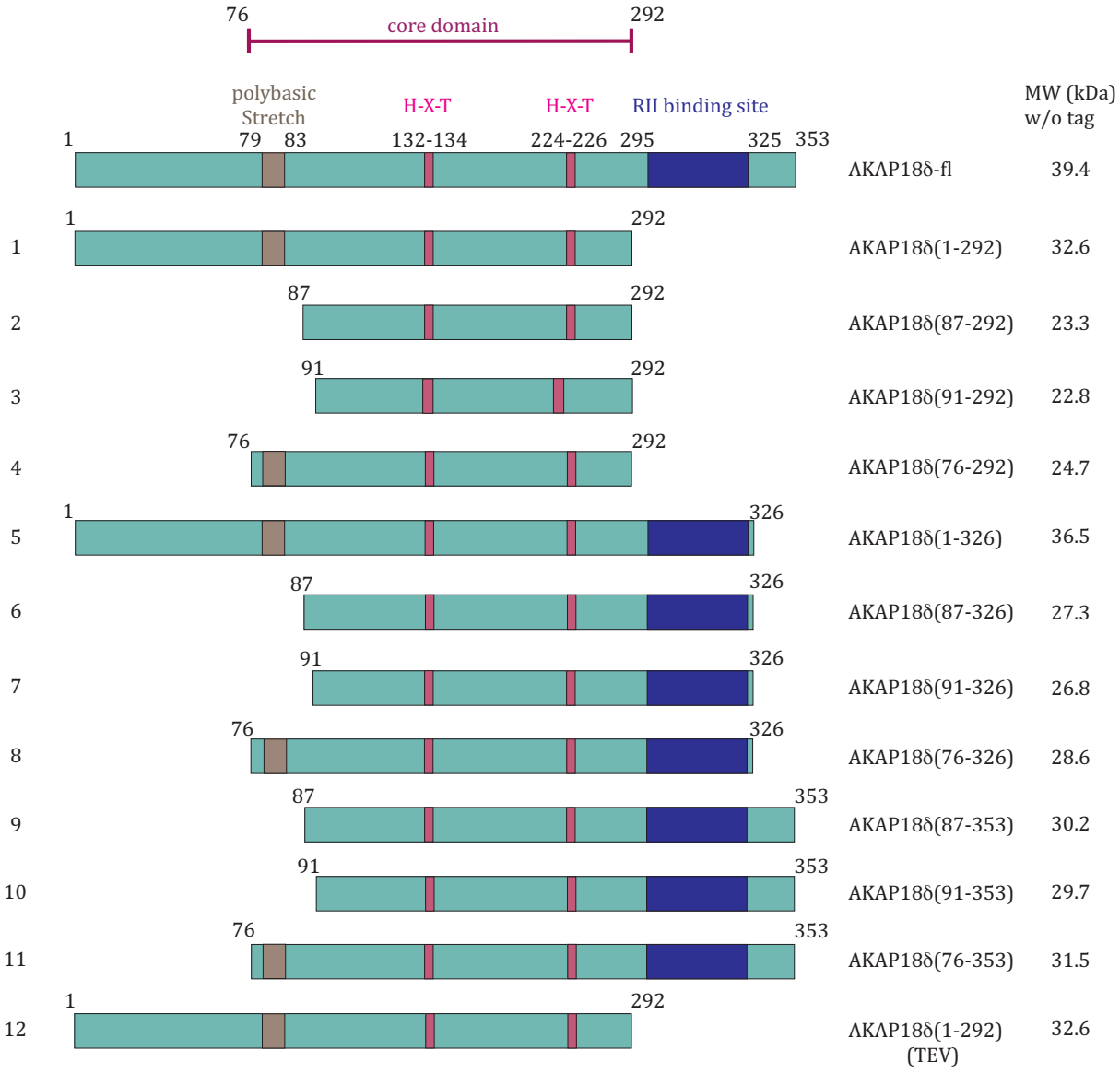

Fig. 8 Schematic representation of expression constructs of rat AKAP18δ. Eleven truncation constructs containing an N-terminal His_6-tag and a thrombin cleavage site in addition to the existing thrombin and enterokinase cleavage site were cloned into the vector pET30 Ek/LIC. Identical constructs were created with an additional tobacco etch virus (TEV) cleavage site. The conserved PKA RII-binding domain is shown in dark blue and the conserved residues of the His-X-Thr motifs are marked in red. On the right, the theoretical molecular weight (MW) of the tag-free constructs is indicated in kDa. The His_6-tag of the pET30 Ek/LIC vector has a MW of ~5 kDa.

In general, small-scale test expression of the AKAP18δ constructs shown in **Fig. 8** was carried out in 24-well format as described in chapter **2.3.4**. Four clones of each construct were tested. As an example, test expression of AKAP18δ constructs 1 through 6 is shown in **Fig. 9**.

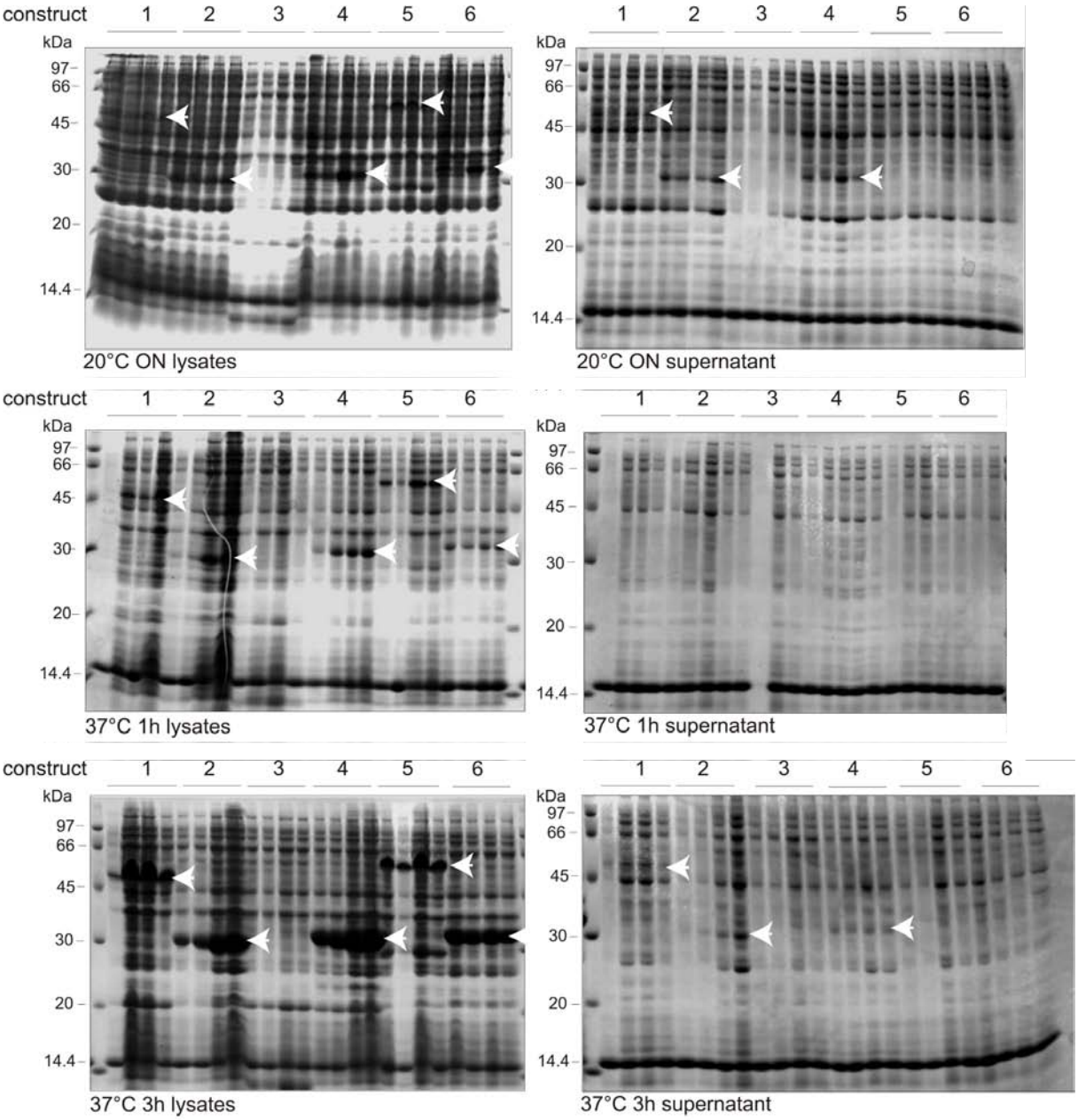

Fig. 9 Test expression of AKAP18d deletion constructs 1-6 (**Fig. 8**). *E. coli* Rosetta 2 DE3 were transformed with the respective construct and grown at 37 °C under constant shaking. After induction with 1 mM IPTG, cells were either grown at 20 °C overnight (upper row) or at 37 °C for 1 h (middle row) or 3 h (lower row). Cells were harvested, shock frozen at -80 °C, and lysed with lysis buffer containing 1 mg/ml lysozyme for 1 h at 4°C. Whole cell lysates (left) and supernatants (right) after centrifugation at 25000 x g at 4 °C were separated by SDS-PAGE. Proteins were Coomassie stained for visualization. Overexpressed as well as soluble proteins are indicated by arrows.

All of the twelve AKAP18δ constructs were expressed except for construct 3. Constructs 1, 2, 4, and 12 were soluble even when expressed at 37 °C for 3 h. Notably, constructs containing the full N-terminus run significantly higher than would be expected from their theoretical molecular weight (in this case constructs 1 and 5).

3.1.2 Expression and purification of rat AKAP18δ(76-292)

As it was known from the literature that AKAP18δ(76-292) (construct 4), also called the core-domain, can be purified in amounts and at a purity sufficient for crystallization [135], first purification attempts focused on this construct. The protein indeed proved to be soluble (**Fig. 9**), thus large-scale purification was performed. In order to yield protein for interaction studies with peptides derived from the putative interaction partners PDE4D3 and phospholamban, AKAP18δ(76-292) containing an N-terminal His_6-tag was expressed in *E. coli* Rosetta 2 DE3 (see chapter **2.3.5**) and purified using affinity chromatography and gel filtration (see chapter **2.3.7** and **2.3.8**). A typical purification of ^{15}N-labeled AKAP18δ(76-292) for NMR studies is depicted in **Fig. 10**. The protein is already ~80 % pure after the first purification step (**Fig. 10**a). Cleavage was performed with enterokinase and thrombin, as thrombin alone did not suffice to remove the tag (**Fig. 10**b). This could be explained by sterical hindrance if the full tag is present. It might shield the thrombin cleavage site, but if the tag is partly removed by enterokinase, thrombin can access its recognition site and cleave off the remaining amino acids. Afterwards, a gel filtration run was performed to remove the cleaved tag and other contaminating proteins to yield ~95 % pure protein (**Fig. 10**c). In **Fig. 10**d, the corresponding SDS-PAGE is shown.

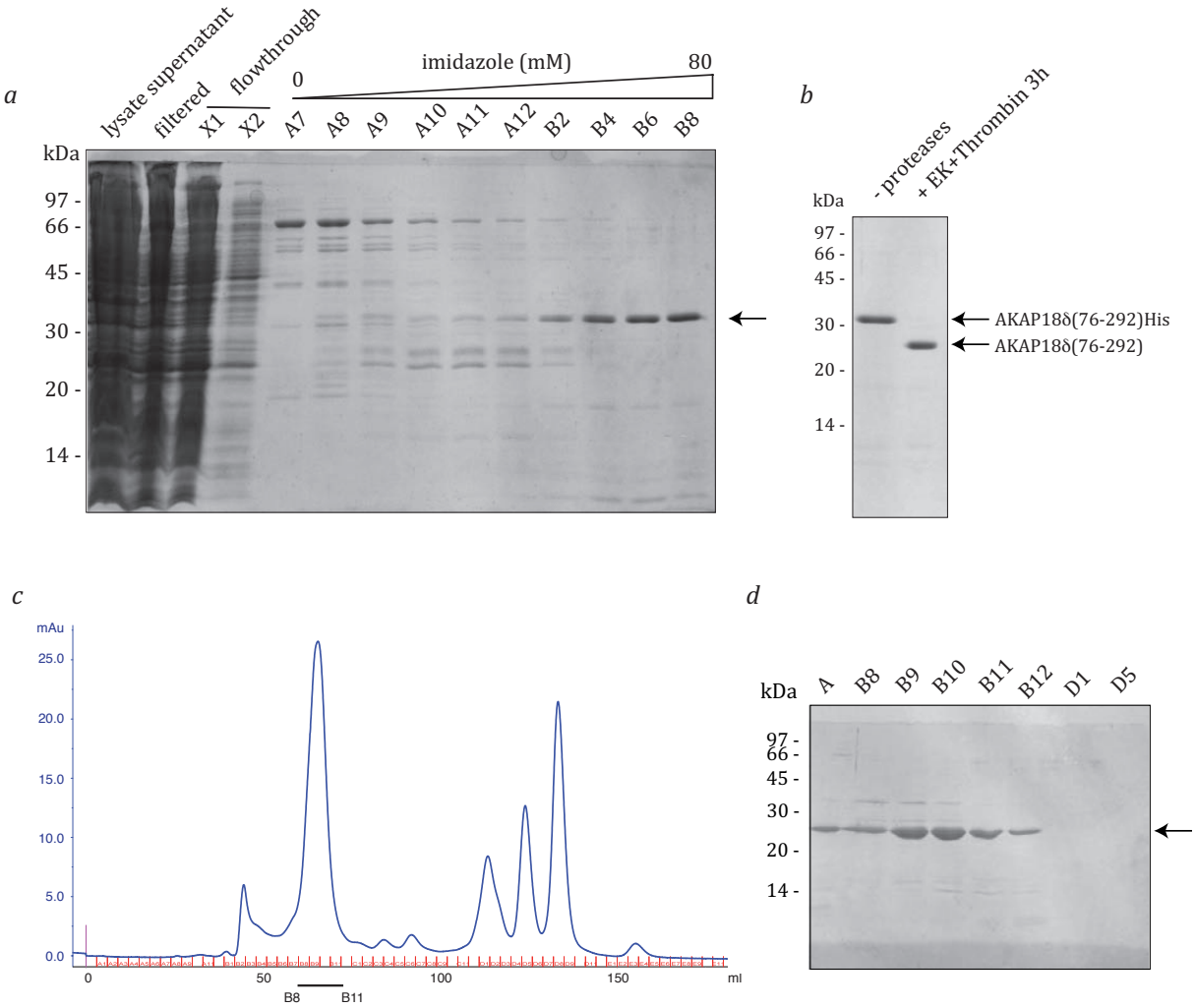

Fig. 10 Purification of rat AKAP18δ(76-292). ***a***, Affinity purification of AKAP18δ(76-292)-His. AKAP18δ(76-292)-His was purified via Co^{2+} affinity chromatography using Talon® material. The protein of interest elutes as a broad peak starting at an imidazole concentration of about 50 mM. Shown is the Coomassie-stained SDS-PAGE of different purification steps and affinity chromatography fractions. ***b***, Cleavage of AKAP18δ(76-292)-His. The Coomassie-stained SDS-PAGE shows protease cleavage with enterokinase and thrombin (each with 1U/100µg protein). ***c***, Chromatogram of gel filtration run (Unicorn software, GE) purifying AKAP18δ(76-292) using Superdex75 16/60 prep grade. The blue trace represents the UV absorption at 280 nm. The fractions pooled are indicated beneath the chromatogram. ***d***, Coomassie-stained SDS-PAGE of the fractions collected in the gel filtration run shown in *c*. The protein is > 90 % pure.

3.1.3 Co-expression and co-purification of AKAP18γ and δ with RIIα D/D

As AKAP18δ constructs containing the RII binding region turned out to be poorly soluble or even insoluble, co-expression of these constructs with the RIIα D/D domain was tested. By co-expressing the binding partner, it is expected that the hydrophobic site of the amphipathic helix, the RII binding region, is shielded by complex formation during expression.

In order to test this, different AKAP18δ constructs containing the RII binding site were co-transformed together with a plasmid containing a tag-free RIIα D/D domain into *E.coli* Rosetta 2

DE 3 cells as described before (see **2.3.4**). **Fig. 11** shows the test expression of AKAP18δ constructs 7, 8, and 9 (compare **Fig. 8**), each co-expressed with the D/D domain.

Co-expression with D/D (red box **Fig. 11**b) resulted in soluble rat AKAP18δ(76-326)-His (construct 8), though the bulk of the protein (about 80%) remained in the insoluble fraction.

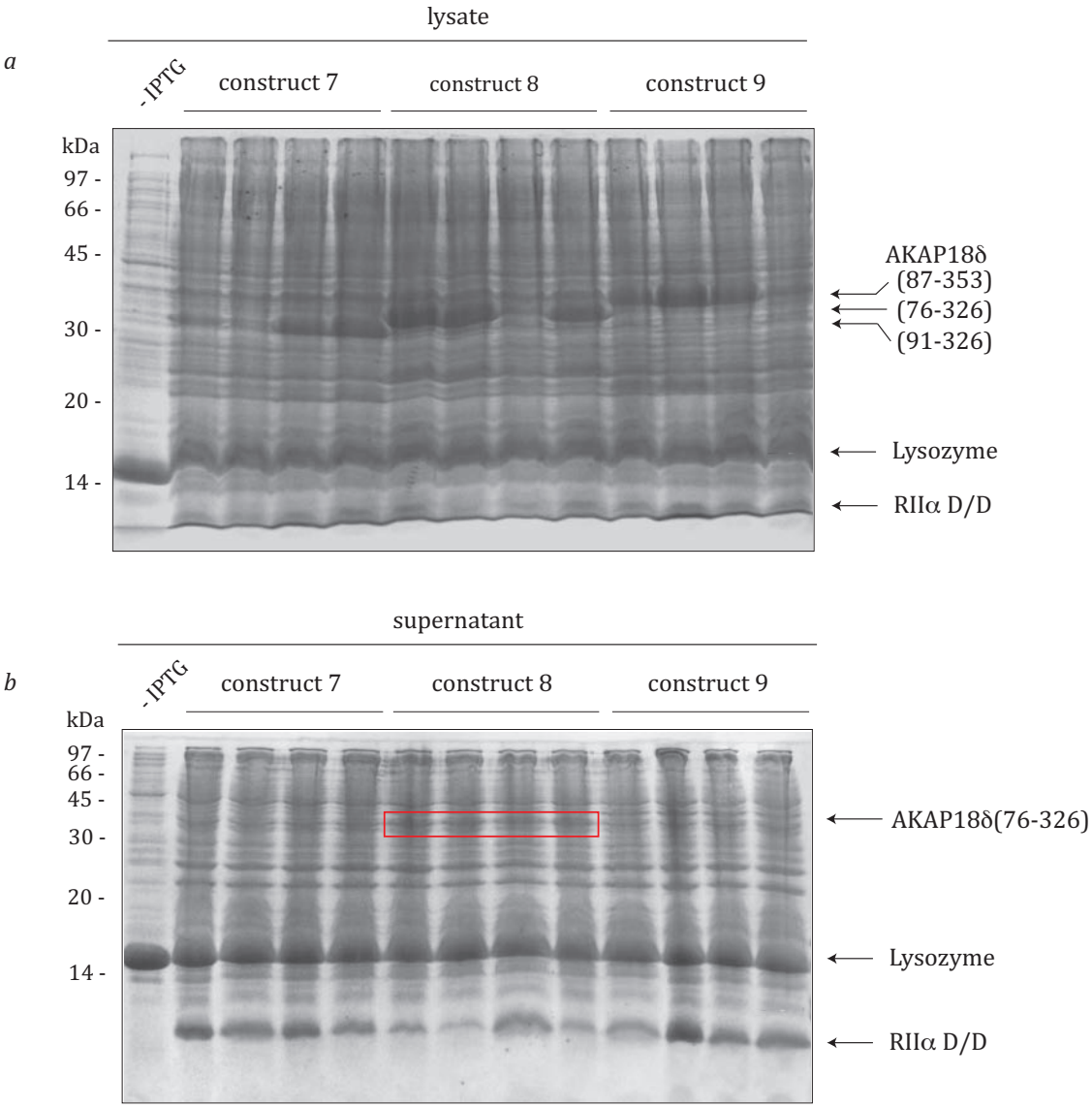

Fig. 11 Test expression of rat AKAP18δ constructs 7, 8, and 9 in *E. coli* Rosetta 2 DE3 cells co-expressing the RIIα D/D domain. ***a***, Coomassie-stained SDS-PAGE showing whole cell extract after cell lysis with lysozyme. Four clones were analyzed for each of the three AKAP18δ constructs co-transformed with RIIα D/D. The overexpressed constructs are indicated by arrows. Not all of the clones show the same expression level. For comparison, uninduced *E. coli* cultures (- IPTG) are shown in the first lane. ***b***, Supernatants corresponding to the samples shown in *a*. Solubly overexpressed AKAP18δ(76-326) is indicated by a red box.

Several problems were observed during large-scale purification of rat AKAP18δ(76-326)-His with D/D. First, cleavage of the tag had to be performed with two proteases as mentioned earlier. In addition, this needed to be performed at room temperature, because cleavage remained incomplete at 4 °C overnight. However, as AKAP18δ and its deletion constructs are prone to aggregation and degradation, longer incubations at room temperature were problematic. Further degradation was observed during the course of purification of rat AKAP18δ(76-326)-His with D/D. To optimize the purification, especially the cleavage procedure, rat AKAP18δ(76-326)-His was transferred from the pET30 Ek/LIC vector into the pSKB2LNB vector, which contains a shorter His_6-tag and a PreScission cleavage site instead of enterokinase and thrombin cleavage sites. To further optimize purification, and to obtain protein pure and homogenous enough for crystallization, several new mouse and human AKAP18γ as well as rat AKAP18δ constructs were cloned using standard cloning procedures described in **2.2** (see **Fig. 12**).

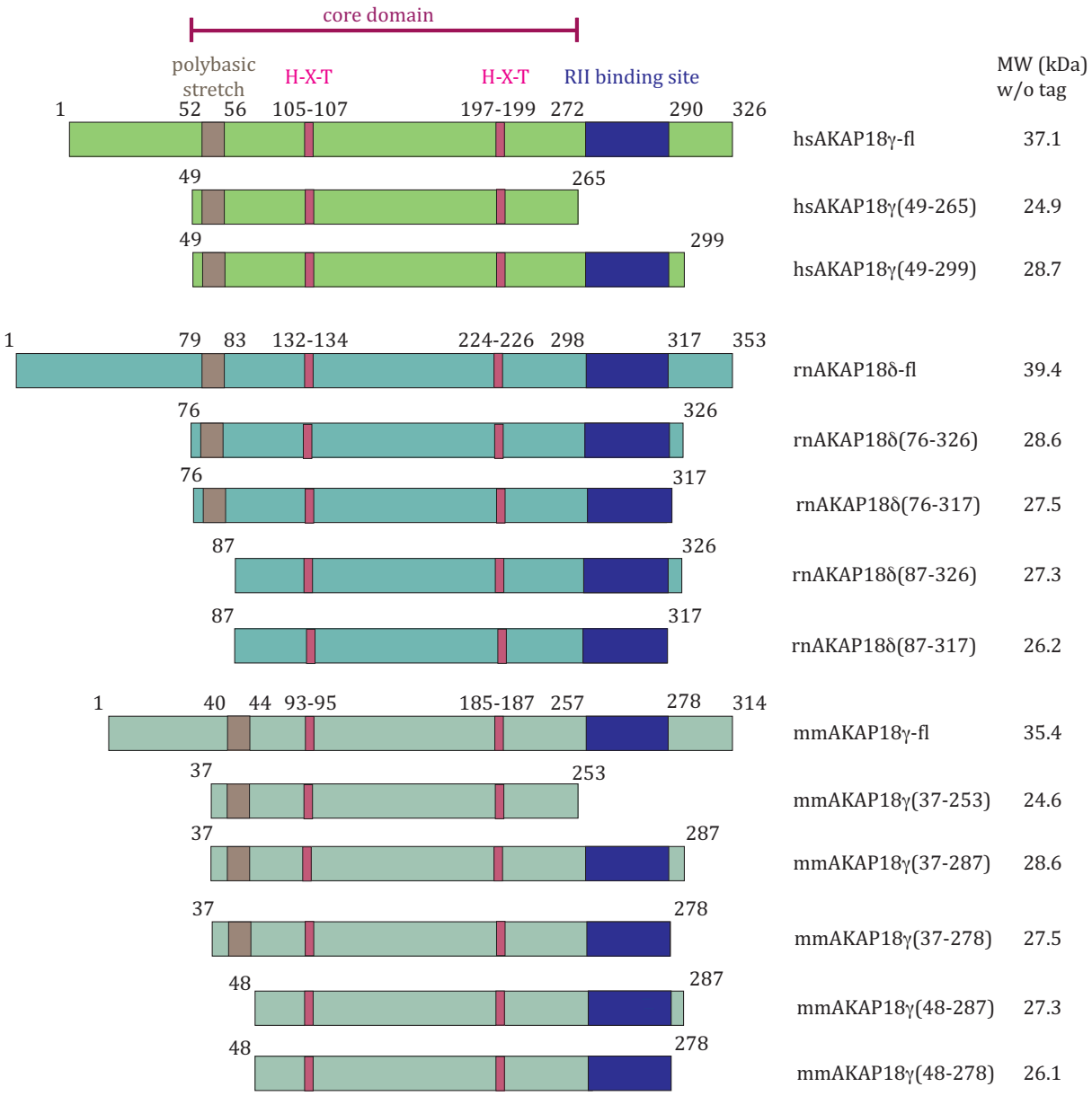

Fig. 12 Schematic representation of new AKAP18γ and δ expression constructs corresponding to initial AKAP18δ constructs. Homologous deletion constructs of human and mouse AKAP18γ and rat AKAP18δ were cloned into pSKB2LNB vector containing an N-terminal His_6-tag and a PreScission protease cleavage site. The amphipathic helix constituting the PKA RII binding site is shown in blue. It is highly conserved in these species. The polybasic stretch with the putative nuclear localization signal is depicted in gray and contains the amino acid sequence KKRKK. The highly conserved His-X-Thr motif is indicated in magenta. On the right, the theoretical molecular weight (MW) of the tag-free constructs is indicated in kDa. The His_6-tag of the pSKB2LNB vector has a MW of ~2.8 kDa.

All of these constructs contain the homologous AKAP18 core domain, but only some of them possess the RII binding site. The latter were always co-transformed and co-purified with tag-free RIIα D/D. A typical purification is shown in **Fig. 13**. In this case, mouse AKAP18γ(37-278)-His with D/D was purified via Co^{2+} affinity and gel filtration chromatography (for details see chapter **2.3.7** and **2.3.8**).

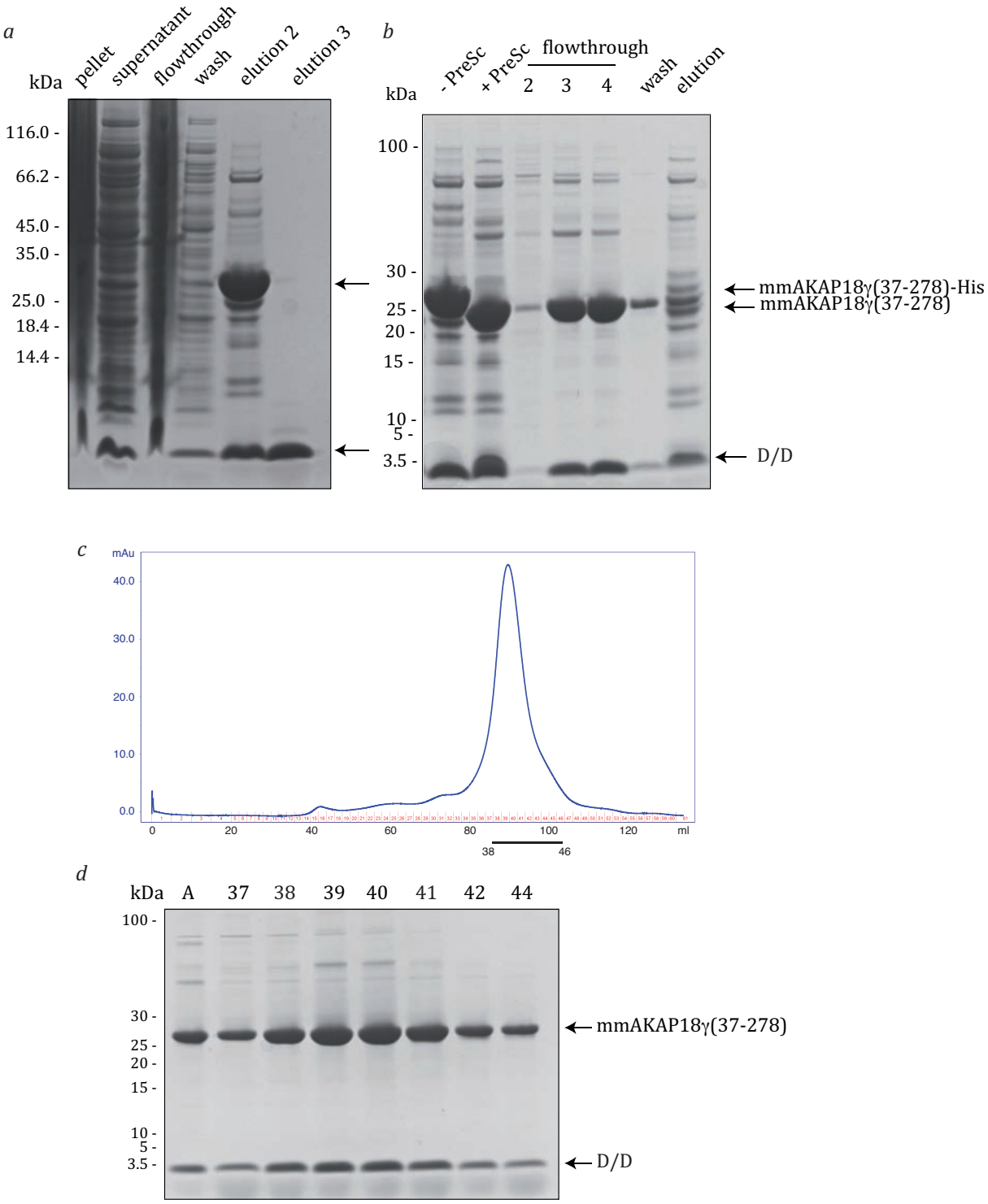

Fig. 13 Purification of mmAKAP18γ(37-278)-His with RIIα D/D. ***a***, Coomassie-stained SDS-PAGE of the first Co^{2+} affinity column. The complex of mouse AKAP18γ(37-278)-His +D/D is highly enriched by this purification step. ***b***, PreScission cleavage of the His_6-tag and second Co^{2+} affinity column. Most of the protein of interest is in the flowthrough. ***c*** and ***d***, Preparative gel filtration run, showing chromatogram and Coomassie-stained SDS-PAGE, respectively. Mouse AKAP18γ(37-278) with D/D is > 90 % pure after this purification step. The black bar beneath the chromatogram depicts the fractions pooled.

It turned out to be crucially important to maintain high salt concentrations (600 mM NaCl) during the first two steps of purification, as this stabilized the protein and prevented degradation. Contamination with DNA as seen in UV spectra when determining protein concentration could also be avoided in this way.

Purification of the other mouse and rat constructs containing the RII binding site was performed in an analogous fashion. Typical yields for the complex of AKAP and D/D are in the range of 4 to 6 mg per liter *E. coli* culture. Notably, purification of the human homolog was less successful. In this case, expression levels were very low and degradation was a major problem. Thus, the human AKAP18γ constructs were not pursued further.

3.1.4 Expression and purification of mouse AKAP18γ(37-253)

As purification yields for mouse AKAP18γ turned out to be higher than for the equivalent rat construct, a construct analogous to the rat AKAP18δ core domain (amino acids 76-292) was cloned and purified. **Fig. 14** shows a representative purification of this construct, mmAKAP18γ(37-253). In general, the purification was performed as described for the other AKAP constructs (see **3.1.3**, **2.3.7**, and **2.3.8**) and yields were slightly higher than for purification of the complex (~8 mg/l culture).

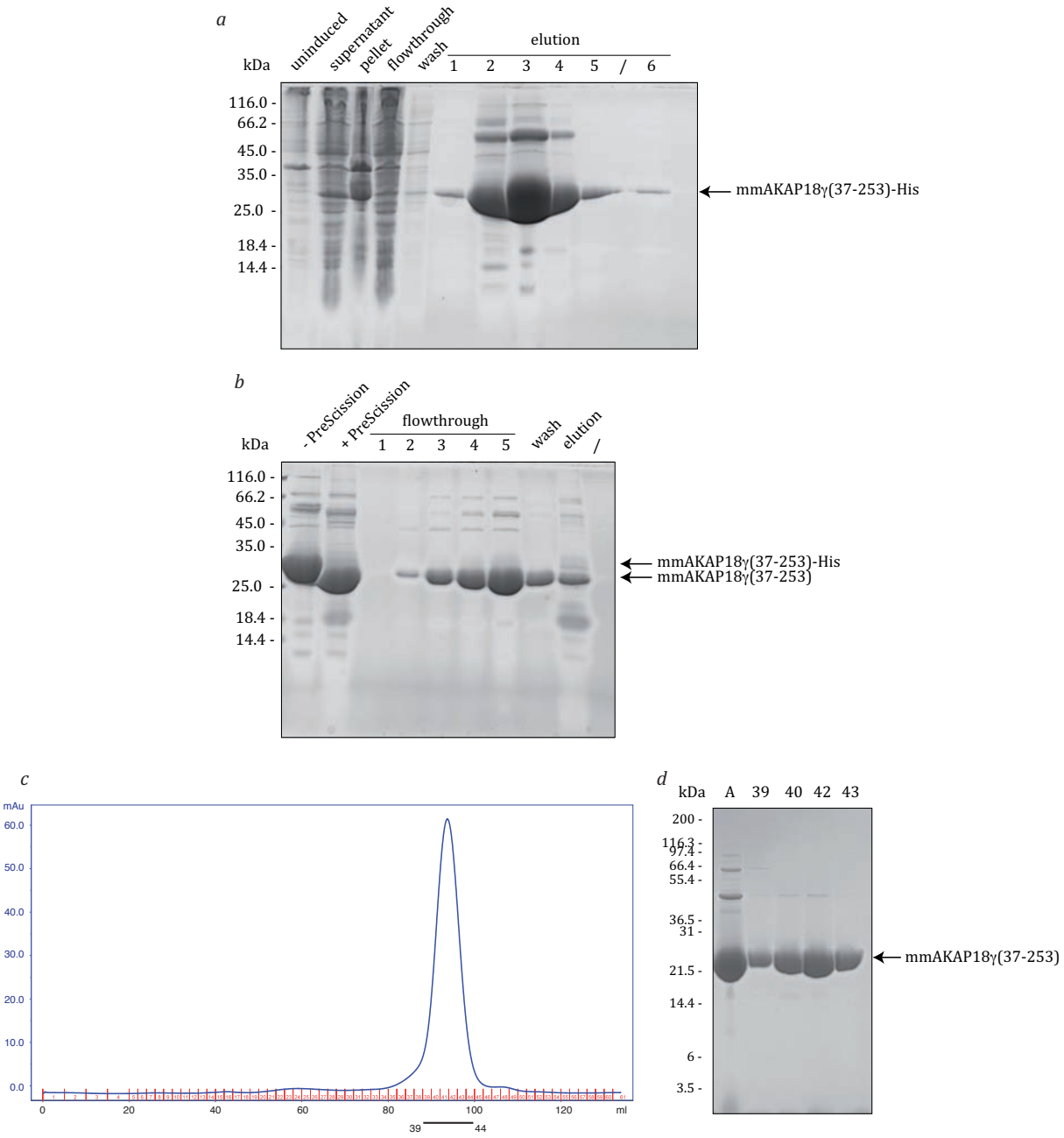

Fig. 14 Purification of mmAKAP18γ(37-253)-His. ***a***, Coomassie-stained SDS-PAGE of the first Co^{2+} affinity column. Mouse AKAP18γ(37-253)-His is highly enriched by this purification step even though a fraction of the protein is found in the pellet and in the flowthrough as well. ***b***, PreScission cleavage of the His_6-tag and second Co^{2+} affinity column. This time, most of the protein of interest is in the flowthrough. ***c*** and ***d***, Preparative gel filtration run, showing chromatogram and Coomassie-stained SDS-PAGE, respectively. Mouse AKAP18γ(37-253) runs as a single peak and is > 95 % pure after this purification step. The black bar beneath the chromatogram depicts the fractions pooled.

3.1.5 Expression and purification of human AKAP18β(43-83)

In the attempt to solve the structure of AKAP18 in complex with RIIα D/D domain, several truncated expression constructs of human AKAP18α and β corresponding to the RII binding domain were cloned. Again, pSKB2LNB was used as expression vector. Human AKAP18β(43-83)-His was co-expressed with RIIα D/D employing the same co-expression and co-purification strategy used for the longer AKAP18γ and δ constructs (see **3.1.3**). Surprisingly, it was not possible to co-purify the complex of hsAKAP18β(43-83)-His and D/D in significant amounts. Instead, hsAKAP18β(43-83) with or without His_6-tag formed higher order oligomers without binding the D/D domain.

A typical purification of hsAKAP18β(43-83) is shown in **Fig. 15**. From **Fig. 15**a it can be seen that hsAKAP18β(43-83)-His as well as the D/D domain were both overexpressed to similar levels but predominantly hsAKAP18β(43-83)-His is eluted from the column. Less than 5 % of the eluted protein consists of the D/D domain. After cleavage of the tag and a second round of affinity chromatography (**Fig. 15**b), gel filtration was performed. The elution profile from gel filtration showed several peaks, which contained mostly hsAKAP18β(43-83), but only trace amounts of the D/D domain (**Fig. 15**c and d).

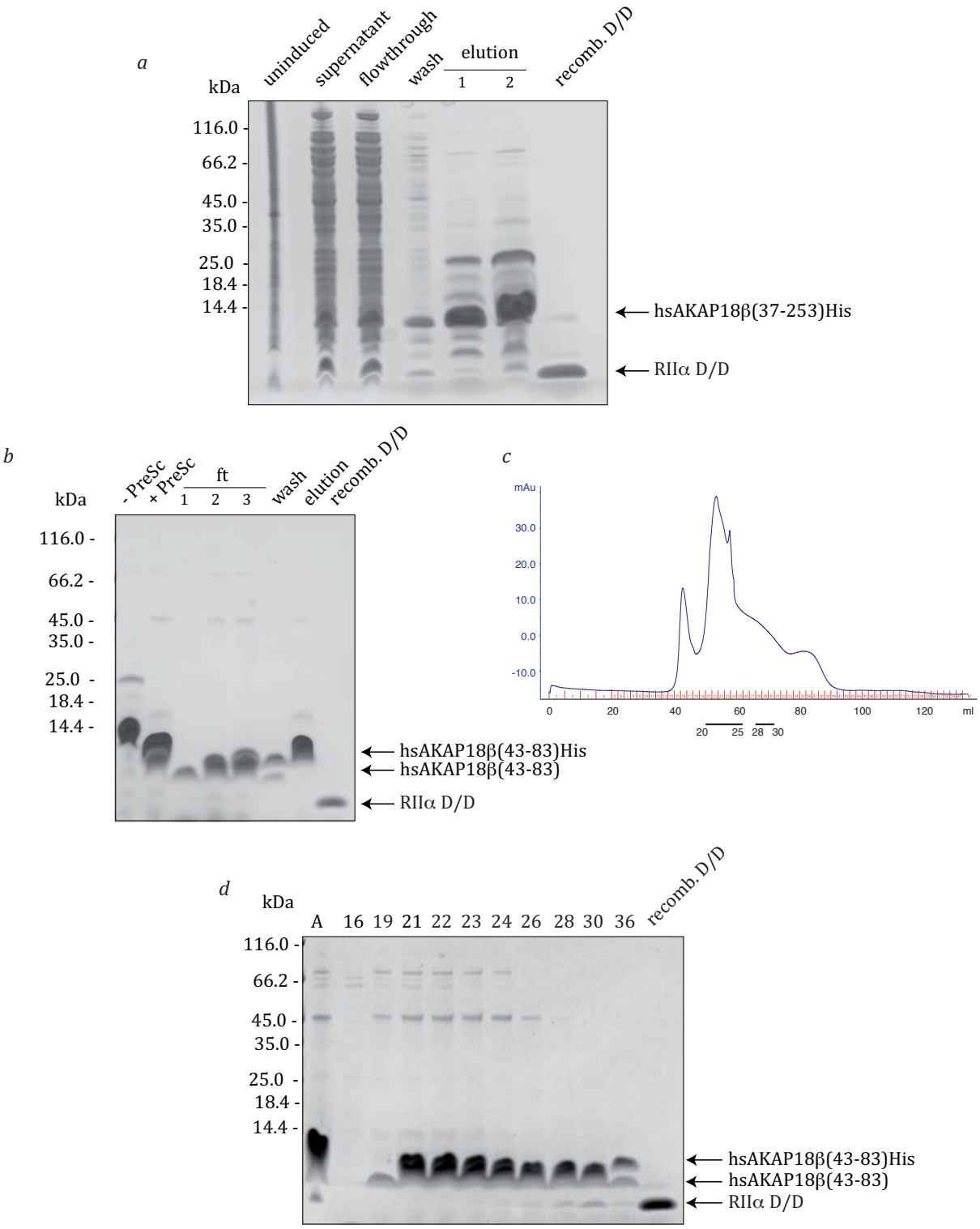

Fig. 15 Purification of hsAKAP18β(43-83)-His. ***a***, Coomassie-stained SDS-PAGE of the first Co^{2+} affinity column. Human AKAP18β(43-83)-His and RIIα D/D are both overexpressed to similar amounts. Nevertheless, only a small fraction of D/D domain is co-purified. ***b***, PreScission cleavage of the His_6-tag and second Co^{2+} affinity column. Most of the protein of interest is in the flowthrough (ft). ***c*** and ***d***, Preparative gel filtration run as a final polishing step, showing chromatogram and Coomassie-stained SDS-PAGE, respectively. Human AKAP18β(43-83) is present in several peaks but is ~90 % pure after this purification step. A fraction of AKAP18β(43-83) is found to form a complex with D/D. The black bars beneath the chromatogram indicate the fractions pooled.

3.2 Initial structural characterization of rat AKAP18δ(76-292) and its interaction partners PDE4D3 and phospholamban

3.2.1 Nuclear magnetic resonance studies

In order to investigate the structural determinants of the interaction between rat AKAP18δ and its binding partners phosphodiesterase (PDE) 4D3 and phospholamban (PLN), nuclear magnetic resonance (NMR) studies were performed. ^{15}N-labeled rat AKAP18δ(76-292) was expressed as described in chapter **2.3.7** and **2.3.8** and purified as shown in **Fig. 10**. Synthetic peptides derived from the mapped interaction sites of PDE4D3 and PLN with AKAP18δ(76-292) were added to detect an interaction.

One-dimensional ^{1}H spectra and two-dimensional heteronuclear single quantum coherence spectra (HSQCs) were recorded to investigate if AKAP18δ(76-292) was folded and if ligand binding was observed (see **2.4.5**). In the ^{1}H-^{15}N HSQC spectra, the resonances for ^{1}H and ^{15}N frequencies are correlated, which each lead to one signal in the NMR spectrum that can be assigned to an N-H atom pair in the protein. The increase in the dimensionality of the NMR experiment is important for observing also subtle chemical shift changes upon binding of a ligand.

The ^{1}H proton and the ^{1}H-^{15}N HSQC spectrum of rnAKAP18δ(76-292), **Fig. 16**a and b respectively, indicate that the protein is well folded, because the overall dispersion of the signals is good: They range from 6 to 10 ppm for the amide region and from -0.5 to 4.5 ppm for the aliphatic region in the ^{1}H spectrum. In the HSQC spectrum, the signals lie between 6.5 and 10.2 ppm in the ^{1}H dimension and between 104 and 132 ppm in the ^{15}N dimension. In theory, there should be 238 peaks for this construct but there are only about 200. This is a hint at conformational heterogeneity.

As it is known from the literature that 5´AMP binds to rnAKAP18δ(76-292) [135], addition of this nucleotide was used as a positive control before application of peptides from interaction partners. **Fig. 16**c shows the overlay of the ^{1}H-^{15}N HSQC spectra without and with 1 mM 5´AMP. As expected, chemical shift changes due to binding of 5´AMP to rnAKAP18δ(76-292) were observed and are shown in **Fig. 16**c and d (marked by arrows). These data suggest that purified rnAKAP18δ(76-292) is properly folded and functional.

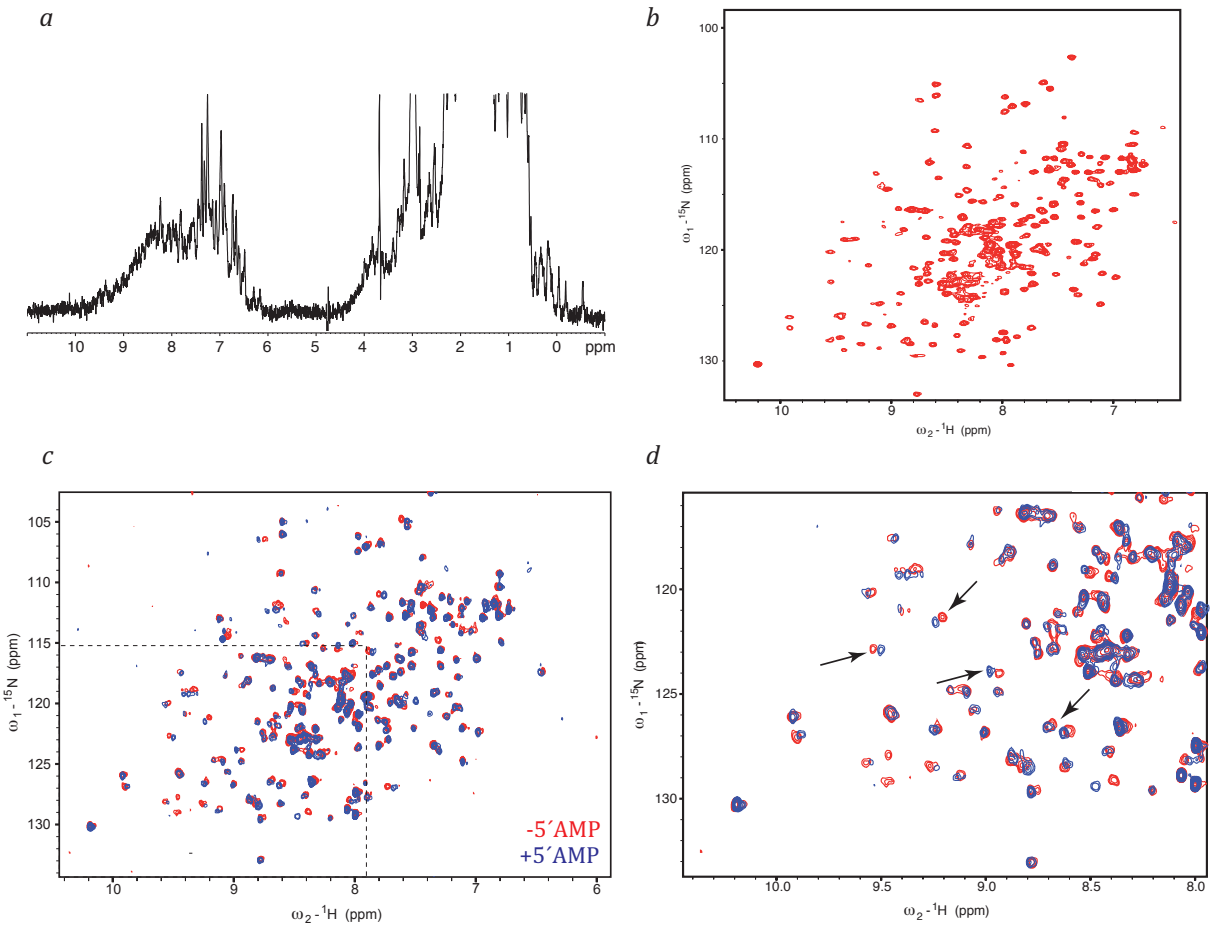

Fig. 16 Initial structural investigation of rat AKAP18δ(76-292) by NMR. All spectra were recorded at 300 K on a 600 MHz spectrometer (DRX-600, Bruker) with a cryo probe head. The buffer contained 20 mM NaH_2PO_4 pH 7.2, 50 mM NaCl, and 10% D_2O. ***a***, ^{1}H-NMR spectrum of rnAKAP18δ(76-292) at a concentration of 105 µM. ***b***, ^{1}H-^{15}N HSQC spectrum of rnAKAP18δ(76-292) at a concentration of 105 µM. ***c***, Overlay of ^{1}H-^{15}N HSQC spectra of rnAKAP18δ(76-292) at a concentration of 75 µM in the absence (red) and in the presence (blue) of 1 mM 5´AMP. ***d***, Zoomed view of ***c*** (boxed region). Examples of relatively large chemical shift changes upon binding of 5´AMP are indicated by arrows.

Similar to the binding of 5´AMP, addition of short peptides derived from AKAP18δ interaction partners, PLN and PDE4D3, should lead to chemical shift perturbations in the AKAP18δ(76-292) HSQC spectra, if the peptides bind.

First, binding of a synthetic peptide representing amino acids 4-32 of rat phospholamban (PLN(4-32)) was tested (see **2.1.10** for amino acid sequence). This region is supposed to contain the interaction site with rnAKAP18δ (residues 12-20) [124]. In AKAP18δ, amino acids 124-138 and 201-220 were mapped to be the PLN binding sites, which both are present in AKAP18δ(76-292) used for NMR studies. ^{1}H-^{15}N HSQC spectra were recorded in the absence or presence of PLN(4-32) in four fold excess. An overlay of the two spectra is shown in **Fig. 17**a. No chemical

shift changes were observed, but the peptide was clearly visible in the ^{1}H spectrum. Accordingly, there is no binding of this PLN peptide to AKAP18δ(76-292).

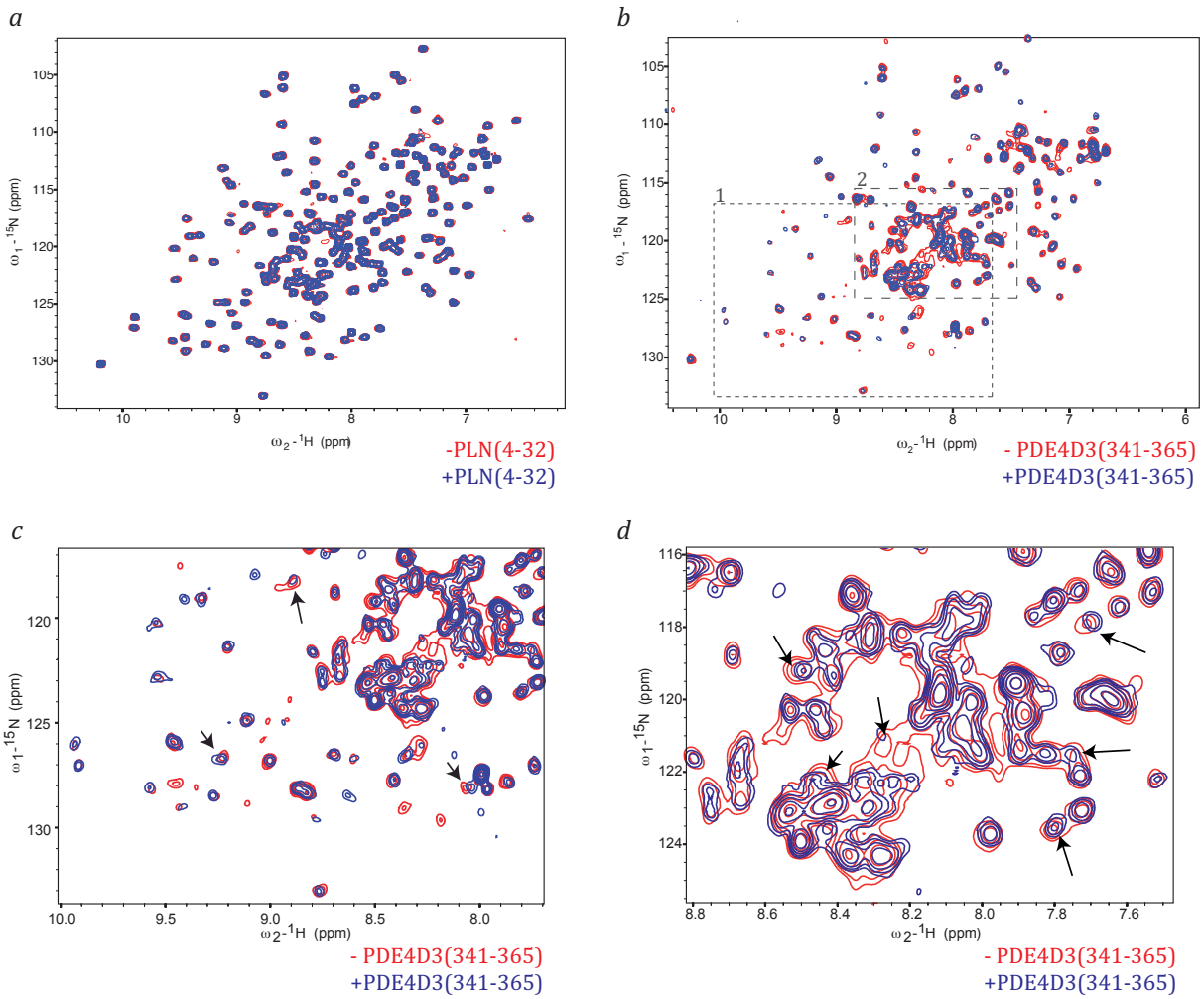

Fig. 17 Two-dimensional HSQC spectra of rat AKAP18δ(76-292) in the presence or absence of putative binding peptides. All spectra were recorded at 300 K on a 600 MHz spectrometer (DRX-600, Bruker) equipped with a cryo probe head. The buffer contained 20 mM NaH_2PO_4 pH 7.0, 100 mM NaCl, and 10% D_2O. ***a***, Overlay of ^{1}H-^{15}N HSQC spectra of rnAKAP18δ(76-292) at a concentration of 70 µM in the absence (red) or in the presence (blue) of 250 µM PLN(4-32). No chemical shift changes are observed. ***b***, Overlay of ^{1}H-^{15}N HSQC spectra of rnAKAP18δ(76-292) at a concentration of 105 µM in the absence (red) or in the presence (blue) of 200 µM PDE4D3(341-365). Subtle chemical shift changes are observed. For more details, zoomed views 1 and 2 (dashed boxes) are shown in ***c*** and ***d***, respectively. Chemical shift changes upon addition of PDE4D3(341-365) are indicated by arrows.

In a similar approach, the binding of peptides derived from PDE4D3 to rnAKAP18δ(76-292) was tested. Two peptides were chosen, PDE4D3(341-365) and PDE4D3(586-610) (see **2.1.10** for amino acid sequences), that were found to bind to rnAKAP18δ-GST in peptide spot arrays [122]. Again, ^{1}H and ^{1}H-^{15}N HSQC spectra of AKAP18δ(76-292) were recorded, this time in the presence and in the absence of PDE4D3 peptides. The results for PDE4D3(341-365) are shown

in **Fig. 17**b-d. In this case, chemical shift perturbations were observed. Additionally, some of the peaks disappeared when the peptide was added, indicating minor structural changes. However, since the signal to noise ration was low in this experiment, the chemical shift changes remained less significant than those observed for 5´AMP binding, even though several repetitions of the experiment with different peptide concentrations were performed. In contrast, the PDE4D3(586-610) peptide clearly did not bind, as it was the case for PLN(4-32) (data not shown).

In addition to the shorter core domain construct of rat AKAP18δ, AKAP18δ(76-292), both the longer construct rnAKAP18δ(76-326) and the co-expressed and co-purified D/D domain (**Fig. 13**) were uniformly ^{15}N-labeled and assessed via NMR spectroscopy. The proteins of the complex were properly folded, as determined by the ^{1}H and the ^{1}H-^{15}N HSQC spectra. **Fig. 18** shows the overlay of the ^{1}H-^{15}N HSQC spectra of AKAP18δ(76-292) (red) and AKAP18δ(76-326) in complex with D/D (blue).

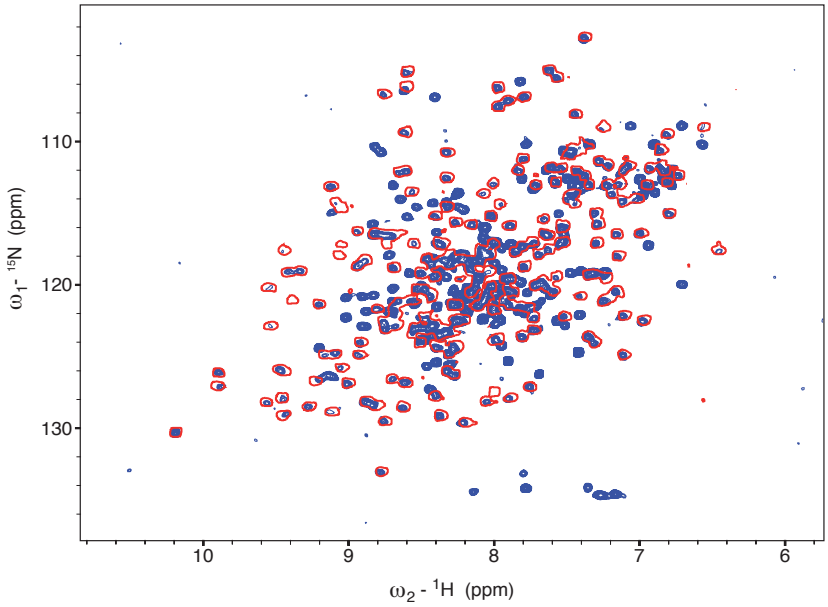

Fig. 18 Overlay of ^{1}H-^{15}N HSQC spectra of rat AKAP18δ(76-292) (red contours) and AKAP18δ(76-326)+D/D (blue). The spectrum for AKAP18δ(76-292) was recorded at 300 K on a 600 MHz spectrometer (DRX-600, Bruker) equipped with a cryo probe, the complex spectrum was recorded on a 900 MHz spectrometer (AV900, Bruker). The buffer contained 20 mM NaH_2PO_4 pH 7.0, 100 or 150 mM NaCl, respectively, and 10% D_2O. Approximately 70 new peaks appear in the AKAP18δ(76-326)+D/D spectrum, which correspond to the additional amino acids in the complex in comparison to AKAP18δ core domain.

Approximately 70 new peaks appeared in the spectrum of AKAP18δ(76-326) in complex with D/D. This is slightly fewer than expected, as there are 76 additional amino acids present in the

complex in comparison to AKAP18δ(76-292) alone. Furthermore, the overall resolution was reduced because many peaks overlap, which can be expected for a complex of the size of about 40 kDa.

In general, assignment of the peaks would be possible but approaches the limits of solution NMR spectroscopy, especially because large amounts not only of ^{15}N- but also of ^{13}C-labeled protein would be needed. Purification yields of the complex are about 4 mg per liter TB medium, which is markedly reduced when proteins are expressed in minimal medium required for labeling. This makes it complicated and expensive to purify sufficient amounts of labeled protein for NMR experiments, where protein concentrations of about 100 µM are advisable. Therefore, structure determination of AKAP18δ(76-326) in complex with D/D by NMR spectroscopy was not pursued.

Since the phospholamban derived peptide PLN(4-32) did not show any interaction with AKAP18δ(76-292), two shorter peptides, PLN(1-20) and PLN(3-22), were tested for interaction with AKAP18δ(76-326) + D/D by ^{1}H-^{15}N HSQC measurements (data not shown). Neither of the two peptides appeared to bind to the AKAP18δ(76-326) – D/D complex. Because phospholamban is a transmembrane protein and therefore complicated to purify in comparison to soluble proteins, working on the PLN – AKAP18δ interaction was not pursued any further.

3.2.2 Crystallization trials of AKAP18δ(76-292) with PDE4D3(341-365)

In parallel to NMR studies on the interaction between rat AKAP18δ(76-292) and synthesized peptides from PLN and PDE4D3, crystallization trials were performed. After observation of a putative interaction of AKAP18δ(76-292) with PDE4D3(341-365) in the ^{1}H-^{15}N HSQC spectra, the same sample was directly used for crystallization screening. Long rod-shaped crystals grew by sitting-drop vapor-diffusion within one day and under various conditions mostly at neutral to higher pH (7 – 9) using commercially available screens (see **2.5.1**). Crystals were tested at BESSY for X-ray diffraction and data sets of best diffracting crystals were collected as described in **2.5.2**. **Fig. 19** shows the crystals used for data set collection.

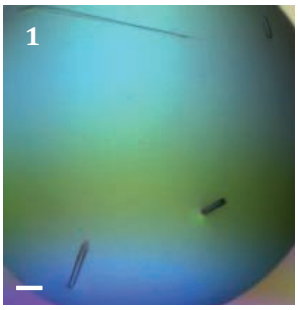

0.2 M TMAO,
0.1 M Tris/HCl pH 8.5,
20 %(w/v) PEG 2000 MME

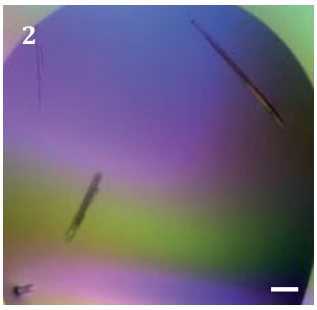

0.1 M Hepes/NaOH pH 7.0
30 % (v/v) Jeffamine ED-2001

Fig. 19 Crystals of rat AKAP18δ(76-292) grown in the presence of PDE4D3(341-365) and in the buffer condition indicated. The white bar represents 100 µm.

In **Table 1**, data collection statistics are given. Crystals diffracted to a maximal resolution of 2.1 Å and 2.3 Å, respectively. Both crystals belonged to a trigonal space group, $P3_1$ or $P3_2$. It was possible to solve the structures by molecular replacement (see **2.5.2**). The cell dimensions of crystal 1 are nearly identical with the published ones [135]. Since no difference electron density was visible for the PDE4D3(341-365) peptide, no further refinement was carried out. The peptide apparently was not present in either of the crystals.

Tab. 1 Data collection statistics rnAKAP18δ(76-292)

Data collection	**rnAKAP18δ(76-292) +PDE4D3(341-365) crystal 1**	**rnAKAP18δ(76-292) +PDE4D3(341-365) crystal 2**
X-ray source	BESSY	BESSY
wavelength (Å)	0.9184	0.9184
space group	$P3_1$	$P3_2$
cell dimensions		
a (Å)	42.76	42.89
b (Å)	42.76	42.89
c (Å)	97.80	195.55
unit cell (Å)	$a = b = 90°$, c = 120 °	$a = b = 90°$, c = 120 °
mol/asu	1	2
Resolution (Å)	2.1 (2.16-2.10)[a]	2.3 (2.36-2.30)
Completeness (%)	92.9 (74.2)	91.5 (79.9)
R_{sym} (%)	5.3 (34.1)	7.6 (33.9)
$I/\sigma I$	14.4 (2.76)	9.6 (3.1)

[a] The numbers in parentheses correspond to the highest resolution shell.
[b] $R_{sym} = \Sigma \mid I(h)_i - \langle I(h) \rangle \mid / \Sigma I(h)_i$ where $I(h)_i$ is the scaled observed intesity of the i-th symmetry related observation of the reflection h, $\langle I(h) \rangle$ is the mean value

3.3 Interaction studies of AKAP18 with longer PDE4D3 constructs

The results for binding of PDE4D3 peptides in the NMR experiments were ambiguous, showing at least an influence of the presence of PDE4D3(341-365) on the chemical shifts in AKAP18δ(76-292) ^{1}H-^{15}N HSQC spectra. Even though it was not possible to co-crystallize AKAP18δ(76-292) with the PDE4D3(341-365) peptide, it cannot be ruled out that there is an interaction between AKAP18δ and full-length PDE4D3. In the peptide, critical amino acid residues may be missing that are essential for the interaction or for adopting the correct fold, e.g. an α-helical fold.

To investigate the secondary structure content of the peptides, CD spectroscopy was performed (see **2.4.1**). It revealed that PDE4D3(341-365) is α-helical whereas PDE4D3(586-610) is disordered (**Fig. 20**).

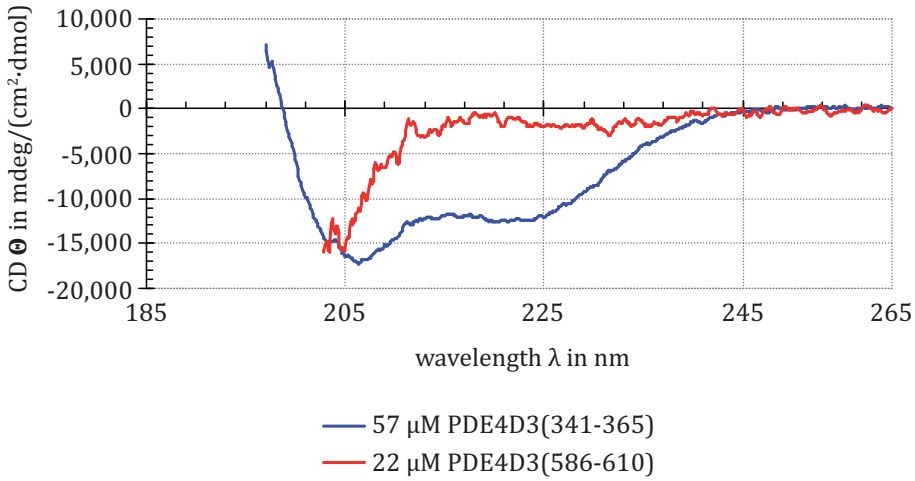

PDE4D3(341-365) LLSTPALEAVFTDLEILAAIFASAI
PDE4D3(586-610) DQEDGRQGQTEKFQFELTLEEDGES

Fig. 20 Circular dichroism spectra of PDE4D3 peptides. The ellipticity is plotted against the wavelength showing a typical α-helical spectrum for PDE4D3(341-365) with the characteristic minima at 222 nm and 208 nm wavelength and a disordered PDE4D3(586-610) peptide spectrum. The amino acid sequences of both peptides are depicted below the spectrum.

3.3.1 Purification of PDE4D3 constructs and activity test

In order to verify the direct interaction of AKAP18δ with PDE4D3 *in vitro*, and to prepare a complex for crystallization, longer PDE4D3 constructs consisting of at least the catalytic domain were cloned into the pET30 Ek/LIC vector (see **2.2.5**ff). The constructs chosen for the interaction studies are shown in **Fig. 21**a. They were designed on the basis of the structure of

the catalytic domain of PDE4D2 (pdb code iptw), which is identical to the catalytic domain of PDE4D3 as those isoforms are produced by alternative splicing. Construct 1 refers to the residues visible in electron density in the crystal structure and construct 2 refers to the expression construct that was used for purification and crystallization by Huai and co-workers [167]. Both constructs only contain the first AKAP18δ binding site, i.e. the first peptide sequence derived from peptide spot analysis [122]. The second AKAP18δ binding site is included in construct 3 and 4, the latter containing the full C-terminus. Purification of PDE4D3 constructs was performed as described in **2.3.4-2.3.8** (**Fig. 21**).

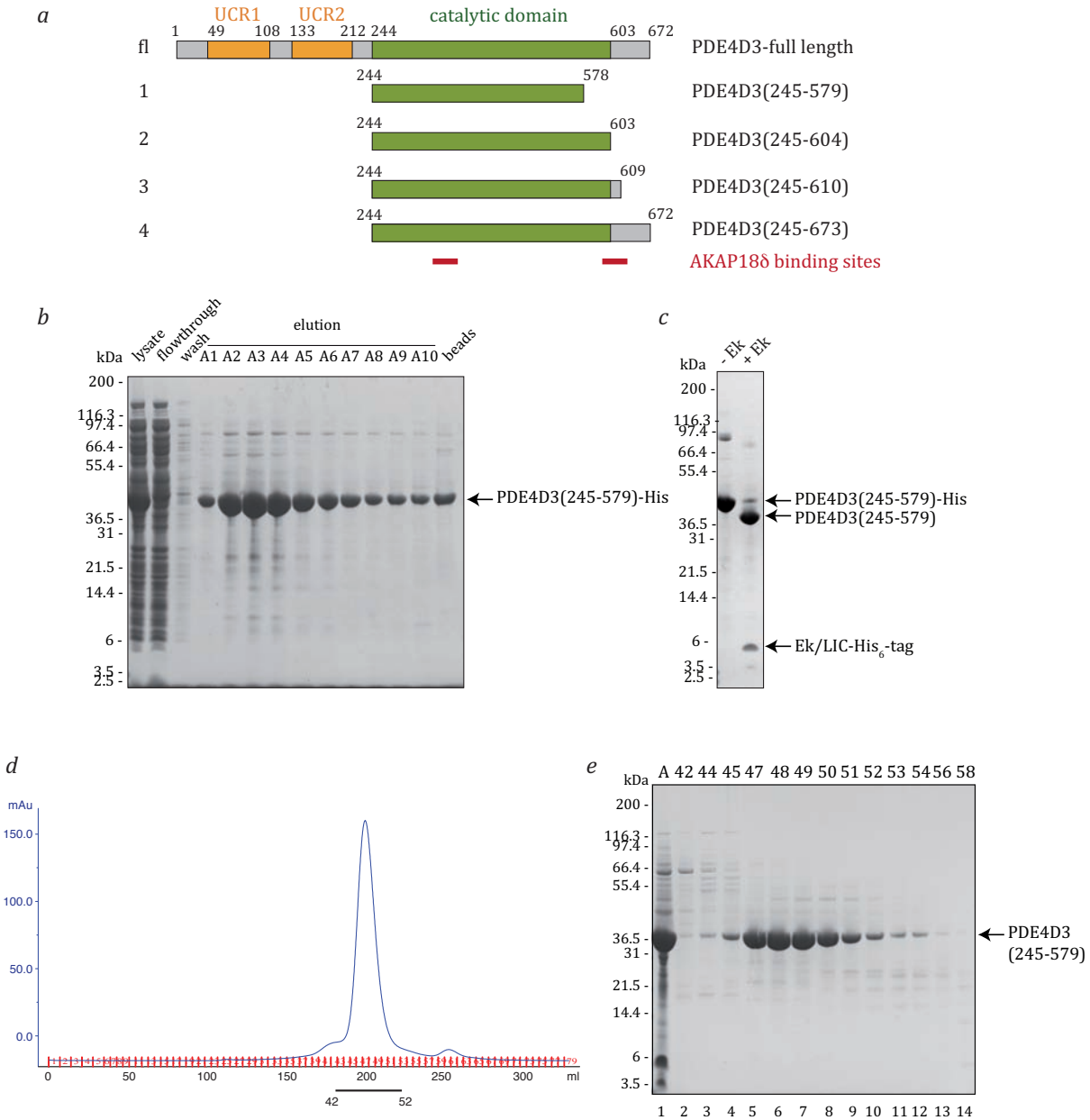

Fig. 21 Purification of human PDE4D3(245-579)-His. ***a***, Schematic representation of full length hsPDE4D3 and deletion constructs cloned into the pET30 Ek/LIC vector containing an N-terminal His_6-tag and an enterokinase (Ek)

cleavage site. At the N-terminus, there are two upstream conserved regions (UCRs) shown in yellow. The highly conserved catalytic domain is shown in green. The mapped regions of the AKAP18δ binding sites are indicated in red. ***b***, Coomassie-stained SDS-PAGE of fractions from the Co^{2+} affinity column. Human PDE4D3(245-579)-His was overexpressed in *E.coli* Rosetta 2 DE3 cells. One-step purification by affinity chromatography yielded ~ 80 % pure protein. ***c***, Coomassie-stained SDS-PAGE showing cleavage of the His_6-tag. ***d***, and ***e***, Chromatogram and Coomassie-stained SDS-PAGE of fractions collected from gel filtration (Superdex 200 26/60). PDE4D3(245-579) elutes as a single peak. Fractions pooled are indicated by a black bar.

All of the four constructs proved to be soluble. Purification of construct 1 and 4 was established in large scale. For both constructs, protein yields of around 30-40 mg from one liter *E. coli* cell culture were achieved.

To ensure that the purified PDE4D3 constructs were correctly folded and therefore enzymatically active, an HPLC based activity assay was performed as described in **2.3.11**. As standards, cAMP, 5´AMP, adenosine diphosphate (ADP), and ATP were separated on the hydrophobicity column and the retention times recorded (**Fig. 22**a). In the absence of PDE4D3(245-579), cAMP is relatively stable (**Fig. 22**b). Catalytic activity of PDE4D3(245-579) was confirmed by observing time-dependent degradation of cAMP to 5´AMP in the chromatogram at 254 nm (**Fig. 22**c and d). The corresponding experiment was performed using PDE4D3(245-673)-His with a similar result. Thus, both PDE4D3(245-579) and PDE4D3(245-673)-His are correctly folded and active enzymes.

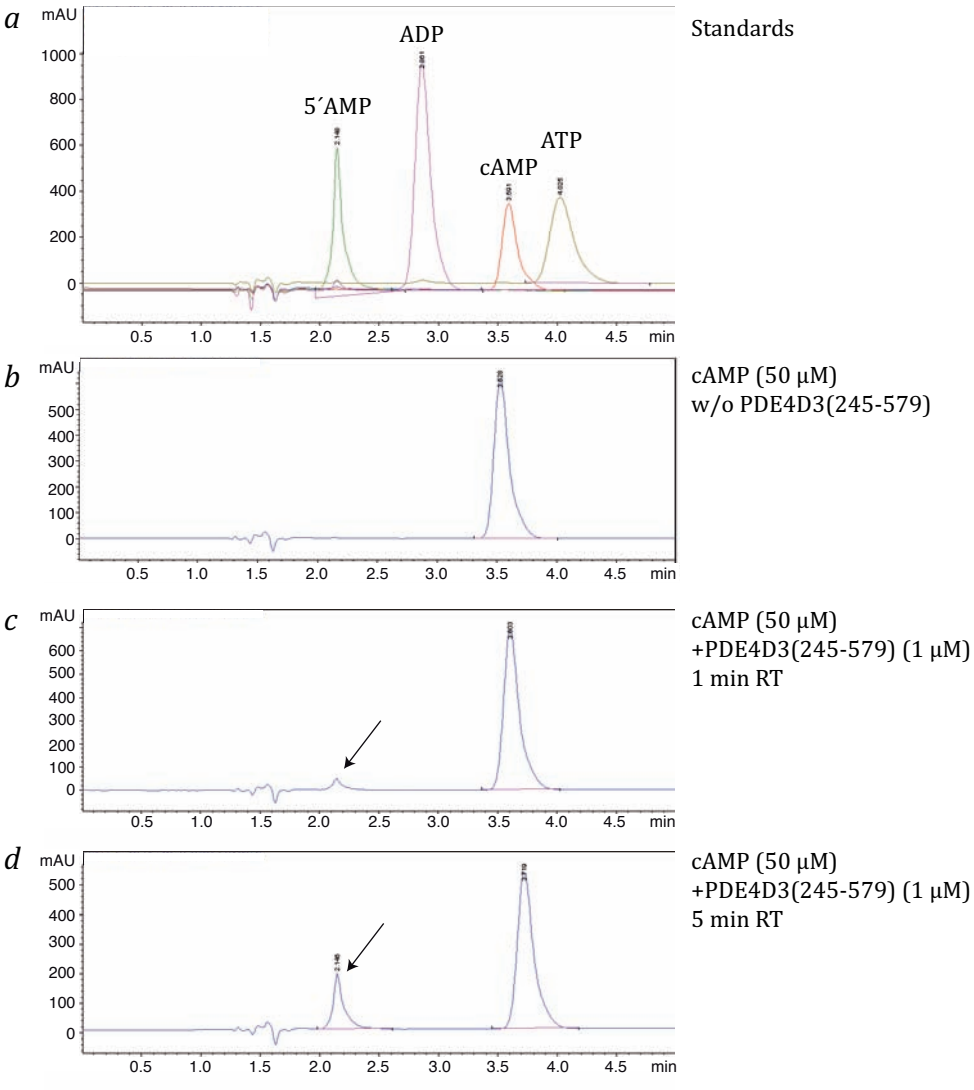

Fig. 22 HPLC-based activity test for purified PDE4D3 mutants. ***a***, Elution profile of nucleotide standards at a concentration of 30 µM as separated on a Hypersil column using potassium phosphate buffer containing 10 mM tetra butyl ammonium bromide (TBAB) and 7.5% acetonitrile. ***b***, ***c***, and ***d***, Purified PDE4D3(245-579) is functional and degrades cAMP to 5´AMP in a time dependent manner. This can be seen from the increase in the 5´AMP peak area with time in the presence of PDE4D3(245-279).

3.3.2 Interaction studies of PDE4D3 with AKAP18δ

Purified and active PDE4D3(245-579) and PDE4D3(245-673)-His were used for interaction studies with AKAP18δ(76-292) and AKAP18δ(76-326) in complex with the D/D domain. Analytical gel filtration with purified rnAKAP18δ and PDE4D3 constructs was used to analyze complex formation (see **2.3.8**). As an example, analytical gel filtration results for AKAP18δ(76-292) and PDE4D3(245-673)-His are shown in **Fig. 23**.

The proteins were mixed and incubated on ice for 30 min either in the absence or in the presence of cAMP (10 mM). Precipitated protein was removed by filtering the samples through a

0.45 µm membrane before applying it on a Superdex200 size exclusion column. **Fig. 23**a shows the chromatogram with the UV absorption at 280 nm plotted against the elution volume for both samples. Both in the absence (blue) and in the presence (green) of cAMP, there is no complex formation with an affinity high enough to be isolated on a gel filtration column. This was verified by SDS-PAGEs of the fractions collected during the run (**Fig. 23**b without cAMP, c with cAMP). The additional peak around an elution volume of 20 ml in the green chromatogram curve is due to the presence of cAMP, which is also detected at 280 nm.

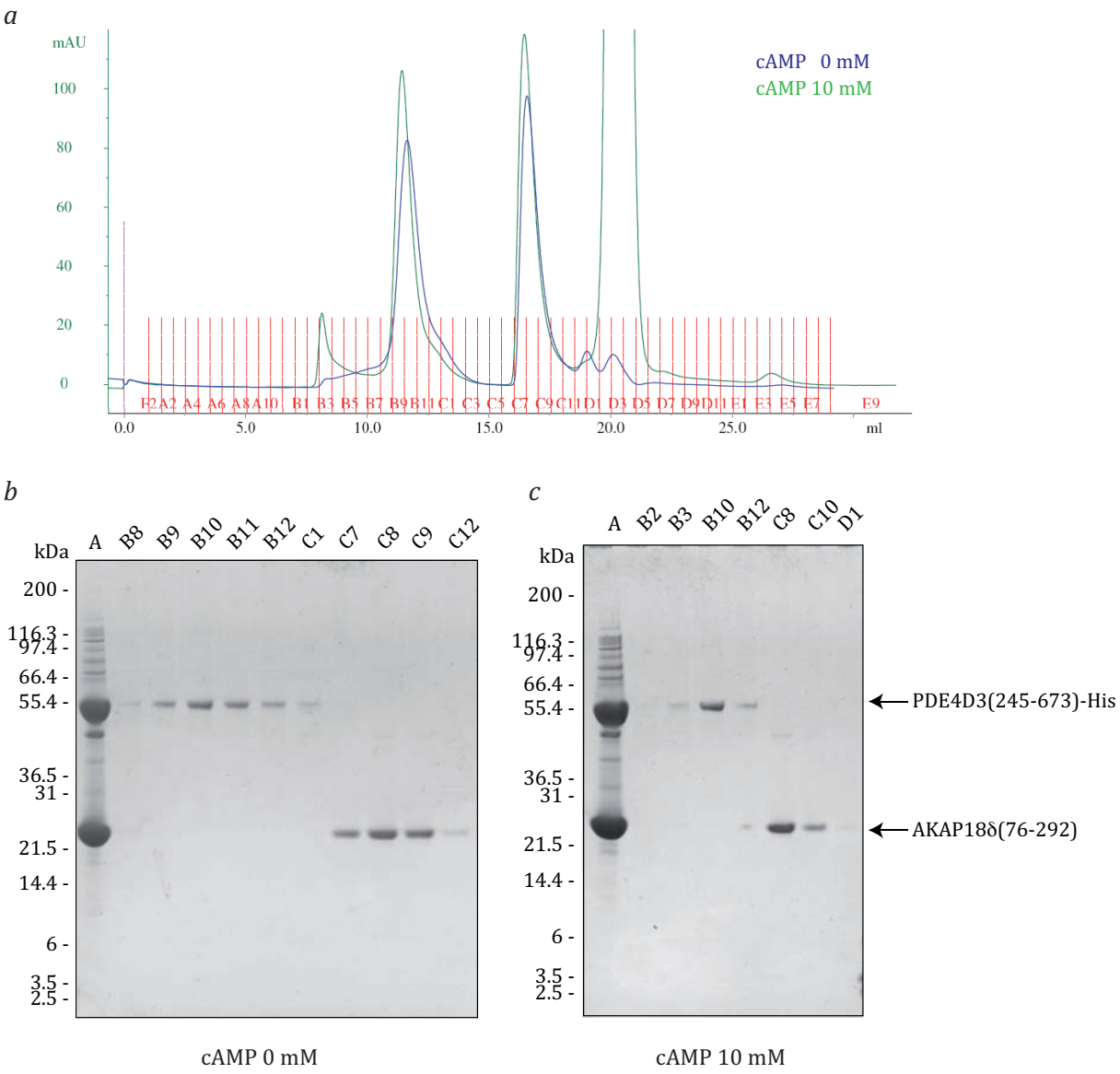

Fig. 23 Analytical gel filtration to analyze a possible interaction between rnAKAP18δ(76-292) and PDE4D3(245-673)-His. ***a***, Chromatogram depicting the elution profile of a mixture of rnAKAP18δ(76-292) and PDE4D3(245-673)-His in the absence (blue) and in the presence (green) of cAMP detected by UV absorption at 280 nm. ***b***, Coomassie-stained SDS-PAGE of fractions collected during the gel filtration run without cAMP. ***c***, Coomassie-stained SDS-PAGE of fractions collected during the gel filtration run with 10 mM cAMP. Both proteins elute as well seperated peaks and do not form a complex.

In an alternative approach, isothermal titration calorimetry (ITC) experiments were carried out (see **2.4.3**) to determine thermodynamic parameters of any interaction that could be detected. The results of the ITC experiments are shown in **Fig. 24**. PDE4D3(245-579) was titrated into a solution containing 30 µM rnAKAP18δ(76-292) (**Fig. 24**a). However, no binding was observed as indicated by the missing changes in the differential heating power. As a control, PDE4D3(245-579) with the same concentration as in *a* was titrated into the ITC buffer in the absence of protein (**Fig. 24**b), which also did not yield a heat signal. The results are identical with the results shown in *a*, indicating that indeed there is no difference in the differential heating power in the presence or absence of AKAP18δ(76-292). Additionally, to test for a possible influence of 5´AMP on the interaction between rnAKAP18δ(76-292) and PDE4D3(245-579), the same experiment as in *a* was performed in the presence of 250 µM 5´AMP and with higher protein concentrations (**Fig. 24**c). Again, no binding was observed.

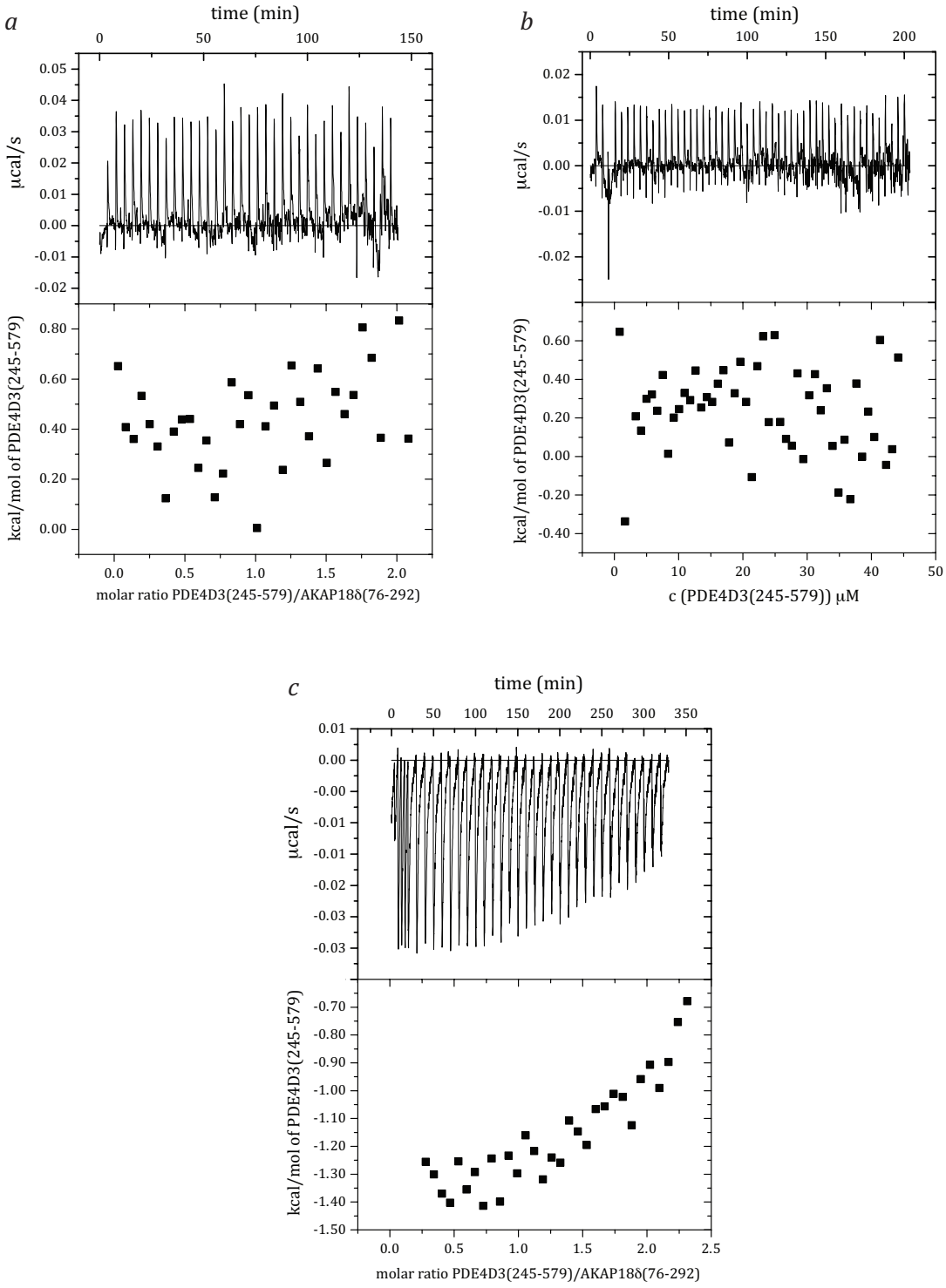

Fig. 24 Isothermal titration calorimetry (ITC) experiments to characterize the rat AKAP18δ - PDE4D3 interaction. In each diagram, the upper panel shows the differential heating power plotted against time, whereas the lower panel depicts the heat of reaction against the molar ratio between the titrated ligand and its putative binding partner. In the case of the control (*b*), the latter is the heat of reaction versus total PDE4D3(245-579) concentration. ***a***, 300 µM PDE4D3(245-579) was titrated into 30 µM AKAP18δ(76-292). ***b***, 300 µM PDE4D3(245-579) was titrated into ITC buffer as a control. ***c***, 500 µM PDE4D3(245-579) was titrated into 40 µM AKAP18δ(76-292) in the presence of 5´AMP (250 µM) in both samples.

In addition to ITC and analytical gel filtration, pull down experiments and cross-linking experiments were performed (data not shown), which also did not result in detection or even isolation of a complex between the rnAKAP18δ and PDE4D3 constructs. Therefore, these constructs were not pursued any further.

3.4 Biophysical characterization of AKAP18 isoforms

Several different biophysical methods failed to identify complex formation between rnAKAP18δ and PDE4D3. Therefore, the focus of the work was changed to understanding the interaction between AKAP18 isoforms with PKA RIIα in general. Homologous proteins from other organisms were identified by performing the BLAST search on the webpage of the National Center of Biotechnology Information (NCBI, http://www.ncbi.nlm.nih.gov/). Human and mouse AKAP18 isoforms were chosen for further investigation and comparison with rat AKAP18δ isoform.

3.4.1 Nucleotide binding to mouse AKAP18γ constructs

Binding of 5´AMP to rat AKAP18δ(76-292) was shown by Gold and co-workers [135] in co-crystallization studies and by equilibrium fluorescence binding using 2′- (or 3′)-O-(N-methylanthraniloyl) adenosine 5′-monophosphate (MANT-AMP) instead of 5´AMP. They determined the K_D to 194±30 μM. The addition of the fluorescent methylisatoic acid to AMP may decrease the binding affinity of MANT-AMP in comparison to 5´AMP, because ITC measurements gave a ten-fold lower dissociation constant K_D of 18±0.6 μM for 5´AMP binding to rnAKAP18δ(76-292) (see **Fig. 25**a). Clear changes in the differential heating power were observed, which are an indication for the heat evolved when the ligand binds to the protein [152]. The corresponding control of titration of 5´AMP alone into ITC buffer can be seen in **Fig. 25**d. In this case, no changes in the differential heating power are observed.

In order to test nucleotide binding to the AKAP18γ mouse isoform (93 % identity with rat) in complex with the D/D domain and to the core domain of mouse AKAP18γ, ITC experiments were performed to study a possible influence of the D/D domain on nucleotide binding. The results are shown in **Fig. 25**b and c, respectively.

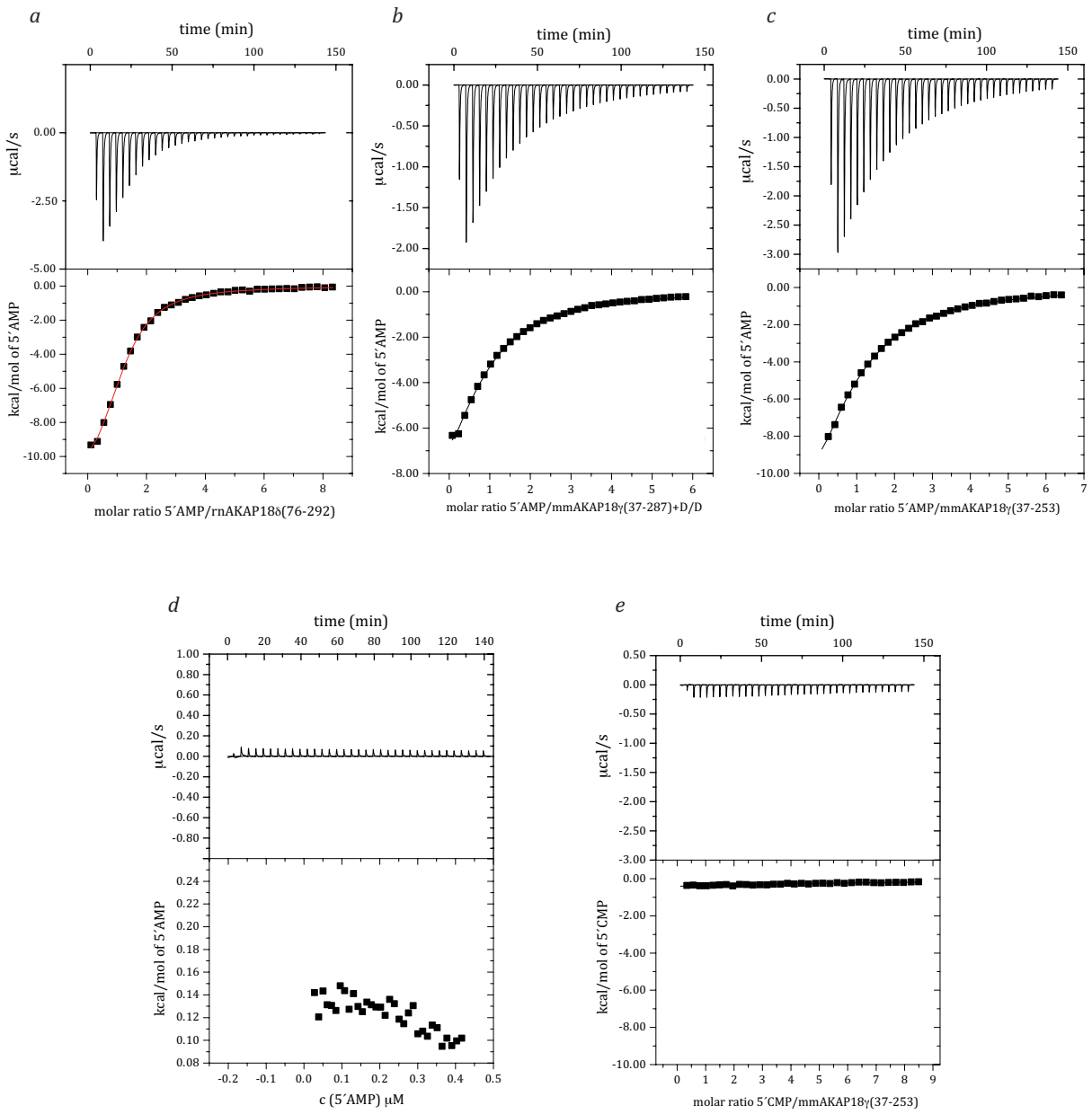

Fig. 25 Isothermal titration calorimetry (ITC) experiments to characterize nucleotide binding to rat AKAP18δ and mouse AKAP18γ constructs. In each diagram, the upper panel shows the differential heating power versus time, whereas the lower panel depicts the heat of reaction versus the molar ratio between the titrated ligand and its putative binding partner. In the case of the control (*c*), the latter is the heat of reaction versus total 5´AMP concentration. ***a***, 2 mM 5´AMP was titrated into 50 µM AKAP18δ(76-292). The dissociation constant, K_D, of 18±0.6 µM was calculated using MicroCal ORIGIN software. ***b***, 1.4 mM 5´AMP was titrated into 50 µM mmAKAP18γ(37-287) with D/D. The dissociation constant, K_D, of 43±2 µM was calculated using the MicroCal ORIGIN software. ***c***, 1.4 mM 5´AMP was titrated into 52 µM mmAKAP18γ(37-253) and the calculated K_D was 60±2 µM. ***d***, As a control, 5´AMP at a concentration of 2 mM was titrated into ITC buffer without any protein. ***e***, 2 mM of 5´CMP was titrated into 49 µM mmAKAP18γ(37-253). No binding was observed.

Both mmAKAP18γ(37-287) in complex with D/D (*a*) and mmAKAP18γ(37-253) (*b*) were able to bind 5´AMP in the low micromolar range (K_D of 43±2 and 60±2 µM, respectively).

In addition to 5´AMP, binding of 5´CMP and cAMP to both mmAKAP18γ(37-287) in complex with D/D and mmAKAP18γ(37-253) was tested. 5´CMP was co-crystallized by Gold and colleagues with rat AKAP18δ(76-292) but did not bind to the mouse proteins. As an example, **Fig. 25**e shows the titration of 5´CMP into a solution of mmAKAP18γ(37-253). No changes in the differential heating power were observed, thus no interaction of the nucleotide with this construct took place. Similarly, cAMP also did not bind to the mouse AKAP18γ constructs.

3.4.2 Crystallization trials of mouse and rat AKAP18γ and δ in complex with D/D

There is no structure of an AKAP longer than the PKA binding domain in complex with the PKA RIIα D/D domain. Consequently, it is not known how the adjacent domains/regions in AKAPs influence binding parameters of PKA. Based on the promising purification protocol for mouse and rat AKAP18 constructs with D/D, it was a primary goal to study the interplay between the AKAP18 core domain, the PKA binding helix of AKAP18, and the PKA RIIα D/D domain using X-ray crystallography. Therefore, a broad variety of crystallization conditions were screened ranging from different commercially available screens to self-developed screens (see chapter **2.5.1**).

To crystallize the complex of AKAP18γ or δ with the D/D domain, the following approaches were tested: Concerning construct design, several shorter variants of the starting constructs, rat AKAP18δ(76-326) and mouse AKAP18γ(37-287), were cloned in order to remove flexible regions (see **Fig. 12**). The rationale was that flexible parts of the AKAPs may prevent crystallization by disturbing the formation of crystal contacts.

Another reason that nucleation does not occur, is aggregation of the protein, precluding crystal growth. High NaCl concentrations were used during purification of AKAP18 in complex with D/D (compare **3.1.3**) to prevent aggregation. In addition, thermal shift assays (TSAs) were performed (see **2.4.2**), in order to find buffer conditions stabilizing AKAP18γ and δ in complex with D/D. **Fig. 26** shows TSA results for mmAKAP18γ(48-287) co-expressed and co-purified with D/D.

a

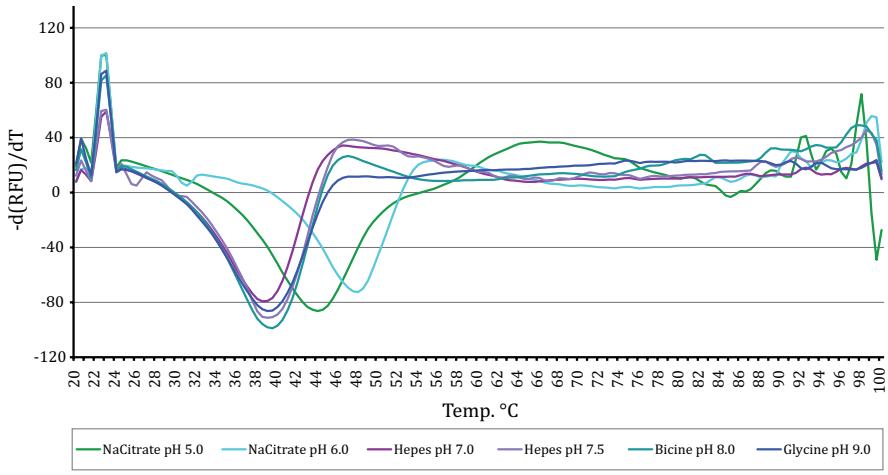

b

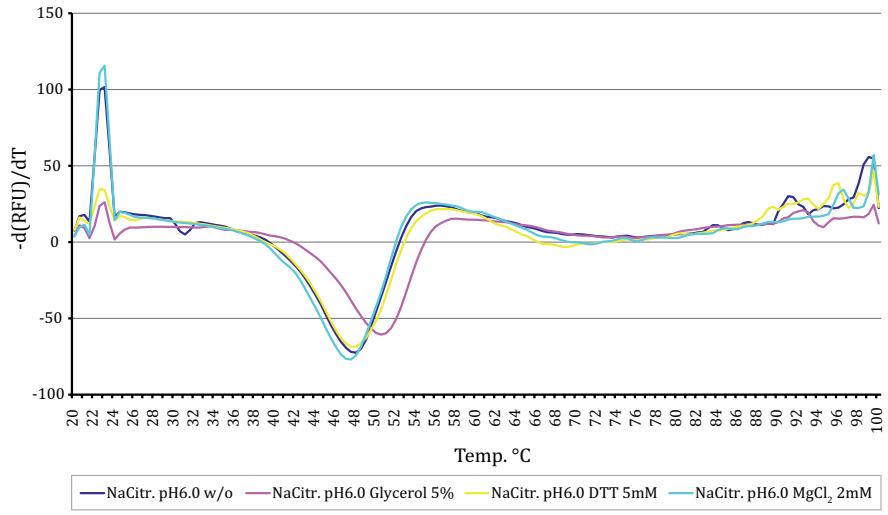

Fig. 26 Thermal shift assay (TSA) showing denaturation of mouse AKAP18γ(48-287) in complex with D/D. 30 µg of protein was used in each sample containing different buffer and/or additive conditions. Sypro®Orange was added and the temperature was raised in steps of 0.5 °C per minute, while measuring fluorescence at each interval. Each condition was tested in duplicate. The first derivative of time -d(RFU)/dT is plotted against the temperature (in °C) with the melting point of the protein T_m located at the minimum of the curve. ***a***, Comparison of different buffers and pH values as indicated below the diagram. Citrate buffer increases the T_m markedly. ***b***, Comparison of different additives to the protein buffered in sodium-citrate pH 6.0. The addition of 5 % glycerol leads to an increase in T_m. *RFU*, *relative fluorescence unit*.

The melting temperature T_m is at the minimum of the first derivative of RFU of time -d(RFU)/dT plotted against temperature. Citrate buffer at pH 5.0 and 6.0 increased T_m of mmAKAP18γ(48-287) with D/D by about 5 °C and 9 °C, respectively, i.e. the stability of the protein was increased. The addition of 5 mM DTT or 2 mM $MgCl_2$ did not change protein stability. As expected, addition of 5 % glycerol increased the melting temperature, in this case by about 4 °C. For subsequent crystallization screens, citrate buffer at pH 6.0 was used to increase complex stability.

Unfortunately, none of these approaches was successful to grow crystals of the AKAP18 – D/D complex.

One amphipathic helix of an AKAP is expected to bind a dimer of the D/D domain [40, 78, 81, 82] In the beginning, it was not clear whether the sample of purified rnAKAP18δ(76-326) and D/D was homogenous after purification. Therefore, in one early attempt to reconstitute a defined 1:2 complex of rnAKAP18δ(76-326) and the D/D domain, co-expressed and co-purified rnAKAP18δ(76-326) and D/D were separated using 1M NaCl. Subsequently, separately purified D/D domain was added to rnAKAP18δ(76-326) in a 1:2 molar ratio directly before the crystallization screens were set up. This yielded crystals of the D/D domain that grew at various pH values under different conditions, mostly in the presence of ammonium sulfate (**Fig. 27**).

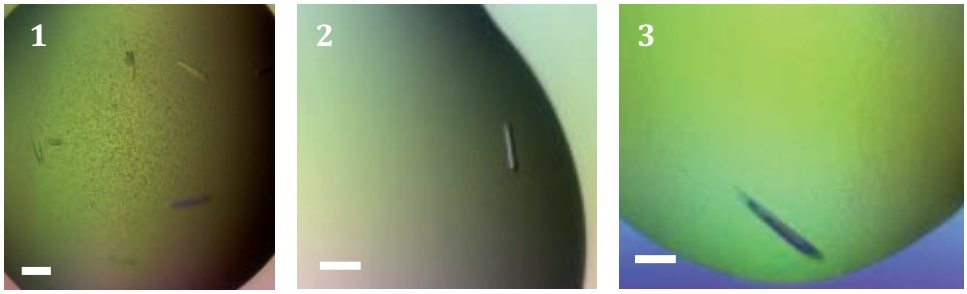

0.2 M K^+/Na^+ tartrate,
2.0 M NH_4 sulfate,
0.1 M tri-sodium citrate
pH 5.6

2.0 M NH_4 sulfate,
0.1 M MES pH 6.0

2.4 M NH_4 sulfate,
0.1 M BICINE pH 9.0

Fig. 27 Crystals of the D/D domain grown from a solution of rnAKAP18δ(76-326) with the D/D domain added after purification. The respective crystallization condition is indicated below each picture. The white bar represents 100 µm.

Similar to the rnAKAP18δ(76-292) crystals, the D/D crystals also were rod-shaped and appeared after one day at 4 °C. Glycerol was used as cryo protectant and X-ray data were collected as described in **2.5.2**. Data collection statistics for three datasets are summarized in **Table 2**.

Tab. 2 Data collection statistics of D/D crystals. The numbers of the crystals refer to numbers in **Fig. 27**

Data collection	D/D (added to rnAKAP18δ(76-326)) crystal 1	D/D (added to rnAKAP18δ(76-326)) crystal 2	D/D (added to rnAKAP18δ(76-326)) crystal 3
X-ray source	BESSY BL14.1	BESSY BL14.1	BESSY BL14.1
wavelength (Å)	0.9184	0.9184	0.9184
space group	$P6_522$	$P3_121$	$P6_522$
cell dimensions			
a (Å)	42.02	42.31	41.74
b (Å)	42.02	42.31	41.74
c (Å)	145.10	72.45	145.66
unit cell (Å)	$a = b = 90°$, c = 120 °	$a = b = 90°$, c = 120 °	$a = b = 90°$, c = 120 °
mol/asu	2	2	2
Resolution (Å)	2.4 (2.46-2.40)[a]	1.7 (1.74-1.70)	2.7 (2.74-2.70)
Completeness (%)	95.7 (88.5)	96.9 (90.3)	94.0 (71.5)
R_{sym} (%)	10.0 (85.2)	5.5 (61.1)	9.8 (71.5)
$I/\sigma I$	20.3 (3.5)	19.8 (2.9)	14.3 (2.75)

[a] The numbers in parentheses correspond to the highest resolution shell.
[b] $R_{sym} = \Sigma \mid I(h)_i - \langle I(h) \rangle \mid / \Sigma I(h)_i$ where $I(h)_i$ is the scaled observed intesity of the i-th symmetry related observation of the reflection h, $\langle I(h) \rangle$ is the mean value

All three crystals belong to a hexagonal space group, either $P6_522$ or $P3_121$. There is always one dimer found per asymmetric unit. After molecular replacement, it became clear that these crystals only contained the D/D domain and no AKAP, because no difference electron density for AKAP18δ was found. Thus, no further refinement was carried out. Furthermore, this result showed that the complex of AKAP18δ(76-326) and the D/D domain should not be separated after co-expression and co-purification.

3.4.3 Oligomerization state of mouse AKAP18γ constructs

To gain insights into the oligomerization state of the mouse AKAP18γ constructs and to be able to determine their molecular weights (MW), analytical gel filtration (aGF) in combination with static light scattering was performed. From the purification of the D/D domain, it was suggested that this protein might not only dimerize but also form higher oligomers.

The results for purified mmAKAP18γ(37-253) or mmAKAP18γ(37-287)+D/D are shown in **Fig. 28**. Both mmAKAP18γ(37-253) and mmAKAP18γ(37-287)+D/D elute as a single species from the aGF column.

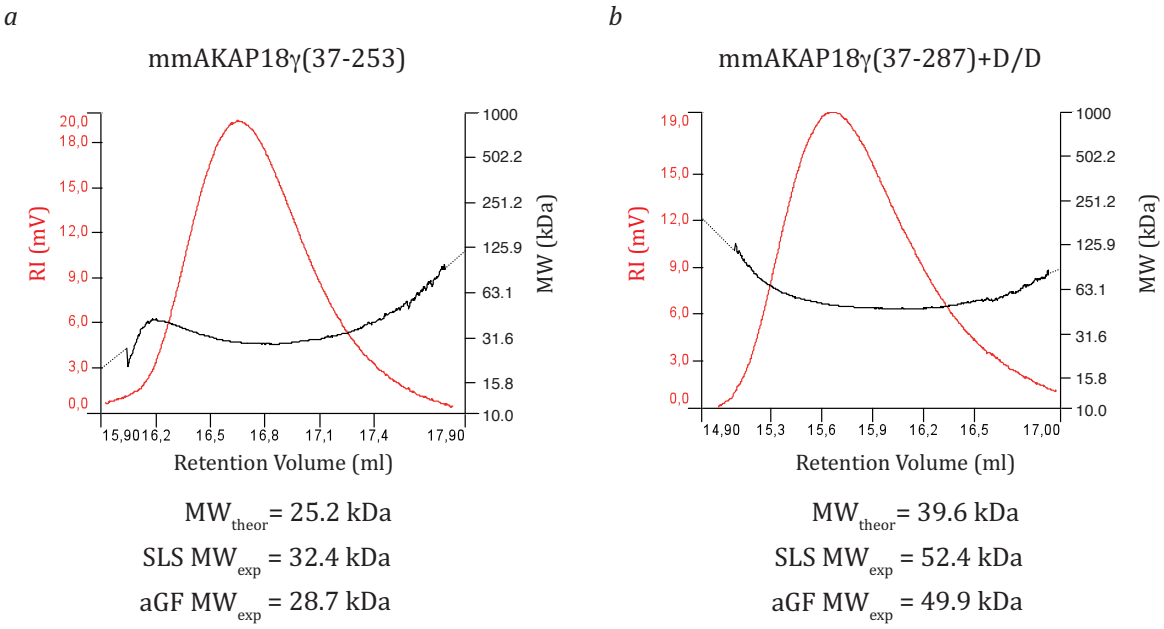

Fig. 28 Static light scattering (SLS) of mmAKAP18γ(37-253) and mmAKAP18γ(37-287) in complex with D/D. 100 µg of mmAKAP18γ(37-253) (***a***) or 200 µg of mmAKAP18γ(37-287) with D/D (***b***) were applied on a pre-equilibrated Superdex 200 size exclusion column and detection of UV at 280 nm, refractory index (RI), and right angle light scattering signal was performed by in-line detectors. Analysis of the results was carried out using the OmniSEC software. In the chromatograms, the RI is shown in red. The black lines indicate the calculated molecular weight of the respective protein/complex throughout the peak. Beneath each chromatogram, the theoretical molecular weight (MW_{theo}), and the experimental molecular weight (MW_{exp}) determined by analytical GF and static light scattering (SLS) are given.

The theoretical MW of mmAKAP18γ(37-253) is 25.2 kDa, whereas aGF gave a MW of 28.7 kDa and RALS 32.4 kDa. Accordingly, under these conditions mmAKAP18γ(37-253) was predominantly monomeric.

For mmAKAP18γ(37-287) in complex with a dimer of the D/D domain, the theoretical MW was 39.6 kDa. In aGF, a MW of 49.9 kDa was found and RALS resulted in a MW of 52.4 kDa. Additionally, the sample was polydisperse, as there was a difference of ~10 kDa between the left side of the peak (retention volume ~15.3 ml) and the right side of the peak (retention volume ~16.4 ml). The difference between the theoretical MW and the mean molecular weight found in RALS could be explained by the following: The refractive index increment dn/dc, the rate of change of the refractive index versus the concentration of the protein in solution at a given temperature, is set to 0.185 ml/g in the OmniSec software, but could slightly differ from that value for different proteins in solution [153]. The accuracy of the MW determination is highly dependent on this value, therefore an error in the MW is often observed.

The result obtained for mmAKAP18γ(37-287) in complex with D/D, i.e. a D/D dimer, would better fit to one mmAKAP18γ(37-287) with two D/D dimers bound to it, at least as observed at the retention volume of ~15.3 ml. Still, a tetrameric D/D domain is not known to bind to AKAPs. More likely, mmAKAP18γ(37-287) forms a complex with a D/D dimer with some unusual characteristics in RALS, and the mmAKAP18γ(37-287) – D/D complex itself does not form higher oligomeric structures.

3.4.4 Oligomerization state of human AKAP18β(43-83)

Human AKAP18β(43-83) was co-expressed and co-purified with D/D as described in chapter **3.1.5**. Surprisingly, it was observed that the D/D domain, even though overexpressed, was not co-purified as judged from SDS-PAGE (**Fig. 15**). At the most, D/D was present only in small amounts in comparison to that seen in the purification of AKAP18γ and δ isoforms. A sample of the pooled fractions after purification of hsAKAP18β(43-83) was analyzed by mass spectroscopy. Indeed, hsAKAP18β(43-83) was found but only traces of the D/D domain.

In order to investigate the oligomerization state of hsAKAP18β(43-83), analytical gel filtration and static light scattering was performed, similar to the experiments shown for mouse AKAP18γ constructs (see **3.4.3**). In **Fig. 29**a the result is given for the light scattering experiment for human AKAP18β(43-83) co-expressed with D/D. The corresponding gel filtration profile is depicted in **Fig. 29**b.

Human AKAP18β(43-83) has a theoretical molecular weight of 4.6 kDa. The main peak in the gel filtration profile corresponds to an experimental molecular weight of 18.9 kDa as determined by static light scattering. This hints at a tetrameric conformation of AKAP18β(43-83). The small peak around a retention volume of 10 ml has an experimental molecular weight of 42 kDa (data not shown). This could correspond to an octamer. The third peak visible in the gel filtration profile is aggregated protein in the void volume.

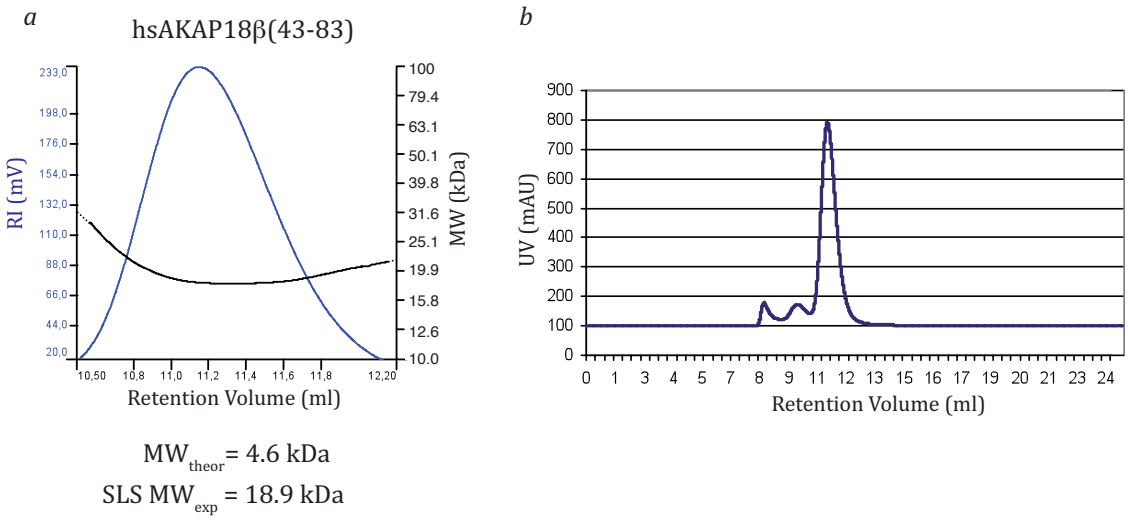

Fig. 29 Static light scattering (SLS) of human AKAP18β(43-83) co-expressed with D/D. 1 mg of hsAKAP18β(43-83) was applied on a pre-equilibrated Superdex 75 size exclusion column eith detection at 280 nm, refractory index (RI), and right angle light scattering signal was performed by in-line detectors. Analysis of the results was carried out using the OmniSEC software. In the chromatogram (***a***), the RI is shown in blue. The black line indicates the calculated molecular weight of hsAKAP18β(43-83) along the peak retention volume. Beneath the chromatogram, the theoretical molecular weight (MW_{theo}) and the experimental molecular weight (MW_{exp}) determined by static light scattering (SLS) are given. ***b***, UV Chromatogram of the standard size exclusion column run. Three peaks are visible. The chromatogram in *a* represents the result for the main peak.

3.5 Crystallization and preliminary X-ray diffraction analysis of human AKAP18β

Human AKAP18β(43-83) was shown to be a tetramer in solution (**3.4.4**). To understand the molecular basis for this assembly, structural studies of this short construct were performed with commercially available crystallization screens (**2.5.1**).

Crystals grew at 4 °C in two different conditions: 100 mM Hepes/NaOH pH 7.5, 25 % isopropanol, 100 mM $MgCl_2$ (ComPas, JBS) and 100 mM sodium-acetate pH 4.6, 30 %MPD, 20 mM $CaCl_2$ (JCSG, JBS). In the first condition, very fine needles appeared within 2 days. In the second condition, single, mostly hexagonal, and relatively large crystals of different shape and size were obtained after three weeks. Starting with these conditions, various fine screens were performed to optimize freezing and cryo conditions as well as crystal quality. **Fig. 30**a shows some representative examples of hsAKAP18β(43-83) crystals.

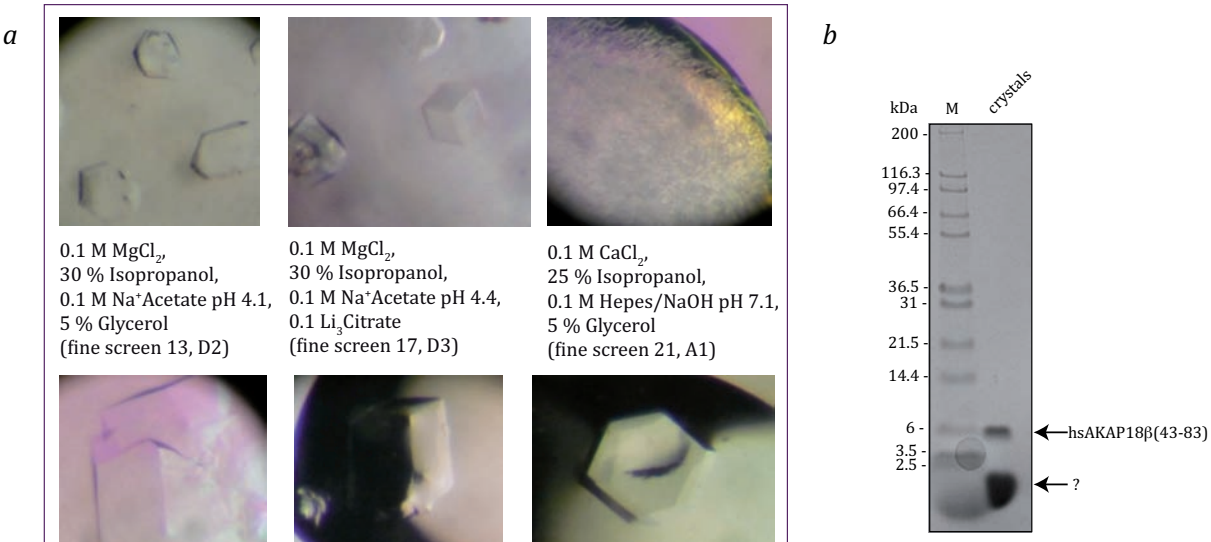

Fig. 30 Crystallization of hsAKAP18β(43-83) ***a***, Crystals of hsAKAP18β(43-83) with the respective crystallization conditions. Crystals grew in either isopropanol or 2-methyl-2,4-pentanediol (MPD) predominantly at acidic pH. ***b***, Analysis of crystal content by SDS-PAGE. Bands were cut out and tested by mass spectroscopy. Only the upper band could be clearly defined as protein.

To analyze the protein content, six crystals were dissolved in SDS sample buffer and separated by SDS-PAGE. Two Coomassie-stained bands were excised from the gel and analyzed by mass spectroscopy. It turned out that the upper band was indeed hsAKAP18β(43-83) but in the lower band, no protein was detected (**Fig. 30**b). The D/D domain in general can be detected by mass spectroscopy. The lower band might consist of degradation products of hsAKAP18β(43-83) that could not be detected by mass spectroscopy.

Crystals of hsAKAP18β(43-83) were very fragile upon disturbance of the saturated atmosphere within the crystallization plate. They tended to crack and dissolve easily. For that reason, it was necessary to quickly soak the crystals in the cryo solution and freeze them as rapidly as possible in liquid nitrogen. Extensive optimization of the cryo solution was necessary to minimize ice formation. The best results were obtained using 20 % ethylene glycol and 20 % isopropanol. Two examples of diffraction patterns are shown in **Fig. 31**. In total, more than 50 crystals were tested at BESSY synchrotron. In most cases, the resolution limit was worse than 6 to 7 Å.

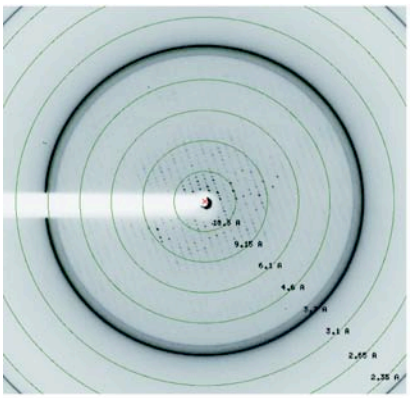

0.1 M $MgCl_2$,
30 % Isopropanol,
0.1 M Na^+Acetate pH 3.9,
(fine screen 5, D5b)
cryo: + 20 % PEG 200
resolution: ~ 7Å

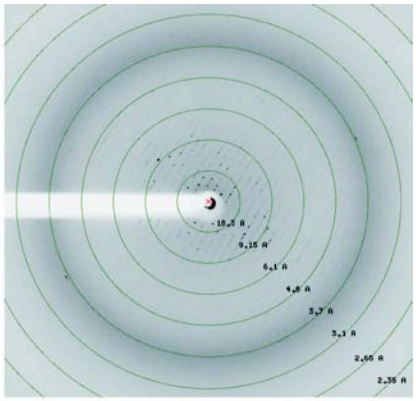

0.1 M $MgCl_2$,
29 % Isopropanol,
0.1 M Na^+Acetate pH 3.9,
(fine screen 5, C5)
cryo: + 30 % MPD
resolution: ~ 4-8 Å

Fig. 31 Diffraction pattern of hsAKAP18β(43-83) crystals collected at BESSY.

The best dataset obtained from hsAKAP18β(43-83) crystals is summarized in the data collection statistics in **Table 3** (see also chapter **2.5.2**).

Tab. 3 Data collection statistics hsAKAP18β(43-83) crystals.

Data collection	**hsAKAP18β(43-83)**
X-ray source	BESSY 14.1
wavelength (Å)	0.9184
space group	F222
cell dimensions	
a (Å)	136.5
b (Å)	186.7
c (Å)	188.8
unit cell (Å)	$a = b = c = 90°$
predicted mol/asu	14-36
solvent content (%)	74-32
Resolution (Å)	50-4.25 (4.5-4.25)[a]
No. of measured reflections	37765 (5972)
No. of unique reflections	8489 (1322)
R_{sym} (%)	6.2 (60.9)
$I/\sigma I$	12.43 (2.78)
Completeness (%)	93.7 (95.5)

[a] The numbers in parentheses correspond to the highest resolution shell.

[b] $R_{sym} = \Sigma \mid I(h)_i - \langle I(h) \rangle \mid / \Sigma I(h)_i$ where $I(h)_i$ is the scaled observed intesity of the i-th symmetry related observation of the reflection h, $\langle I(h) \rangle$ is the mean value

The best crystal diffracted to 4.25 Å resolution and belonged to space group F222, with relatively large unit cell dimensions of a = 136.5 Å, b = 186.7 Å, c = 188.8 Å, and $\alpha = \beta = \gamma = 90$ °, but also high symmetry. Matthews coefficient analysis indicated that the asymmetric unit contained between 14 and 36 molecules (corresponding to a solvent content of 74 % and 32 %, respectively). Phasing trials via molecular replacement using the programs Molrep and Phaser and using the structure of the AKAP-*IS* helix crystallized in complex with D/D (pdb file 2izx) as a search model were not successful, nor were attempts using a poly-alanine helix with the program Coot [168]. Also no molecular replacement solution was found with the structure of the D/D domain (pdb file 2izy). Because of the low resolution diffraction and the unusually high number of proteins in the asymmetric unit, structure solution was not further pursued.

3.6 Functional characterization of mouse AKAP18γ

3.6.1 AKAP18γ and δ localization

There are ambiguous results published concerning the localization of AKAP18γ isoforms. In most cases, AKAP18γ was found in the cytosol, in contrast to the AKAP18α and β isoforms that are membrane-bound. Only in one study, it was shown that endogenous AKAP18γ translocates to the nucleus of murine oocytes, and overexpressed human AKAP18γ localized to the nucleus of HEK293 cells. This effect was attributed to the existence of a nuclear localization signal (NLS) in [109]. Human, mouse, and rat AKAP18γ or δ isoforms, respectively, all contain this polybasic stretch near their N-terminus (KKRKK) which is known as a classical NLS motif [169].

To further investigate the localization of the longer AKAP18 constructs used for *in vitro* studies and to test for their functionality, mammalian expression vectors of rnAKAP18δ-fl and mmAKAP18γ(37-287) N- or C-terminally tagged with mCherry fluorescent protein were created. The truncated mouse construct was used, because it was not possible to clone the full-length construct from mouse brain cDNA. Nevertheless, its function as an AKAP should be tested *in vivo*. The constructs were transfected into HeLa and CHO cells as described in **2.6.2**. As a control, mCherry alone was overexpressed. Cells were fixed and mounted for confocal microscopy (see **2.6.3**). As can be seen from the overview in **Fig. 32**a, first tests showed a uniform distribution of AKAP18 isoforms in these cells, comparable to that of mCherry alone. A formerly observed reticular localization of AKAP18γ and δ constructs could not be verified. In addition, there were no differences in the localization of the truncated mmAKAP18γ(37-287) and full-length rnAKAP18δ.

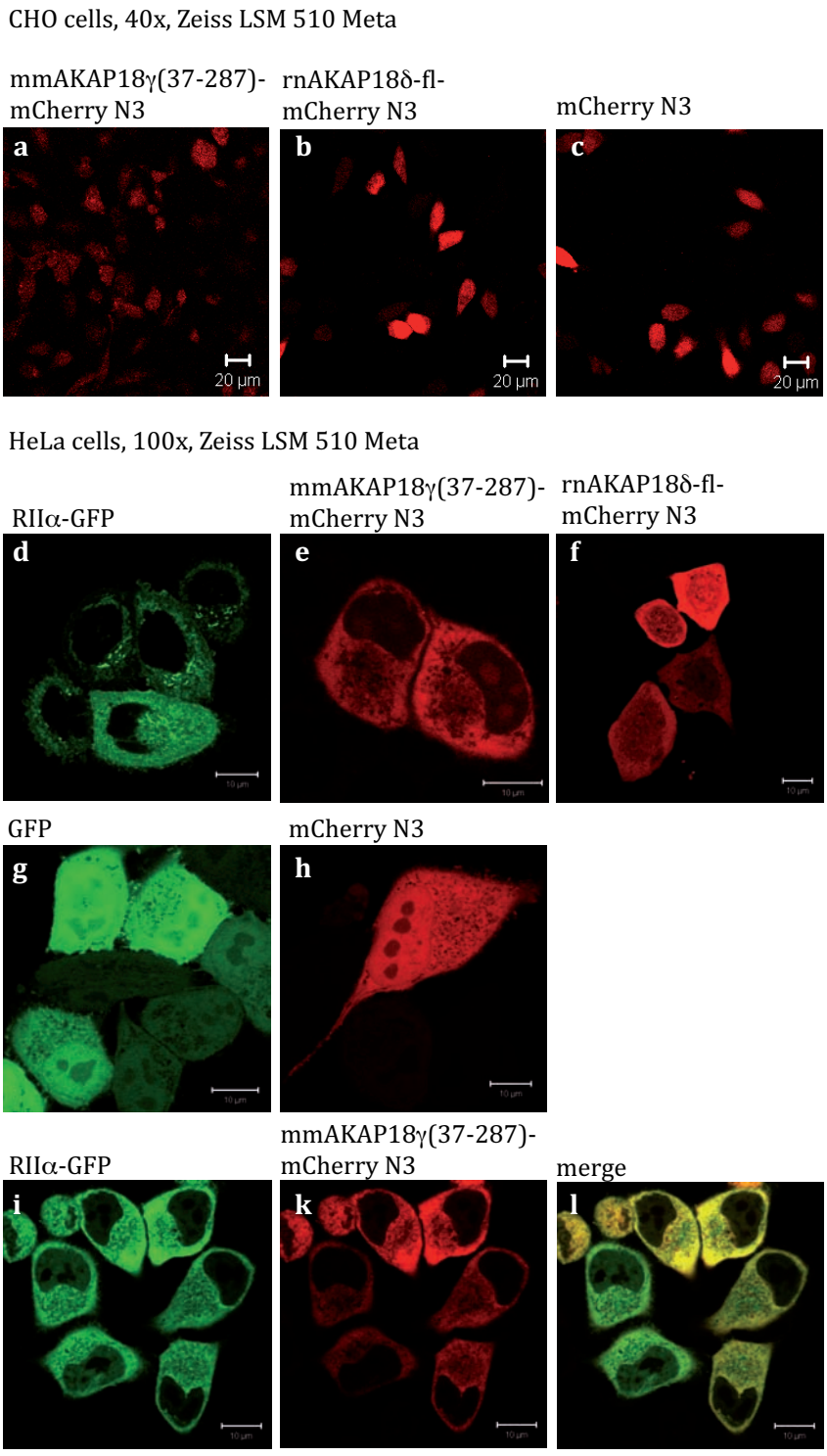

Fig. 32 Confocal microscopy images of ***a***, ***b***, and ***c***, fixed CHO cells over-expressing mCherry-tagged mouse AKAP18γ(37-287) or rat AKAP18δ wild type, or mCherry alone. ***d*** – ***l***, Living HeLa cells over-expressing RIIα-GFP alone (d), mCherry-tagged mouse AKAP18γ(37-287) alone (e), rat AKAP18δ wild type (f), and as a control GFP (g), or mCherry (h). Co-transfection of RIIα-GFP (i) mmAKAP18γ(37-287) (k) shows partial co-localization (merge, l).

In order to have a closer look at AKAP18 localization and its effect on co-expressed RIIα (C-terminally GFP-tagged), mmAKAP18γ(37-287) and rnAKAP18δ-fl with a C-terminal mCherry-tag were overexpressed in HeLa cells with or without RIIα-GFP. As shown in **Fig. 32**d, RIIα-GFP

alone localizes in the cytoplasm to a subcellular compartment near the nucleus that could be the Golgi apparatus. The nucleus is free of RIIα-GFP. Overexpressed mmAKAP18γ(37-287)-mCherry (**Fig. 32**e) or rnAKAP18δ-fl-mCherry (**Fig. 32**f) both are distributed all over the cytosol. Only about 5 % are found in the nucleus. In comparison, overexpression of GFP (**Fig. 32**g) and mCherry (**Fig. 32**h) alone gave a very different picture: The two fluorescent proteins are uniformly distributed in the cytoplasm, but tend to accumulate in the nucleus.

In the case of co-expression of mmAKAP18γ(37-287)-mCherry with RIIα-GFP (**Fig. 32**i-l) the overexpressed AKAP seemed to delocalize RIIα, and no Golgi-like staining was observed. In part, both proteins seemed to co-localize, leaving out the area close to the nucleus as observed before for mmAKAP18γ(37-287)-mCherry alone. Similar results were found for co-expression of rnAKAP18δ-fl-mCherry with RIIα-GFP (not shown).

Taken together, mmAKAP18γ(37-287)-mCherry and rnAKAP18δ-fl-mCherry both are found in the cytosol and do not translocate to the nucleus. The truncated mouse construct apparently is binding to RIIα-GFP as efficiently as the full-length rat construct, because it was able to re-localize RIIα in the same fashion. It represents a functionally active AKAP.

3.6.2 Cellular localization of mouse AKAP18γ(37-287) mutants

To analyze the function of the conserved His-X-Thr motif found by Gold and co-workers, mmAKAP18γ(37-287)-mCherry mutants were created that lack amino acid residues essential for 5´AMP binding. On the basis of the AKAP18δ core domain structure [135] mmAKAP18γ residue Phe^{140} (corresponding to Phe^{179} in rnAKAP18δ), His^{93} and Thr^{95} (His^{132} and Thr^{134}), or His^{185} and Thr^{187} (His^{224} and Thr^{226}) were mutated to alanine creating single or double mutants, respectively. To search for a cellular read-out for AKAP18γ function, mouse renal collecting duct (MCD4) cells, stably expressing aquaporin (AQP) 2 were transfected with wild-type mmAKAP18γ(37-287)-mCherry or either of the mutants (see **2.6.2**). Cells were stimulated with forskolin (FSK) for 30 min or left untreated and then prepared for immunofluorescence microscopy as described in **2.6.3**. The results are summarized in **Fig. 33**.

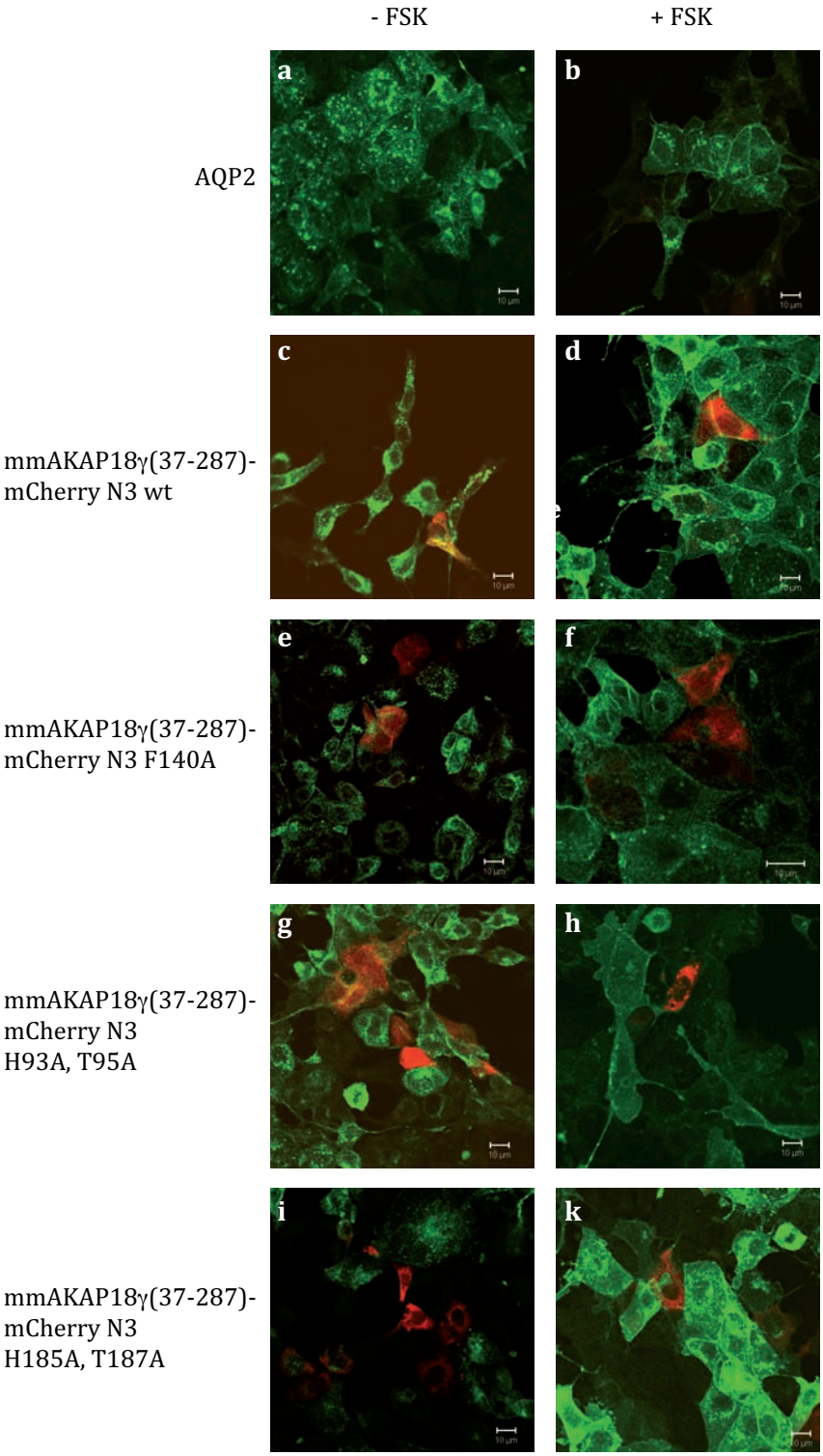

Fig. 33 Confocal microscopy images of MCD4 cells stably overexpressing aquaporin 2 (AQP2) with transient overexpression of different C-terminally mCherry-tagged mmAKAP18γ mutants. Cells were either left untreated (a, c, e, g, i) or treated with FSK for 30 min (b, d, f, h, k). ***a***, ***b***, AQP2 was stained by immunofluorescence, no additional plasmid was transfected. ***c***, ***d***, MCD4 cells were transfected with mmAKAP18γ(37-287)-mCherry wild type. ***e***, ***f***, MCD4 cells were transfected with mmAKAP18γ(37-287)-mCherry F140A mutant. ***g***, ***h***, MCD4 cells were transfected with mmAKAP18γ(37-287)-mCherry H93A, T95A double mutant. ***i***, ***k***, MCD4 cells were transfected with mmAKAP18γ(37-287)-mCherry H185A, T187A double mutant.

Upon stimulation with forskolin, a direct activator of adenylyl cyclases, cAMP levels increase and PKA is activated to phosphorylate AQP2 and thereby trigger AQP2 redistribution from intracellular vesicles to the plasma membrane [170]. As rat AKAP18δ has been implicated to play a role in AQP2 shuttling by bringing PKA in close vicinity to its substrate AQP2 in inner medullary collecting duct cells [118], it was tested whether overexpression of the mouse AKAP18γ constructs used in *in vitro* studies, including the nucleotide-binding deficient mutants, would influence AQP2 redistribution in MCD4 cells. Overexpression of the different mmAKAP18γ mutants did not seem to have any influence on AQP2 shuttling. Localization of mmAKAP18γ(37-287)-mCherry did not differ from its localization in HeLa cells (**Fig. 32**) and was mostly cytosolic. Co-localization with AQP2 was not observed. Only the mmAKAP18γ(37-287)-mCherry F140A mutant localized as well to the nucleus, at least in comparison to the other constructs. Taken together, overexpression of mmAKAP18γ(37-287) deficient in binding 5´AMP by does not interfere with AQP2-shuttling in MCD4 cells.

4 Discussion

AKAPs, like other scaffolding/anchor proteins, constitute the core of multi-protein signaling complexes by performing multiple functions. They possess a dynamic structure that adapts simultaneously to different binding partners, thereby bringing them into close proximity. They are additionally localized to specific compartments within the cell, thereby targeting the scaffolded proteins to these sites. The amount of structural information available on AKAPs is relatively low, as their structural flexibility and membrane binding properties, the very characteristics that define their function, hamper recombinant protein production and make AKAPs less amenable to structure determination.

Specifically because of that lack of information, solving the structure of an AKAP, including the PKA binding helix and in complex with its binding partners, was the aim of this work. This knowledge would provide us with fundamental insights into how these kinds of complexes are organized, and might reveal possible regulatory mechanisms of AKAP signaling modules. Structural characterization of AKAPs in complex with their binding partners is also of interest, as mutual influences between the scaffold and the recruited proteins are not well investigated.

To approach this topic, AKAP18 was chosen for structural investigation, with special regard to its interaction with PKA RIIα, phosphodiesterase 4D3, and phospholamban. Biochemical and biophysical characterization of these proteins was carried out to provide additional information on their properties and to inform the crystallization attempts.

4.1 Purification of A-kinase anchoring protein 18 isoforms

In general, milligram amounts of highly pure protein are a prerequisite for structural characterization. Target proteins can be engineered to increase their solubility and propensity to form single crystals that diffract X-rays. Therefore, various truncation constructs of different AKAP18 isoforms were cloned for expression in *E. coli* and tested for their expression and solubility. Protocols were established for large-scale purification of the most promising constructs.

Purification of full-length rnAKAP18δ proved to be very difficult, in large part because the protein is strongly prone to aggregation. An added GST-tag was found to promote solubility, in contrast to a His_6-tag that was not effective in preventing aggregation. Cleavage of the tag led to loss of the protein through precipitation, which could be reduced with high salt concentrations in the purification buffer (600 mM NaCl). When the crystal structure of the so-called AKAP18δ core domain, comprising amino acid residues 76 to 292, was published by Gold and co-workers [135], this structure along with secondary structure and disorder predictions was used as the

basis for the design of improved truncation constructs (see **Fig. 8**). It was subsequently possible to purify four different truncated forms of AKAP18δ that together cover the whole amino acid sequence of this protein: Constructs 1 (aa 1-292), 4 (76-292), 8 (aa 76-326), and 11 (aa 76-353). Constructs 8 and 11 both contained the PKA RIIα binding site and were co-expressed with their binding partner, RIIα or the D/D domain of RIIα. This strategy was successful in preventing the otherwise insoluble AKAP18δ constructs from aggregating and rendering them amenable to purification in large scale. As the affinity between AKAP18δ and RIIα or D/D is in the nanomolar range, co-purification of the two proteins was possible, and neither the RIIα nor the D/D domain contained an affinity tag for complex purification. The RIIα binding site of an AKAP in general is expected to be an amphipathic helix [78, 81, 82]. This also holds true for AKAP18 isoforms, as can be seen from the helical wheel projection of the PKA binding site of human AKAP18β (**Fig. 34**). It was therefore hoped that the hydrophobic part of this helix, which could trigger aggregation, would be protected by co-expression with the binding partner. The D/D domain was found to be most suitable for this approach, because full-length human RIIα was prone to degradation. Construct 4, the "core domain", and construct 8 both were chosen for further experiments, as purification of the other two AKAP18δ constructs yielded less protein.

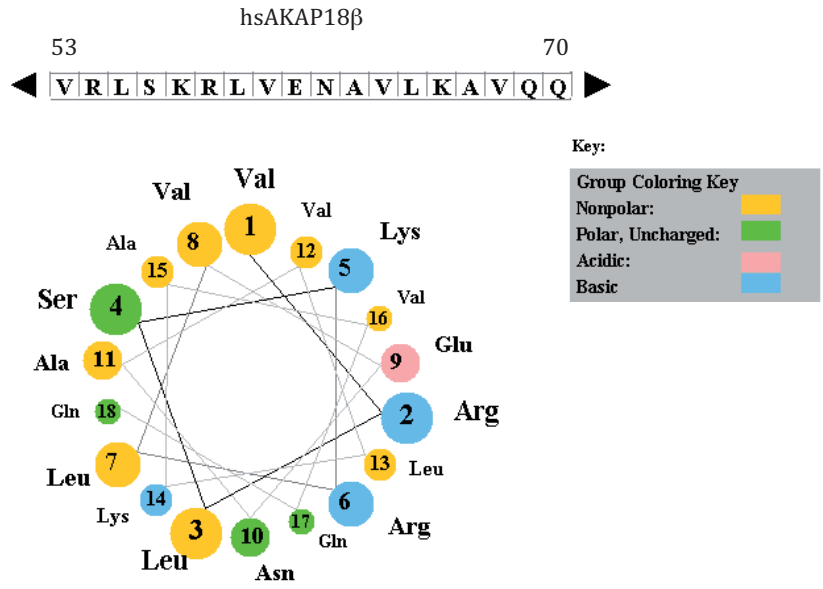

Fig. 34 Helical wheel projection of the amino acid sequence of human AKAP18β(53-70). The positions of the amino acid side chains are depicted along the axis of an α-helix in a view orthogonal to the paper plane. The color key of the different amino acid groups is given in the grey box. The section of hsAKAP18β comprising residues 53 to 70 was chosen as an example of an amphipathic portion of AKAP18β(43-83). On the left side of the helix, mostly nonpolar and uncharged residues are found whereas the right side of the helix contains several charged residues. The figure was produced using a Java Applet by Edward K. O´Neil and Charles M. Grisham (Univ. of Virginia), which is accessible online at http://cti.itc.virginia.edu/~cmg/Demo/wheel/wheelApp.html.

It has long been recognized that amino acid differences between homologous proteins from different species may be exploited to identify proteins that form single crystals for X-ray crystallography [171-173]. In the attempt to obtain highly purified protein suitable for crystallization, human and mouse AKAP18γ constructs comprising the AKAP18 core domain and the core domain plus the PKA binding site were also cloned in the rat AKAP18δ construct formats. The mouse constructs were cloned from mouse brain RNA after reverse transcription into cDNA. It was not possible to clone full-length mmAKAP18γ.

To eliminate flexible parts of the protein that might interfere with crystallization, several shorter constructs of mouse and human AKAP18γ and rat AKAP18δ were cloned (**Fig. 12**). These additional truncations by 10 to 20 amino acids did not influence the solubility of the proteins or the yield of complex purification. Optimization of the purification conditions resulted in protein more than 95 % pure. 600 mM sodium chloride in the purification buffers not only kept the AKAP18γ or δ - D/D complexes in solution, but also helped to remove bound DNA.

Using the co-expression and co-purification strategy applied for the longer AKAP18 isoforms containing the PKA binding site, hsAKAP18β(43-83) was also co-expressed with the D/D domain with the intention of purifying the complex. The PKA binding regions in AKAP18 isoforms are highly conserved as can be seen from the alignment in **Fig. 35**.

```
                          *   10    *   20    *   30    *   40
hsAKAP18beta    43 : NGGEPDDAELVRLSKRLVENAVLKAVQQYLEETQNKNKPGE :  83
hsAKAP18gamma  265 : NGGEPDDAELVRLSKRLVENAVLKAVQQYLEETQNKNKPGE : 305
mmAKAP18gamma  253 : DRREPEDAELVRLSKRLVENAVLKAAQQYLEETQNKKQPGE : 293
rnAKAP18delta  292 : DRKEPEDAELVRLSKRLVENAVLKAVQQYLEETQNKKQPGE : 332
```

Fig. 35 Alignment of the PKA RII-binding sites of different AKAP18 isoforms in human (hs), mouse (mm) and rat (rn). Conserved residues are boxed in dark green, 80 % conserved residues are boxed in light green and yellow boxes indicate 60 % sequence conservation.

Both the D/D domain and hsAKAP18β(43-83) showed good over-expression in *E. coli*. But surprisingly, purification and crystallization of hsAKAP18β(43-83) revealed that this 41 amino acid peptide forms crystals without the D/D domain (**Fig. 30**). Less than 5 % of the final purification yields contained the hsAKAP18β(43-83) – D/D complex, while more than 95 % of the over-expressed D/D domain is lost after the first affinity chromatography column (**Fig. 15**). These results were confirmed both by SDS-PAGE analysis and mass spectroscopy and are in contrast to the observation that constructs of the longer AKAP18 isoforms γ and δ, which contain the PKA RIIα binding site, must be co-expressed with D/D or RIIα to render them soluble and to prevent aggregation.

4.2 Structural investigation of AKAP18 isoforms

4.2.1 Crystallization and preliminary X-ray diffraction of human AKAP18β(43-83)

It could be shown that hsAKAP18β(43-83) forms higher homo-oligomeric complexes that remain soluble in the absence of the D/D domain. This can be concluded from the apparent molecular weight in analytical gel filtration ranging from 16 to 34 kDa (trimer to heptamer) with 4.6 kDa as the theoretical molecular weight of hsAKAP18β(43-83). In addition, static light scattering indicated a tetrameric conformation with an experimental molecular weight of 18.9 kDa (**Fig. 29**). An additional small peak corresponding to an experimental molecular weight of 42 kDa could be explained by formation of an octamer.

To understand the molecular determinants of this assembly, structural investigations of hsAKAP18β(43-83) were performed. Crystals of this peptide grew under different conditions containing 20 – 30 % isopropanol or MPD. But despite many efforts to optimize crystal quality by varying these conditions, most crystals only diffracted X-rays with a resolution limit above 6 to 7 Å.

The statistics of the best data set that was collected (summarized in **Table 3**) showed a resolution of 4.25 Å. At least 14 to 36 hsAKAP18β(43-83) peptides were present in the asymmetric unit of the crystal and the unit cell was relatively large (a = 136.5 Å, b = 186.7 Å, c = 188.8 Å). Unfortunately, it was not possible to solve the crystal structure of hsAKAP18β(43-83), since molecular replacement was impossible with this high number of molecules in the asymmetric unit. Neither the AKAP-*IS* helix from the crystal structure in complex with D/D by Gold and co-workers [81], nor a poly-alanine helix created from this template, nor the D/D domain proved suitable for molecular replacement. Of course, there is the possibility of trying to generate a different crystal form of hsAKAP18β(43-83). In order to achieve this, it may be necessary to design shorter constructs of the PKA binding helix to remove flexible residues at the N- and C-termini of the original construct. Should this effort yield crystals that diffract to a higher resolution than 4 Å and/or that belong to a different space group and have smaller unit cell dimensions, molecular replacement may be possible.

Without a crystal structure, it can only be speculated how hsAKAP18β(43-83) oligomerizes and why it is soluble in the absence of the D/D domain. During the co-expression and co-purification process, the peptide alone does not bind the D/D domain as efficiently as it does in the context of the longer AKAP18 constructs. **Fig. 34** shows the section of the PKA binding site of AKAP18β (highly similar to that of the other AKAP18 isoforms) that forms the amphipathic helix. It is possible that several of these amphipathic helices oligomerize, most likely forming a tetramer, and that in this way the hydrophobic faces of the helices are shielded from the environment. This interaction seems to be of an even higher affinity than that determined for the AKAP18 -

RIIα interaction, which is already in the nanomolar range [108]. Thus, the D/D domain was not necessary to solubilize hsAKAP18β(43-83) and therefore was not co-purified.

The longer AKAP18γ and δ isoforms did not oligomerize like hsAKAP18β(43-83), although containing exactly the same amino acid sequence as the short peptide. Static light scattering results indicated that mouse AKAP18γ constructs did not form oligomers, neither the core domain (amino acids 37-253 in mouse) alone, nor the construct containing the PKA binding site in complex with D/D (amino acids 37-287 in mouse) (**Fig. 28**). Separation of the preformed complex of rnAKAP18δ(76-326) and D/D led to the aggregation of AKAP18δ and formation of D/D crystals (see **Fig. 27**). The aggregation of AKAP18δ(76-326) was likely triggered by the amphipathic helix, because the core domain (amino acids 76-292 in rat) does not aggregate. Thus, the D/D domain was required to "buffer" hydrophobic patches in the protein, thereby rendering AKAP18 γ and δ constructs containing the PKA-binding helix soluble.

It would be very interesting to know the structure of the AKAP18β(43-83) oligomer. Perhaps oligomerization is of physiological relevance for the stability or activity of the AKAP18α and β isoforms, which both contain this highly conserved sequence. They localize to the plasma membrane, where they might form oligomers in the absence of their interaction partners and could disassemble into monomers in the presence of an interacting protein.

4.2.2 Structural investigation of AKAP18γ and δ in complex with D/D

As mentioned above, one aim of this work was to determine the structure of a complex of AKAP18γ or δ with the D/D domain of RIIα by X-ray crystallography to understand the molecular basis of this interaction and to study the interplay between the AKAP18γ/δ core domain and the PKA RIIα D/D domain. Unfortunately, despite many efforts, crystallization was not successful, either with commercially available or self-developed screens.

Besides optimization of the expression constructs and purification conditions described above (**4.1**), thermal shift assays (TSAs) were performed to further optimize the buffer conditions of the AKAP18γ and δ constructs in complex with D/D and to stabilize the proteins (**Fig. 27**). Crystallization screens had already shown that citrate buffer stabilized the complex since in this buffer precipitation was only apparent at higher protein concentrations (15 to 20 mg/ml instead of 10 mg/ml). In TSAs it was found that citrate buffer at pH 5.0 and 6.0 increased the thermal stability of AKAP18 – D/D complexes (T_m shifted from ~39 °C to ~44 °C for pH 5.0 and ~49 °C for pH 6.0). Additionally, it was verified that increasing NaCl concentrations from 100 mM to 300 mM led to stabilization of AKAP18δ(76-292). The presence of 5´AMP also increased the melting temperature of AKAP18δ(76-292) by 2 °C (data not shown). However, incorporating

these stabilizing conditions into the crystallization screens did not result in crystals of rat AKAP18δ or mouse AKAP18γ constructs in complex with D/D.

Two further attempts to modify the complexes to enhance the chances for crystallization were made: methylation of lysine residues to reduce surface entropy and limited proteolysis of the protein using trypsin and chymotrypsin; neither approach resulted in crystals.

One explanation for why AKAP18γ or δ in complex with the D/D domain failed to crystallize could be heterogeneity of the sample. Despite the high purity of the complex (>90 %, see **Fig. 13**d), the chromatogram shows a small shoulder (**Fig. 13**c), which hints at the presence of a different protein species, e.g. degradation products or contamination with other proteins or nucleic acids not visible in SDS-PAGE. In addition, NMR experiments suggested conformational heterogeneity of the rnAKAP18δ(76-326) - D/D complex, because comparison with the ^{1}H-^{15}N HSQC spectrum of rnAKAP18δ(76-292) (**Fig. 18**) revealed that only about 70 new peaks appear despite the presence of 76 additional amino acids in the complex, which should at least give rise to 76 new peaks. Because of signal overlapp, the exact number of missing peaks cannot be determined. Furthermore, static light scattering showed polydispersity of the sample containing the complex between mmAKAP18γ(37-287) and D/D (**Fig. 28**). The mean experimental MW was 52.4 kDa, but the MW at the left side of the peak (retention volume ~15.3 ml) was about 10 kDa higher than at the right side of the peak (retention volume ~16.4 ml). This 10 kDa discrepancy could account for the presence of an additional D/D dimer in the AKAP – D/D complex, because the theoretical MW of a D/D monomer is 4.6 kDa, and suggests heterogeneity of the sample. This may have interfered with crystallization of the mmAKAP18γ(37-287) - D/D complex.

In general, the co-purified AKAP18γ or δ - D/D complexes were left intact. However, the molar ratio of AKAP and D/D is expected to be 1:2, as the D/D domain always forms a dimer that binds to the PKA binding helix in the AKAP [40, 78, 81, 82]. It was not clear whether the sample of the purified complex was homogenous. Therefore, in an early attempt to reconstitute a defined complex of rat AKAP18δ(76-326) and the D/D domain with a 1:2 molar ratio, the purified complex was first separated using a very high salt concentration (1 M NaCl) and separately purified D/D was added to free AKAP18δ(76-326) (see also chapter **3.4.2**). Instead of the complex, the D/D domain crystallized alone despite the presence of AKAP18δ (**Fig. 27**). The D/D structure was not refined any further since the structure of this D/D domain (e.g. pdb file 2izy [81]) was already known. In this context, it became clear that in the absence of the D/D domain, AKAP18γ or δ containing the PKA binding site is suited neither for crystallization nor for solution binding studies.

In NMR spectroscopy experiments, it was found that purified rat AKAP18δ(76-292) adopted a stable compact structure, as overall dispersion of the ^{1}H and ^{1}H-^{15}N HSQC spectra was good. The

addition of 5´AMP led to chemical shift perturbations (**Fig. 16**), consistent with the finding by Gold and co-workers that this nucleotide binds to AKAP18δ(76-292) [135]. This result further implied that the purified protein was correctly folded. However, only an assignment of the peaks could answer the question of whether those peaks that shift correspond to the amino acid residues involved in 5´AMP binding in the crystal structure. This would require additional labeling of the protein with ^{13}C as well as deuteration of the sample. Structure determination by NMR spectroscopy was not pursued as the structure of the core domain in complex with 5´AMP had already been solved by X-ray crystallography [135].

In contrast, NMR spectroscopy may be the method of choice to determine the structure of the longer AKAP18δ(76-326) construct bound to the D/D domain, as this complex failed to crystallize (see above). It was also ^{15}N-labeled and probed using NMR spectroscopy as shown in **Fig. 18**. Comparison with the spectrum of the short AKAP18δ construct revealed that the overall resolution was reduced, as seen by peak overlap. However, an assignment of the peaks and, eventually, structure determination would in principle be possible though difficult, since the size of the complex (~40 kDa) approaches the limits of what is attainable with standard solution-state NMR. Nevertheless, the complex with D/D was also folded, because the ^{1}H-^{15}N HSQC spectrum showed the good peak dispersion expected for a folded protein, thus making peak assignment tractable.

4.3 Binding studies on AKAP18

4.3.1 Interaction studies of rat AKAP18δ with PDE4D3 and phospholamban

Rat AKAP18δ has previously been found not only to interact with PKA, but to form a signaling complex with other proteins involved in signal transduction, like phosphodiesterase PDE4D3 on aquaporin bearing vesicles in inner medullary collecting duct cells of the kidney [122]. Additionally, AKAP18δ was identified as the anchoring protein responsible for mediating the interaction between PKA and phospholamban (PLN) in cardiac myocytes, which influences SERCA activity [124]. To understand the underlying molecular mechanisms of these interactions, structural investigation of the interaction of rnAKAP18δ with both PLN and PDE4D3 was undertaken.

Interaction of AKAP18δ(76-292) and AKAP18δ(76-326)+D/D with synthesized PDE4D3 and PLN peptides was probed in NMR experiments (see chapter **3.2.1**). The amino acid sequence of these peptides was chosen to correspond to the interaction sites with GST-, GFP- or YFP-tagged AKAP18δ as identified in peptide spot arrays and pull-down assays [122, 124]. Additionally, longer PDE4D3 constructs were cloned and purified that contained either one or both of these

interaction sites (**Fig. 21**) and were used for interaction studies with AKAP18δ constructs using ITC, analytical gel filtration, and pulldown studies.

PDE4D3(341-365), but none of the other PDE4D3 or PLN peptides, induced minor structural changes in AKAP18δ(76-292) as inferred from NMR chemical shift changes, including the loss of some peaks (**Fig. 16**). Generally, the signal to noise ratio was low in these experiments, which made the chemical shift perturbations observed less significant than those seen upon addition of 5´AMP (see above). Furthermore, it should be considered that the PDE4D3(341-365) peptide is poorly soluble in aqueous buffers in contrast to PDE4D3(586-610). It is therefore possible that some of the chemical shift changes were due to non-specific interactions with AKAP18δ(76-292).

Crystallization screens set up directly from the NMR sample yielded crystals that only contained AKAP18δ(76-292). No difference electron density for the PDE4D3(341-365) peptide was found in the electron density map. As the structure of AKAP18δ(76-292) was already published, no further refinement was carried out. If there was an interaction between AKAP18δ(76-292) and PDE4D3(341-365), the affinity was too weak for co-crystallization with the peptide.

The other peptides used for interaction studies by NMR spectroscopy did not bind. It is possible that the short peptides used lacked critical portions of the respective binding sites, thereby preventing peptide binding to AKAP18δ(76-292). In the case of the interaction with PLN, it might be that the pentameric form of PLN is needed for the AKAP18δ - PLN interaction, although there were hints that AKAP18δ primarily binds to the monomer [124]. As monomeric PLN interacts with PKA [128], it is more likely that AKAP18δ interacts with the PLN monomer rather than with the pentamer to mediate PLN phosphorylation. Furthermore, the presence of SERCA may also be required for the AKAP18δ - PLN interaction. And since PLN is a membrane protein, lipids as well may promote the interaction. The polybasic stretch in the N-terminus of AKAP18δ might facilitate the interaction with membrane proteins like PLN.

Because of its membrane localization, PLN is much more difficult to investigate than PDE4D3. For this reason, further experiments were carried out focusing on the AKAP18δ - PDE interaction. In order to investigate additional parts of PDE4D3 apart from those regions that were mimicked by the peptides used in NMR spectroscopy, four PDE4D3 expression constructs were cloned as mentioned above. Expression and solubility was tested for all of the four constructs and large-scale purification was established for the shortest and the longest constructs (**Fig. 21**). The purified PDE4D3 constructs were catalytically active as determined by HPLC-based nucleotide detection (**Fig. 22**) and thus folded correctly. They were used for ITC experiments and for analytical gel filtration experiments to detect interaction with rnAKAP18δ(76-292). Neither method verified complex formation. It is possible that these *in*

vitro assays with highly pure proteins lack an additional component present in only partially purified proteins or in the whole cell lysates used in pull down studies. Additionally, the results of the peptide spot assays in general depend not only on the protein used as interaction partner and the method used to detect the interaction, but also on the spot synthesized peptides themselves. If these peptides, for instance, are highly charged, they may lead to non-specific interactions, giving rise to false positive results [174].

The presence of cAMP (expected to be degraded to 5´AMP by PDE4D3) during analytical gel filtration also did not promote complex formation (**Fig. 23**). When working with truncated proteins it is always possible that some parts of the protein essential for the interaction are absent. Unfortunately, full-length PDE4D3 and rnAKAP18δ were not suited for large-scale preparation due to extensive degradation and propensity to aggregation. As a result, structural investigation of PDE4D3 and rat AKAP18δ interaction was not pursued further.

4.3.2 Nucleotide binding to AKAP18γ and δ isoforms

AKAP18δ(76-292) was shown to bind 5´AMP and 5´CMP by Gold and colleagues [135]. They co-crystallized the AKAP18δ core domain with both nucleotides and from that estimated the K_D to be in the mid-micromolar range. By equilibrium fluorescence binding using 2'- (or 3')-O-(N-methylanthraniloyl) adenosine 5'-monophosphate (MANT-AMP) instead of 5´AMP, they determined the K_D for MANT-AMP binding to AKAP18δ(76-292) to be ~ 200 µM. In contrast, ITC measurements conducted in this work indicated an approximately ten fold lower K_D of 18±0.6 µM for 5´AMP binding to rnAKAP18δ(76-292) (**Fig. 24**d). The interaction was additionally verified by NMR spectroscopy (**Fig. 16**c und d). Furthermore, it was shown that not only rat AKAP18δ but also mouse AKAP18γ(37-253), which is thought to be equivalent to the rat core domain, can bind 5´AMP with a K_D of 60±2 µM. This is not very surprising, as there is about 96 % sequence identity between rat and mouse AKAP18δ and γ, respectively, in the core region.

It was expected that the presence of the PKA binding site in mmAKAP18γ in complex with the D/D domain might have an influence on nucleotide binding. But this was not the case. Mouse AKAP18γ(37-287) in complex with D/D bound 5´AMP with a K_D of 43±2 µM, which is only slightly higher affinity than in absence of D/D and the PKA binding site.

In contrast to the results by Gold and co-workers, binding of 5´CMP was never observed in ITC experiments (**Fig. 25**). This is remarkable, as they were able to solve a crystal structure of rnAKAP18δ(76-292) with 5´CMP bound (pdb file 2vfl). Maybe the interaction is very weak, and as the crystals grew in the presence of an excess of 5´CMP (5 mM), the nucleotide might only be found in the crystal under these conditions. Concerning 5´AMP, a nucleotide concentration of

670 µM was sufficient to detect difference electron density for 5´AMP in the electron density map. A K_D value for the binding of 5´CMP to rnAKAP18δ(76-292) was not reported. The finding that cAMP did not bind to rnAKAP18δ(76-292) corresponds to the results found in ITC experiments performed in this thesis.

The question remains, why do mouse and rat AKAP18γ and δ bind nucleotides? In the crystal structure, the phosphate moieties of 5´AMP and 5´CMP are coordinated by the two conserved His-X-Thr motifs [135]. This motif is found in all members of the 2H phosphoesterase family with X most often being a hydrophobic residue [140]. Alignment of the long rat, mouse, and human AKAP18 isoforms as well as alignment of AKAP18δ core domain sequences with amino acid sequences of other members of the 2H phosphoesterase family (see Appendix **5.2** and **5.3**) reveal that all of the proteins contain this motif twice. It forms the active site in most of the proteins but the reactions they catalyze are different, and range from nucleic acid metabolism to signal transduction.

It is remarkable that the overall sequence similarity in the 2H phosphoesterase family is below 20 % (see Appendix **5.3**) whereas the fold is very much conserved [140]. As an example, structural alignment of rat AKAP18δ(76-292) and the 2´-5´RNA ligase of *T. thermophilus* is shown in **Fig. 36**. The sequence identity of the two proteins is only 18 %, but the structures align with an rmsd of 1.9 Å for equivalent Cα atoms. Most importantly, the two signature His-X-Thr motifs have a very similar position at the bottom of the cleft between the two lobes (**Fig. 36**b).

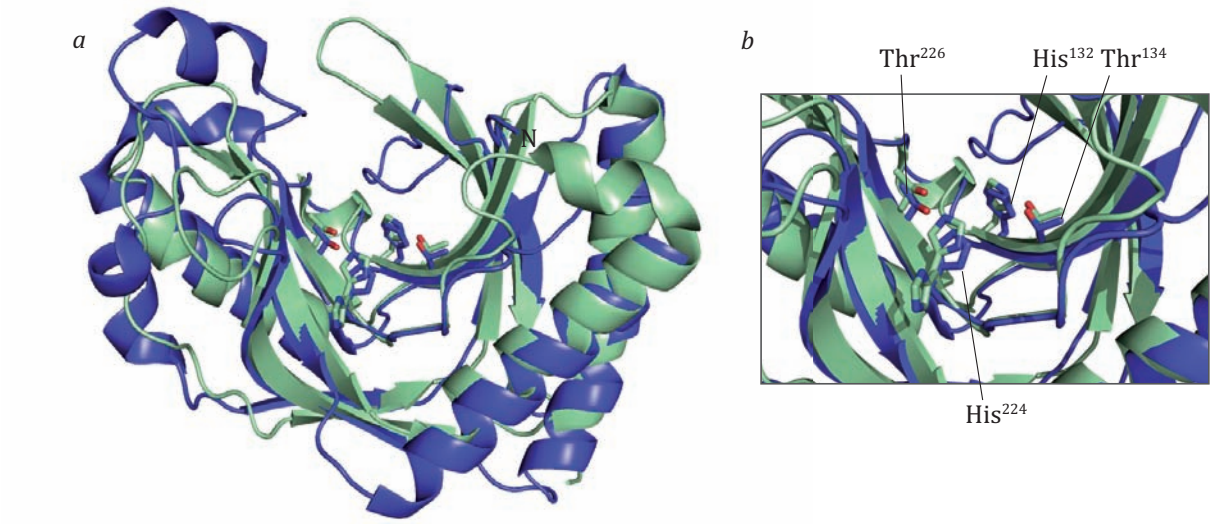

Fig. 36 Structural differences between the rat AKAP18δ core domain and the 2´-5´ RNA ligase from *Thermus thermophilus*. ***a***, The pdb files of AKAP18δ(76-292) (2vfk, in blue) and the 2´-5´RNA ligase (1iuh, in light green) were aligned using the program Coot and further processed using PyMOL (Delano Scientific). The backbone atoms are shown in the ribbon representation with the side chains of the conserved His-X-Thr motifs shown as sticks. ***b***, Close-up view of the His-X-Thr motifs. The residues of the signature motifs of the two molecules align very well. Residue numbers are given corresponding to the AKAP18δ(76-292) structure. His^{224} corresponds to His^{130} in the 2´-5´ RNA ligase, which has two conformations in the crystal.

The overall fold of AKAP18δ(76-292) has the highest similarity with that of the bacterial RNA ligases. Comparison of the structures of AKAP18δ(76-292) with the 2´,3´cyclic phosphodiesterase (CPDase) from *A. thaliana* (pdb file 1fsi, rmsd 2.6 Å, sequence identity 13 %) and human brain 2´,3´cyclic nucleotide phosphodiesterase (CNP) (pdb file 1woj, rmsd 3 Å, sequence identity 12 %) shows that the structures are substantially different from each other. Despite their divergence however, in all cases, the His-X-Thr motifs are found at the bottom of the cleft between the two lobes.

Up to now, no enzymatic activity of AKAP18γ or δ has been found. On the basis of the structure of AKAP18δ(76-292), Gold and co-workers considered how AKAP18δ could theoretically catalyze the ligase reaction. In this scheme, a 5´ and a 3´ half-tRNA molecule with a 2´,3´-cyclic phosphate at the 5´ fragment and a free 5´OH at the 3´ fragment are joined together by the ligase to form a 2´-5´phosphodiester linkage [142].

Maybe AKAP18 γ and δ isoforms do not have any enzymatic activity. Rather, nucleotide binding might be used in the context of signaling and might influence interactions with other proteins and/or the localization of AKAP18γ and δ in the cell. To test this, mCherry-tagged mmAKAP18γ wild type and mutants presumably deficient in nucleotide binding, were over-expressed in MCD4 cells stably over-expressing AQP2 and localization was assessed with immunofluorescence microscopy (**Fig. 33**). Mouse AKAP18γ(37-287) did not co-localize with AQP2 and also did not seem to influence AQP2 redistribution upon FSK stimulation. Mutating residues involved in nucleotide binding, especially the His-X-Thr motifs to alanine (His^{93} and Thr^{95} (corresponding to His^{132} and Thr^{134} in rnAKAP18δ), His^{185} and Thr^{187} (His^{224} and Thr^{226} in rnAKAP18δ), or Phe^{140} (Phe^{179} in rnAKAP18δ)), also did not alter AQP2 shuttling. The overall distribution of the C-terminally mCherry-tagged AKAP18γ constructs was very much the same in HeLa cells (**Fig. 32**) namely mostly cytosolic, except for the mmAKAP18γ(37-287)-mCherry F140A mutant. A minor fraction of this mutant was consistently found in the nucleus.

In general, over-expression of mmAKAP18γ(37-287) deficient in binding 5´AMP did not alter AQP2 shuttling. Maybe a quadruple mutant of both His-X-Thr motifs involved in 5´AMP binding is required to observe an effect, corresponding to the approach by Gravel and co-workers, who describe such a mutant form of the above mentioned brain 2´,3´cyclic nucleotide phosphodiesterase [175]. This mutant lacks catalytic CNPase activity, but RNA-binding is not decreased in comparison to wild type CNP. The authors suggest that catalytic activity and RNA-binding might be two independent properties of this domain [175]. Similarly, in AKAP18γ and δ, nucleotide binding seems to be independent of any obvious catalytic activity and likewise it might not be associated with regulation of the PKA - AKAP interaction (or of that with other binding partners). Of course, AKAP18γ and δ isoforms might be involved in many other signaling

pathways apart from PKA-mediated AQP2-shuttling, e.g. AMP kinase signaling as suggested before [135]. Additionally, there may be an influence of nucleotide binding deficient mutants on SERCA activity in heart muscle cells [124].

Concerning targeting of the longer AKAP18 isoforms, the putative nuclear localization signal (NLS) proposed by Brown and colleagues [109] does not seem to be functional, at least under the experimental conditions used in this study. If there were nuclear translocation of AKAP18γ (or δ) this would raise the question of its function in the nucleus. PKA activity in the nucleus is described as resulting from free C subunits that diffuse passively into the nucleus, as the holoenzyme or the R subunit dimer is too large to enter [12, 176]. In this case, nuclear translocation of AKAP18 would suggest that it would mediate the active transport of the PKA holo-enzyme into the nucleus, although the fact that AKAP18γ and δ are nucleotide-binding proteins allows for the conclusion that these proteins might have a function inside the nucleus apart from PKA anchoring. But, in spite of these considerations, nuclear shuttling was not observed for mCherry-tagged wild-type AKAP18δ or mmAKAP18γ(37-287) co-expressed with RIIα-GFP in confocal microscopy studies (**Fig. 32**), except for the minor fraction of the mmAKAP18γ(37-287) F140A mutant that was found to localize to the nucleus, as mentioned above.

The NLS might also be interpreted as a polybasic stretch that is needed for membrane targeting of the AKAP18 isoforms that do not contain an acylation site, as do the α and β isoforms. Polybasic regions can interact with the negatively charged head groups of phospholipids in the membrane via electrostatic interactions. At least for rat AKAP18δ, it was shown that it interacts with membrane proteins, e.g. phospholamban [124], or resides on AQP2 bearing vesicles [118]. In each case, a phospholipid membrane is in close vicinity and protein – protein interactions could be stabilized by additional membrane attachment of the AKAP.

4.4 Outlook: AKAP18 as drug target

AKAPs have been shown to play a role in a variety of physiological processes such as the control of β-adrenergic signaling and therefore cardiac myocyte contractility in the heart, and of exocytotic processes associated with water reabsorption in polarized epithelial cells of the kidney [12].

In the heart, PKA regulates the force (inotropy) and the rate (chronotropy) of heart contraction through phosphorylation of several target proteins, e.g. the ryanodin receptor (RyR), L-type calcium channels, troponin I, and phospholamban. Targeted PKA action is necessary to coordinate each protein's function. For example, the $Ca_V1.2$ calcium channel is recruited into a

macromolecular complex with PKA mediated by AKAP18α [116]. Recently, it was shown that AKAP18α was necessary for reconstitution of PKA-dependent regulation of $Ca_V1.2$ channel activity in non-muscle cells [177]. Additionally, AKAP18δ anchors PKA in close proximity to PLN and thereby regulates SERCA activity [124]. Disruption of targeting of protein kinase A by AKAPs in cardiac myocytes has been implicated in human disease. A mutation found in AKAP9 (also called Yotiao) leads to impaired interaction with the potassium channel KCNQ1, which renders the potassium channel unresponsive to cAMP-dependent regulation and leads to the phenotype of delayed repolarisation of the ventricular action potential [178].

In the kidney, AKAP18δ was shown to play a role in arginine/vasopressin (AVP) mediated re-distribution of aquaporin 2 (AQP2) from intracellular vesicles to the plasma membrane to increase water reabsorption [118]. AKAP18δ is supposed to mediate the phosphorylation of AQP2 by PKA at Ser^{265} that leads to AQP2 shuttling [170]. AVP is the major regulator of renal water retention and its binding to the vasopressin V2 receptor induces an increase the blood volume. For this reason, V2 receptor antagonists are a major drug target for increasing water excretion, which is important in chronic heart failure to relieve the heart [179].

The specific inhibition of the PKA – AKAP18δ interaction has potential application in the treatment of chronic heart failure [180] and has been shown to increase contractility of cultured cardiomyocytes and isolated rat hearts via a small molecule inhibitor found in a screening approach [181].

The availability of a structure of the RII-binding domain of AKAP18 in complex with the D/D domain or RIIα subunit would be very useful to facilitate rational drug design and lead structure optimization in order to specifically inhibit the PKA RIIα - AKAP18 interaction. Specific inhibition may be possible, as amino acid sequence conservation is low among AKAPs in general, and this includes the sequences of the PKA binding regions of different AKAPs. There are structures known of the D/D domain in complex with AKAP peptides, e.g. from the PKA binding site of D-AKAP2 [82] or with the AKAP-*IS* peptide [81]. A structure of the PKA binding domain of hsAKAP18β(43-83) in complex with D/D would not only be of interest for the comparative study of these domains, but also for the rational drug design approach.

To investigate the influence of the core domain on the interaction with the D/D domain, the structure of the longer AKAP18γ and δ isoforms in complex with D/D is now likely best pursued using NMR spectroscopy. The ^{1}H - ^{15}N HSCQ spectra of this ~40 kDa complex show good peak dispersion and an assignment of the signals would in principle be possible. If there were additional interactions between AKAP18γ or δ and the D/D domain detected, these sites could be additionally targeted with small molecule inhibitors to disrupt PKA anchoring.

This thesis lays the foundation for further structural and functional investigation of the AKAP18 – PKA interaction. Protein purification was established for different truncated constructs of AKAP18 isoforms with yields sufficient for structural biology studies. Furthermore, buffer conditions for optimal handling of AKAP18 constructs were found that could be used for setting up *in vitro* assays. Therefore, these results form the basis for establishing screening and validation assays in the development of new drugs for the treatment of heart failure by the inhibition of the AKAP18 - PKA interaction.

5 Appendix

5.1 Protein Structure Determination by X-ray Crystallography

There are many textbooks covering the field of X-ray crystallography of biological macromolecules. In this chapter, only the basic principles are summarized. For detailed explanations see for example [182, 183]. In order to solve the structure of a protein by X-ray crystallography, crystals of it must be grown that diffract X-rays. The first step in the formation of macromolecular crystals is nucleation that takes place at high levels of supersaturation. Crystals in general have a regular and periodic internal three-dimensional arrangement over a relatively large distance. The smallest repeat unit within a crystal is the unit cell. It builds up the entire crystal by translational symmetry operation. The asymmetric unit contains all the information necessary to build up the unit cell upon application of space group symmetry operations. The space group of the crystal is defined by the dimensions of the unit cell together with the symmetry operations applied to the asymmetric unit. As only one stereoisomer of any biological macromolecule exists in nature (for proteins this is L-amino acids), these crystals only contain symmetry elements with rotation and/or translation (inversion and reflexion are not possible). Thus, out of the 230 possible space groups, proteins can only crystallize in 65 space groups.

X-rays are high energy electromagnetic radiation and X-ray diffraction is the result of the interaction of this radiation with the electrons of the atoms in the crystal. In general, the scattering of X-rays by electrons is elastic and takes place without any energy loss (also called Thomson scattering). The scattering of X-rays by single molecules is extremely weak but if the molecules are periodically arranged in the crystal lattice all the small scattering contributions will sum up to result in sharp diffraction spots at diffraction angles given by the Bragg equation:

(1) $$2d_{hkl}\sin\theta = n\lambda$$

A set of parallel lattice planes having the indices *hkl* and an interplanar spacing of d_{hkl} produces a diffracted beam when X-rays of the wavelength λ impinge upon the planes at an angle θ and are reflected at the same angle. *n* is an integer.

The result of the X-ray diffraction experiment is a list of intensities with the indices *hkl* giving their position in the reciprocal lattice. Thus, the intensity assigned to the reflection *hkl* is a measure of the relative strength of the reflection from the set of lattice planes with the indices *hkl*. Reflections near the origin (indices *000*) arise from sets of widely spaced planes and bear

information on larger features of the molecule in the unit cell. Reflections far from the origin originate from closely spaced lattice planes and carry detailed information on the molecular structure.

Each diffracted X-ray that produces a reflection can also be described as the sum of the contributions of all scatters from a unit cell. This is called structure factor equation:

(2) $$\vec{F}(S) = \sum_{j=1}^{n} f_j e^{(2\pi i \vec{r}_j \vec{S})}$$

where *n* is the number of atoms in the unit cell, r_j is the position of the atom *j* with respect to the origin, f_j is the atomic scattering factor, and $\vec{S}$ is the difference between the scattered wave vector and the incident wave vector.

A crystal is a periodic arrangement of unit cells with the number n_1 in the direction $\vec{a}$, n_2 in the direction $\vec{b}$, and n_3 in the direction $\vec{c}$. If the repeated molecules in the crystal scatter exactly in phase, after a certain number of integer translations t, u, and v along the cell constants $\vec{a}$, $\vec{b}$, and $\vec{c}$, respectively, the scattering functions add up and the resulting scattering factor is strong. The total scattering $\vec{K}(\vec{S})$ by the crystal is the product of the three summations in all three directions:

(3) $$\vec{K}(\vec{S}) = \vec{F}(\vec{S}) \times \sum_{t=0}^{n_1} e^{(2\pi i t \vec{S}\vec{a})} \times \sum_{u=0}^{n_2} e^{(2\pi i u \vec{S}\vec{b})} \times \sum_{v=0}^{n_3} e^{(2\pi i v \vec{S}\vec{c})}$$

The summation is largest, when $\vec{S}\vec{a}$ is an integer *h*, $\vec{S}\vec{b}$ is an integer *k*, and $\vec{S}\vec{c}$ is an integer *l*. These so-called Laue conditions determine the position of the diffraction maxima, i.e. the condition for maximum constructive interference.

To reconstruct the electron density $\rho(\vec{r})$ at the position $\vec{r}$ in the unit cell, the Fourier transformation is used. Integration over all electrons in the unit cell gives

(4) $$\vec{F}(\vec{S}) = \int_{cell} \rho(\vec{r}) e^{(2\pi i \vec{r}_l \cdot \vec{S})} dv$$

Given that x, y, and z are fractional coordinates and V is the volume of the unit cell, it follows that

(5) $$dv = V \cdot dxdydz$$

and

(6) $$\vec{r}\vec{S} = (\vec{a}x + \vec{b}y + \vec{c}z)\vec{S} = hx + ky + lz$$

$\vec{F}(\vec{S})$ can then be written as $\vec{F}(hkl)$:

(7) $$\vec{F}(hkl) = V\int_{x=0}^{1}\int_{y=0}^{1}\int_{z=0}^{1}\rho(x,y,z)e^{(-2\pi i(hx+ky+lz))}dxdydz$$

$\vec{F}(hkl)$ is the Fourier transform of $\rho(xyz)$ and, thus, $\rho(xyz)$ is the inverse Fourier transform of $\vec{F}(hkl)$. Because the reciprocal space is discrete, the continuous Fourier integral can be replaced with a discrete triple summation. With $\vec{F}_{hkl} = |F_{hkl}|e^{i\alpha_{hkl}}$ the electron density equation is given as

(8) $$\rho(xyz) = \frac{1}{V}\sum_{h}\sum_{k}\sum_{l}|F(hkl)|e^{-2\pi i(hx+ky+lz)+i\alpha(hkl)}$$

with $\frac{1}{V}$ being the normalization factor to provide the correct units of e^-/ Å^3 for the electron density. However, the measured intensities of the reflections only provide the structure factor amplitudes $|F_{hkl}|$, but the phase angles $\alpha(hkl)$ are missing. The phases can either be obtained experimentally by isomorphous replacement methods, where isomorphous differences between native and derivative crystals containing a heavy atom are used for phase determination. Another method is to replace methionine in the protein with selenomethionine and make use of anomalous differences in data sets collected at the peak wavelength of the respective anomalous scatterer.

On the other hand, if a structurally similar model is available, this can be used to obtain initial phases. Importantly, the correct orientation and position of the search model in the unit cell must be determined. The search for proper placement of the molecule can be conducted in sequence by a deterministic 3-dimensional rotation search followed by a deterministic 3-dimensional translation search. Or it can be performed as a one-step stochastic 6-dimensional placement search. Many runs of stochastic search may be necessary to find the correct solution, if it exists, depending on the model and the data quality.

5.2 Sequence alignment of AKAP18 isoforms

Sequences of mouse AKAP18γ (SwissProt entry Q7TN79), human AKAP18γ (Q9POM2), and rat AKAP18δ (Q6JP77) were aligned using the ClustalW server [184] and processed using the program GeneDoc (http://www.psc.edu/biomed/genedoc). 100 % conserved residues are boxed dark green, 60 % conserved residues are boxed light green. As an exception, highly conserved residues of the PKA binding site are in red and the two His-X-Thr motifs are colored yellow.

```
                          *         20         *         40         *
mmAKAP18g    1 : ------------------------------------MPFAAVDIQDDCG :  13
hsAKAP18g    1 : ----------------------MSEEFEANTMDSIVDMPFATVDIQDDCG :  28
rnAKAP18d    1 : MERPAAGEIDANKCDHLSRGEEGTGDLETSPVGSIADLPFAAVDIQDDCG :  50

                        60         *         80         *        100
mmAKAP18g   14 : SPDVPQANPKR--SKEEFEDRGDKNDHVKKRKKAKKDYQPNYFLSIPITN :  61
hsAKAP18g   29 : ITDEPQINL-----KRSQENEWVKSDQVKKRKKKRKDYQPNYFLSIPITN :  73
rnAKAP18d   51 : LPDVPQGNVPQGNPKRSKENRGDRNDHVKKRKKAKKDYQPNYFLSIPITN : 100

                          *        120         *        140         *
mmAKAP18g   62 : KKITTGIKSLQNSILQQDKRLTKAMVGDGSFHITLLVMQLLNEDEVNIGT : 111
hsAKAP18g   74 : KEIIKGIKILQNAIIQQDERLAKAMVSDGSFHITLLVMQLLNEDEVNIGI : 123
rnAKAP18d  101 : KKITAGIKVLQNSILRQDNRLTKAMVGDGSFHITLLVMQLLNEDEVNIGT : 150

                        160         *        180         *        200
mmAKAP18g  112 : DALLELKPFVEEILEGKHLALPFQGIGTFQGQVGFVKLADGDHVSALLEI : 161
hsAKAP18g  124 : DALLELKPFIEELLQGKHLTLPFQGIGTFGNQVGFVKLAEGDHVNSLLEI : 173
rnAKAP18d  151 : DALLELKPFVEEILEGKHLTLPFHGIGTFQGQVGFVKLADGDHVSALLEI : 200

                          *        220         *        240         *
mmAKAP18g  162 : AETAKRTFREKGILAGESRTFKPHLTFMKLSKAPMLRKKGVRKIEPGLYE : 211
hsAKAP18g  174 : AETANRTFQEKGILVGESRSFKPHLTFMKLSKSPWLRKNGVKKIDPDLYE : 223
rnAKAP18d  201 : AETAKRTFQEKGILAGESRTFKPHLTFMKLSKAPMLWKKGVRKIEPGLYE : 250

                        260         *        280         *        300
mmAKAP18g  212 : QFIDHRFGEELLYQIDLCSMLKKKQSNGYYHCESSIVIGEKDRREPEDAE : 261
hsAKAP18g  224 : KFISHRFGEEILYRIDLCSMLKKKQSNGYYHCESSIVIGEKNGGEPDDAE : 273
rnAKAP18d  251 : QFIDHRFGEEILYQIDLCSMLKKKQSNGYYHCESSIVIGEKDRKEPEDAE : 300

                          *        320         *        340         *
mmAKAP18g  262 : LVRLSKRLVENAVLKAAQQYLEETQNKKQPGEGNSTKAEEGDRNGDGSDN : 311
hsAKAP18g  274 : LVRLSKRLVENAVLKAVQQYLEETQNKNKPGEGSSVKTEAADQNGNDNEN : 323
rnAKAP18d  301 : LVRLSKRLVENAVLKAVQQYLEETQNKKQPGEGNSVKAEEGDRNGDGSDN : 350

mmAKAP18g  312 : NRK : 314
hsAKAP18g  324 : NRK : 326
rnAKAP18d  351 : NRK : 353
```

5.3 Sequence alignment of AKAP18δ core domain with RNA ligases

Amino acid sequences of rat AKAP18δ core domain (pdb entry 2vfk, SwissProt entry Q6JP77) was aligned with the corresponding sequences of *P. horikoshii* 2´-5´RNA ligase (1vdx, O57823), *P. furiosus* 2´-5´RNA ligase (2fyh, Q8U4Q3), *T. thermophilus* 2´-5´RNA ligase (1iuh, Q84CU4), and *A. thaliana* cyclic nucleotide phosphodiesterase Appr>p (1fsi, O04147). 100 % conserved residues are boxed red, 60 % conserved residues are boxed dark green.

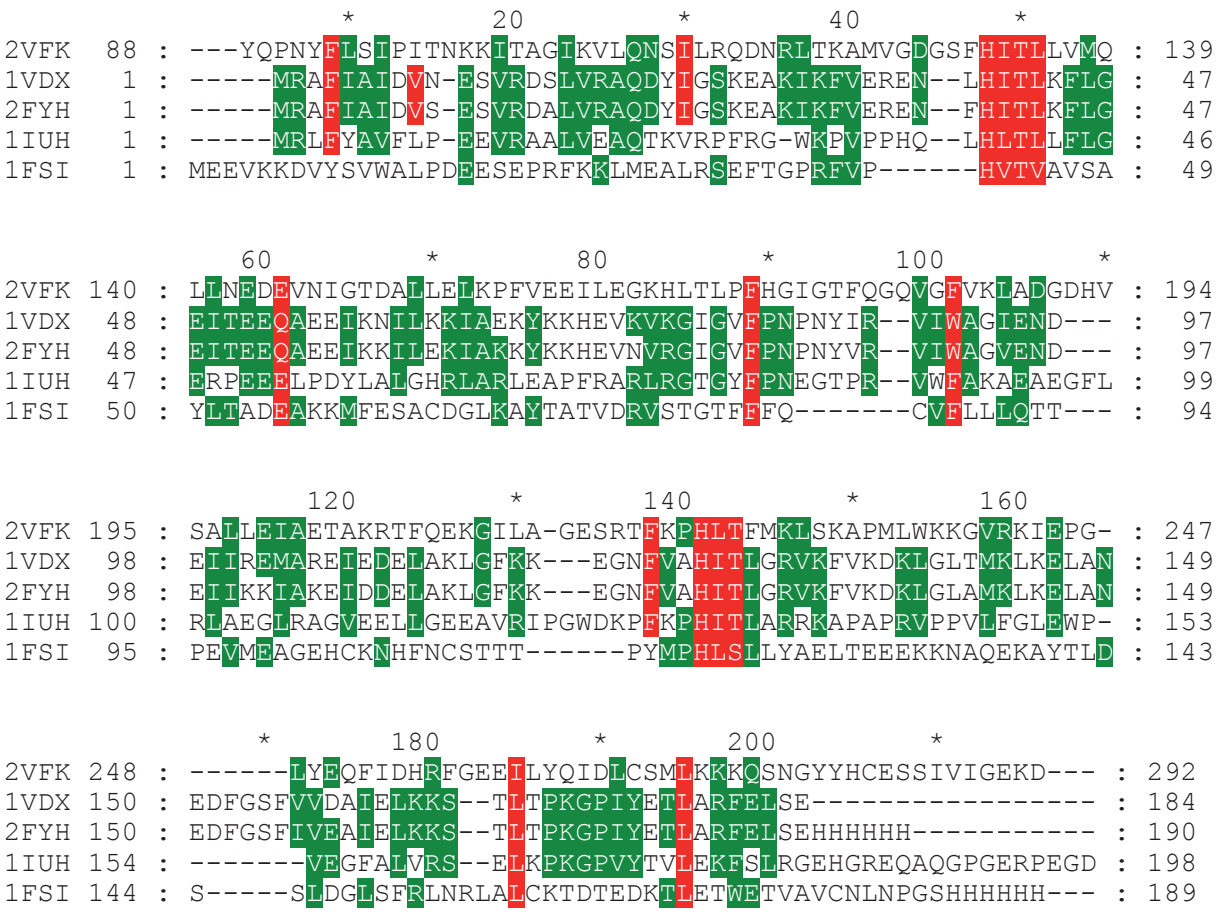

5.4 Abbreviations

Å	Ångström (0.1 nm)
AC	Adenylyl cyclase
5´ADP	Adenosine-5´-diphosphate
AIM	Autoindution medium
AKAP	A-kinase anchoring protein
5´AMP	Adenosine-5´-monophosphate
Amp	Ampicillin
5´ATP	Adenosine-5´-triphosphate
AQP2	Aquaporin 2
BD	Binding domain (of AKAP to PKA RIIα)
BESSY	Berliner Elektronenspeicherring-Gesellschaft für Synchrotronstrahlung
3´,5´cAMP	cyclic 3´,5´-adenosine monophosphate
3´,5´cGMP	cyclic 3´,5´-guanosine monophosphate
C	Catalytic subunit of PKA
Cam	Chloramphenicol
Carb	Carbenicillin
CAP	Catabolite gene activator protein
CBD	cAMP binding domain
CCD	Charge-couple device
CD	Circular dichroism
CHO	Chinese hamster ovarian
5´CMP	5´Cytidine monophosphate
D/D	PKA RIIα Dimerization and docking domain
DTT	Dithiothreitol
EG	Ethylene glycol
FSK	Forskolin
GST	Glutathione-S-transferase

GDP	Guanosine diphosphate
GTP	Guanosine triphosphate
HEK	Human embryonic kidney
Hepes	4-(2-hydroxyethyl)-1-piperazineethanesulfonic acid
HPLC	High pressure liquid chromatography
HSQC	Heteronuclear single quantum coherence
IMCD cells	Inner medullary collecting duct cells
IPTG	Isopropyl β-D-1-thiogalactopyranoside
ITC	Isothermal titration calorimetry
Kan	Kanamycin
LB	Luria bertani
LSM	Laser scanning microscopy
MDCK cells	Madin-Darby canine kidney cells
MES	2-(N-morpholino)ethanesulfonic acid
MPD	2-methyl-2,4-pentandiol
NMR	Nuclear magnetic resonance
PBC	Phosphate binding cassette
PCR	Polymerase chain reaction
PEG	Polyethylene glycol
PDB	Protein data base
PDE	Phosphodiesterase
PKA	cAMP-dependent kinase (Protein kinase A)
PLN	Phospholamban
RIIα	PKA Regulatory Subunit IIα
RALS	Right angle light scattering
SDS-PAGE	Sodium dodecyl sulfate polyacrylamide gel electrophoresis
SEC	Size exclusion chromatography
SERCA	Sarcoplasmic reticulum Ca^{2+}-ATPase
TB	Terrific broth
TMAO	Trimethylamine N-oxide

Tris	Tris(hydroxymethyl)aminomethane
TSA	Thermal shift assay

For abbreviation of the amino acids, the one and the three letter code was used:

A, Ala - alanine	I, Ile - isoleucine	R, Arg – arginine
C, Cys - cysteine	K, Lys - lysine	S, Ser – serine
D, Asp - aspartate	L, Leu - leucine	T, Thr – threonine
E, Glu - glutamate	M, Met - methionine	V, Val – valine
F, Phe - phenylalanine	N, Asn - asparagine	W, Trp – tryptophane
G, Gly - glycine	P, Pro - proline	Y, Tyr – tyrosine
H, His - histidine	Q, Glu - glutamine	X – any amino acid residue

6 Abstract

Cyclic 3´, 5´-adenosine monophosphate (cAMP)-dependent kinase, also known as protein kinase A (PKA), is one of the major effectors of the second messenger cAMP in the cell. By binding of cAMP to its regulatory (R) subunits, the associated catalytic (C) subunits are released from inhibition and are activated to phosphorylate target proteins at serine and threonine residues. One way to confer specificity to PKA action is the so-called compartmentalization of PKA signaling. That means that PKA activity is restricted both in space and in time. A-kinase anchoring proteins (AKAPs) serve as molecular scaffolds that both bind PKA regulatory subunits and target the kinase to certain subcellular departments of the cell. They accomplish this by interaction with target proteins, bringing them in close proximity to the kinase, and with other proteins involved in signal transduction. In this way, AKAPs form multi-protein signaling modules that regulate, focus, and integrate different signals inside the cell.

To understand AKAP function and the mechanism of their interaction with the PKA R subunit as well as with other interaction partners, the structural determinants of the interaction of AKAP18 with RIIα, the phosphodiesterase PDE4D3, and phospholamban (PLN) were investigated.

There are four splice variants of AKAP18 known, called AKAP18α, β, γ, and δ. They share a common PKA-binding site, which is highly conserved. Large-scale purification of the most promising truncated constructs of these isoforms was established and yielded highly pure protein for structural investigation. The constructs containing the PKA binding site were co-purified with the D/D domain, the N-terminal domain of the R subunit that interacts with AKAPs. It was shown that purified proteins and the co-purified complex are correctly folded and functional. AKAP18 binds 5´AMP and the K_d for binding was determined to be in the low micromolar range, independent of the presence of the D/D domain. Crystallization of a complex of AKAP18 γ or δ isoforms in complex with D/D was not successful, but the complex might be amenable to NMR spectroscopy.

The interaction of AKAP18δ with PDE4D3 and PLN was investigated by NMR spectroscopy, isothermal titration calorimetry, analytical gel filtration, co-crystallization with synthetic peptides, and by pull-down studies, but a stable complex could not be verified.

Zusammenfassung

Zyklisches 3´,5´-adenosinmonophosphat (cAMP)-abhängige Kinase, auch bekannt als Proteinkinase A (PKA), ist eines der Hauptzielproteine des sekundären Botenstoffs cAMP in der Zelle. Wenn cAMP an die regulatorische (R) Untereinheit der PKA bindet, werden die vorher gebundenen katalytischen (C) Untereinheiten freigesetzt, wodurch diese aktiviert werden. Ein wichtiges Mittel, um der PKA-Aktivität Spezifität zu verleihen, ist die sogenannte Kompartmentalisierung. Darunter versteht man die räumliche und zeitliche Beschränkung der PKA Signaltransduktion in der Zelle. A-kinase Ankerproteine (AKAPs) dienen dabei als molekulare *scaffolds* („Gerüstproteine“), die einerseits R-Untereinheiten der PKA binden können und diese dann, andererseits, aber auch an bestimmte subzelluläre Kompartimenten verankern können. Zusätzlich interagieren AKAPs mit Substraten der PKA, um diese in die Nähe der Kinase zu bringen, sowie mit anderen Proteinen, die in die Signaltransduktionskette involviert sind. Damit bilden AKAPs die Basis für Signalmodule, die aus unterschiedlichen Proteinen bestehen, und verschiedenste Signale regulieren, bzw. integrieren.

Um die Funktion von AKAPs besser zu verstehen und um Interaktionsmechanismen mit der R-Untereinheit der PKA sowie mit anderen Interaktionspartnern zu beleuchten, wurden die Wechselwirkungen von AKAP18 mit RIIα, der Phosphodiesterase PDE4D3 und Phospholamban (PLN) untersucht.

Es gibt vier verschiedene Splicevarianten von AKAP18, AKAP18 α, β, γ und δ, die alle eine hochkonservierte PKA-bindestelle besitzen. Für strukturelle Untersuchungen wurde die Aufreinigung trunkierter Konstrukte verschiedener AKAP18 Isoformen etabliert, die hochreines Protein im Milligrammmaßstab ergab. Für die Aufreinigung der AKAP18-konstrukte mit der PKA-bindestelle wurde die D/D-domäne, die N-terminale Domäne der R-Untereinheit, die für die Interaktion mit AKAPs zuständig ist, co-aufgereinigt. Mit Hilfe von *nuclear magnetic resonance* (NMR) Spektroskopie und anderen biophysikalischen Methoden konnte gezeigt werden, dass die so hergestellten Proteine korrekt gefaltet und funktional sind. Die längeren AKAP18-isoformen binden 5´AMP und der K_D für die Bindung wurde ermittelt. Er liegt im unteren, mikromolaren Bereich, unbeeinflusst von der Anwesenheit der D/D-domäne. Die Versuche, AKAP18γ und δ Isoformen im Komplex mit der D/D-domäne zu kristallisieren, blieben erfolglos, aber die Struktur ist eventuell durch NMR-Spektroskopie lösbar.

Die Interaktion von AKAP18δ mit PDE4D3 und PLN konnte weder mittels NMR-Spektroskopie, Isothermaler Titrationskalorimetrie, analytischer Gelfiltration, Co-Kristallisation noch in pulldown-Studien verifiziert werden.

7 References

1. Alberts, B.J., A.; Lewis, J.; Raff, M.; Roberts, K.; Walter, P., *Molecular Biology of the Cell*2002, New York: Garland Science.
2. Krauss, G., *Biochemistry of Signal Transduction and Regulation*2001: Wiley-VHC.
3. Taylor, S.S., et al., *Signaling through cAMP and cAMP-dependent protein kinase: diverse strategies for drug design.* Biochim Biophys Acta, 2008. **1784**(1): p. 16-26.
4. Pearce, L.R., D. Komander, and D.R. Alessi, *The nuts and bolts of AGC protein kinases.* Nat Rev Mol Cell Biol, 2010. **11**(1): p. 9-22.
5. Lagerstrom, M.C. and H.B. Schioth, *Structural diversity of G protein-coupled receptors and significance for drug discovery.* Nat Rev Drug Discov, 2008. **7**(4): p. 339-57.
6. Vilardaga, J.P., et al., *G-protein-coupled receptor heteromer dynamics.* J Cell Sci, 2010. **123**(Pt 24): p. 4215-20.
7. Hofmann, K.P., et al., *A G protein-coupled receptor at work: the rhodopsin model.* Trends Biochem Sci, 2009. **34**(11): p. 540-52.
8. Hanoune, J. and N. Defer, *Regulation and role of adenylyl cyclase isoforms.* Annu Rev Pharmacol Toxicol, 2001. **41**: p. 145-74.
9. Nakamura, T. and G.H. Gold, *A cyclic nucleotide-gated conductance in olfactory receptor cilia.* Nature, 1987. **325**(6103): p. 442-4.
10. de Rooij, J., et al., *Epac is a Rap1 guanine-nucleotide-exchange factor directly activated by cyclic AMP.* Nature, 1998. **396**(6710): p. 474-7.
11. Skalhegg, B.S. and K. Tasken, *Specificity in the cAMP/PKA signaling pathway. Differential expression,regulation, and subcellular localization of subunits of PKA.* Front Biosci, 2000. **5**: p. D678-93.
12. Tasken, K. and E.M. Aandahl, *Localized effects of cAMP mediated by distinct routes of protein kinase A.* Physiol Rev, 2004. **84**(1): p. 137-67.
13. Houslay, M.D., G.S. Baillie, and D.H. Maurice, *cAMP-Specific phosphodiesterase-4 enzymes in the cardiovascular system: a molecular toolbox for generating compartmentalized cAMP signaling.* Circ Res, 2007. **100**(7): p. 950-66.
14. Baillie, G.S., J.D. Scott, and M.D. Houslay, *Compartmentalisation of phosphodiesterases and protein kinase A: opposites attract.* FEBS Lett, 2005. **579**(15): p. 3264-70.
15. Walsh, D.A., J.P. Perkins, and E.G. Krebs, *An adenosine 3',5'-monophosphate-dependant protein kinase from rabbit skeletal muscle.* J Biol Chem, 1968. **243**(13): p. 3763-5.
16. Shoji, S., et al., *Complete amino acid sequence of the catalytic subunit of bovine cardiac muscle cyclic AMP-dependent protein kinase.* Proc Natl Acad Sci U S A, 1981. **78**(2): p. 848-51.
17. Uhler, M.D., et al., *Isolation of cDNA clones coding for the catalytic subunit of mouse cAMP-dependent protein kinase.* Proc Natl Acad Sci U S A, 1986. **83**(5): p. 1300-4.
18. Knighton, D.R., et al., *Structure of a peptide inhibitor bound to the catalytic subunit of cyclic adenosine monophosphate-dependent protein kinase.* Science, 1991. **253**(5018): p. 414-20.
19. Potter, R.L. and S.S. Taylor, *Relationships between structural domains and function in the regulatory subunit of cAMP-dependent protein kinases I and II from porcine skeletal muscle.* J Biol Chem, 1979. **254**(7): p. 2413-8.
20. Corbin, J.D., et al., *Hormonal regulation of adenosine 3',5'-monophosphate-dependent protein kinase.* Adv Cyclic Nucleotide Res, 1975. **5**: p. 265-79.
21. Corbin, J.D., T.R. Soderling, and C.R. Park, *Regulation of adenosine 3',5'-monophosphate-dependent protein kinase. I. Preliminary characterization of the adipose tissue enzyme in crude extracts.* J Biol Chem, 1973. **248**(5): p. 1813-21.
22. Reimann, E.M., D.A. Walsh, and E.G. Krebs, *Purification and properties of rabbit skeletal muscle adenosine 3',5'-monophosphate-dependent protein kinases.* J Biol Chem, 1971. **246**(7): p. 1986-95.
23. Zimmermann, B., et al., *PrKX is a novel catalytic subunit of the cAMP-dependent protein kinase regulated by the regulatory subunit type I.* J Biol Chem, 1999. **274**(9): p. 5370-8.

24. Schiebel, K., et al., *FISH localization of the human Y-homolog of protein kinase PRKX (PRKY) to Yp11.2 and two pseudogenes to 15q26 and Xq12-->q13.* Cytogenet Cell Genet, 1997. **76**(1-2): p. 49-52.
25. De Camilli, P., et al., *Heterogeneous distribution of the cAMP receptor protein RII in the nervous system: evidence for its intracellular accumulation on microtubules, microtubule-organizing centers, and in the area of the Golgi complex.* J Cell Biol, 1986. **103**(1): p. 189-203.
26. Rubin, C.S., et al., *Characterization and comparison of membrane-associated and cytosolic cAMP-dependent protein kinases. Physicochemical and immunological studies on bovine cerebral cortex protein kinases.* J Biol Chem, 1979. **254**(10): p. 3797-805.
27. Corbin, J.D., S.L. Keely, and C.R. Park, *The distribution and dissociation of cyclic adenosine 3':5'-monophosphate-dependent protein kinases in adipose, cardiac, and other tissues.* J Biol Chem, 1975. **250**(1): p. 218-25.
28. Scott, J.D., et al., *The molecular cloning of a type II regulatory subunit of the cAMP-dependent protein kinase from rat skeletal muscle and mouse brain.* Proc Natl Acad Sci U S A, 1987. **84**(15): p. 5192-6.
29. Lee, D.C., et al., *Isolation of a cDNA clone for the type I regulatory subunit of bovine cAMP-dependent protein kinase.* Proc Natl Acad Sci U S A, 1983. **80**(12): p. 3608-12.
30. Cadd, G. and G.S. McKnight, *Distinct patterns of cAMP-dependent protein kinase gene expression in mouse brain.* Neuron, 1989. **3**(1): p. 71-9.
31. Jahnsen, T., et al., *Purification and characterization of hormone-regulated isoforms of the regulatory subunit of type II cAMP-dependent protein kinase from rat ovaries.* J Biol Chem, 1985. **260**(29): p. 15980-7.
32. Kennelly, P.J. and E.G. Krebs, *Consensus sequences as substrate specificity determinants for protein kinases and protein phosphatases.* J Biol Chem, 1991. **266**(24): p. 15555-8.
33. Kim, C., N.H. Xuong, and S.S. Taylor, *Crystal structure of a complex between the catalytic and regulatory (RIalpha) subunits of PKA.* Science, 2005. **307**(5710): p. 690-6.
34. Kim, C., et al., *PKA-I holoenzyme structure reveals a mechanism for cAMP-dependent activation.* Cell, 2007. **130**(6): p. 1032-43.
35. Wu, J., et al., *PKA type IIalpha holoenzyme reveals a combinatorial strategy for isoform diversity.* Science, 2007. **318**(5848): p. 274-9.
36. Brown, S.H., et al., *Novel isoform-specific interfaces revealed by PKA RIIbeta holoenzyme structures.* J Mol Biol, 2009. **393**(5): p. 1070-82.
37. Vigil, D., et al., *Solution scattering reveals large differences in the global structures of type II protein kinase A isoforms.* J Mol Biol, 2006. **357**(3): p. 880-9.
38. Boettcher, A.J., et al., *Realizing the allosteric potential of the tetrameric protein kinase A RIalpha holoenzyme.* Structure, 2011. **19**(2): p. 265-76.
39. Heller, W.T., et al., *C subunits binding to the protein kinase A RI alpha dimer induce a large conformational change.* J Biol Chem, 2004. **279**(18): p. 19084-90.
40. Sarma, G.N., et al., *Structure of D-AKAP2:PKA RI complex: insights into AKAP specificity and selectivity.* Structure, 2010. **18**(2): p. 155-66.
41. Grant, B.D., et al., *Kinetic analyses of mutations in the glycine-rich loop of cAMP-dependent protein kinase.* Biochemistry, 1998. **37**(21): p. 7708-15.
42. Hemmer, W., et al., *Role of the glycine triad in the ATP-binding site of cAMP-dependent protein kinase.* J Biol Chem, 1997. **272**(27): p. 16946-54.
43. Johnson, D.A., et al., *Dynamics of cAMP-dependent protein kinase.* Chem Rev, 2001. **101**(8): p. 2243-70.
44. Sastri, M., et al., *A-kinase-interacting protein localizes protein kinase A in the nucleus.* Proc Natl Acad Sci U S A, 2005. **102**(2): p. 349-54.
45. Akamine, P., et al., *Dynamic features of cAMP-dependent protein kinase revealed by apoenzyme crystal structure.* J Mol Biol, 2003. **327**(1): p. 159-71.
46. Narayana, N., et al., *A binary complex of the catalytic subunit of cAMP-dependent protein kinase and adenosine further defines conformational flexibility.* Structure, 1997. **5**(7): p. 921-35.

47. Hemmings, B.A., et al., *Phosphorylation of the type-II regulatory subunit of cyclic-AMP-dependent protein kinase by glycogen synthase kinase 3 and glycogen synthase kinase 5.* Eur J Biochem, 1982. **127**(3): p. 473-81.
48. Carmichael, D.F., et al., *Type II regulatory subunit of cAMP-dependent protein kinase. Phosphorylation by casein kinase II at a site that is also phosphorylated in vivo.* J Biol Chem, 1982. **257**(17): p. 10440-5.
49. Taylor, S.S., J.A. Buechler, and W. Yonemoto, *cAMP-dependent protein kinase: framework for a diverse family of regulatory enzymes.* Annu Rev Biochem, 1990. **59**: p. 971-1005.
50. Titani, K., et al., *Amino acid sequence of the regulatory subunit of bovine type I adenosine cyclic 3',5'-phosphate dependent protein kinase.* Biochemistry, 1984. **23**(18): p. 4193-9.
51. Ogreid, D. and S.O. Doskeland, *The kinetics of association of cyclic AMP to the two types of binding sites associated with protein kinase II from bovine myocardium.* FEBS Lett, 1981. **129**(2): p. 287-92.
52. Ringheim, G.E. and S.S. Taylor, *Effects of cAMP-binding site mutations on intradomain cross-communication in the regulatory subunit of cAMP-dependent protein kinase I.* J Biol Chem, 1990. **265**(32): p. 19472-8.
53. Saraswat, L.D., et al., *Deletion mutants as probes for localizing regions of subunit interaction in cAMP-dependent protein kinase.* J Biol Chem, 1988. **263**(34): p. 18241-6.
54. Corbin, J.D., et al., *Compartmentalization of adenosine 3':5'-monophosphate and adenosine 3':5'-monophosphate-dependent protein kinase in heart tissue.* J Biol Chem, 1977. **252**(11): p. 3854-61.
55. Su, Y., et al., *Regulatory subunit of protein kinase A: structure of deletion mutant with cAMP binding domains.* Science, 1995. **269**(5225): p. 807-13.
56. Weber, I.T., et al., *Predicted structures of cAMP binding domains of type I and II regulatory subunits of cAMP-dependent protein kinase.* Biochemistry, 1987. **26**(2): p. 343-51.
57. Diller, T.C., et al., *Molecular basis for regulatory subunit diversity in cAMP-dependent protein kinase: crystal structure of the type II beta regulatory subunit.* Structure, 2001. **9**(1): p. 73-82.
58. Zawadzki, K.M., et al., *Endogenous tryptophan residues of cAPK regulatory subunit type IIbeta reveal local variations in environments and dynamics.* Proteins, 2003. **51**(4): p. 552-61.
59. Diller, T.C., N.H. Xuong, and S.S. Taylor, *Type II beta regulatory subunit of cAMP-dependent protein kinase: purification strategies to optimize crystallization.* Protein Expr Purif, 2000. **20**(3): p. 357-64.
60. Bubis, J., T.S. Vedvick, and S.S. Taylor, *Antiparallel alignment of the two protomers of the regulatory subunit dimer of cAMP-dependent protein kinase I.* J Biol Chem, 1987. **262**(31): p. 14961-6.
61. Reimann, E.M., *Conversion of bovine cardiac adenosine cyclic 3',5'-phosphate dependent protein kinase to a heterodimer by removal of 45 residues at the N-terminus of the regulatory subunit.* Biochemistry, 1986. **25**(1): p. 119-25.
62. Scott, J.D., et al., *Type II regulatory subunit dimerization determines the subcellular localization of the cAMP-dependent protein kinase.* J Biol Chem, 1990. **265**(35): p. 21561-6.
63. Carr, D.W., et al., *Interaction of the regulatory subunit (RII) of cAMP-dependent protein kinase with RII-anchoring proteins occurs through an amphipathic helix binding motif.* J Biol Chem, 1991. **266**(22): p. 14188-92.
64. Leiser, M., C.S. Rubin, and J. Erlichman, *Differential binding of the regulatory subunits (RII) of cAMP-dependent protein kinase II from bovine brain and muscle to RII-binding proteins.* J Biol Chem, 1986. **261**(4): p. 1904-8.
65. Sarkar, D., J. Erlichman, and C.S. Rubin, *Identification of a calmodulin-binding protein that co-purifies with the regulatory subunit of brain protein kinase II.* J Biol Chem, 1984. **259**(15): p. 9840-6.
66. Hausken, Z.E., et al., *Type II regulatory subunit (RII) of the cAMP-dependent protein kinase interaction with A-kinase anchor proteins requires isoleucines 3 and 5.* J Biol Chem, 1994. **269**(39): p. 24245-51.

67. Luo, Z., B. Shafit-Zagardo, and J. Erlichman, *Identification of the MAP2- and P75-binding domain in the regulatory subunit (RII beta) of type II cAMP-dependent protein kinase. Cloning and expression of the cDNA for bovine brain RII beta.* J Biol Chem, 1990. **265**(35): p. 21804-10.
68. Leon, D.A., et al., *A stable alpha-helical domain at the N terminus of the RIalpha subunits of cAMP-dependent protein kinase is a novel dimerization/docking motif.* J Biol Chem, 1997. **272**(45): p. 28431-7.
69. Banky, P., L.J. Huang, and S.S. Taylor, *Dimerization/docking domain of the type Ialpha regulatory subunit of cAMP-dependent protein kinase. Requirements for dimerization and docking are distinct but overlapping.* J Biol Chem, 1998. **273**(52): p. 35048-55.
70. Newlon, M.G., et al., *The A-kinase anchoring domain of type IIalpha cAMP-dependent protein kinase is highly helical.* J Biol Chem, 1997. **272**(38): p. 23637-44.
71. Carr, D.W., et al., *Association of the type II cAMP-dependent protein kinase with a human thyroid RII-anchoring protein. Cloning and characterization of the RII-binding domain.* J Biol Chem, 1992. **267**(19): p. 13376-82.
72. Herberg, F.W., et al., *Analysis of A-kinase anchoring protein (AKAP) interaction with protein kinase A (PKA) regulatory subunits: PKA isoform specificity in AKAP binding.* J Mol Biol, 2000. **298**(2): p. 329-39.
73. Carr, D.W., et al., *Localization of the cAMP-dependent protein kinase to the postsynaptic densities by A-kinase anchoring proteins. Characterization of AKAP 79.* J Biol Chem, 1992. **267**(24): p. 16816-23.
74. Glantz, S.B., Y. Li, and C.S. Rubin, *Characterization of distinct tethering and intracellular targeting domains in AKAP75, a protein that links cAMP-dependent protein kinase II beta to the cytoskeleton.* J Biol Chem, 1993. **268**(17): p. 12796-804.
75. Kapiloff, M.S., et al., *mAKAP: an A-kinase anchoring protein targeted to the nuclear membrane of differentiated myocytes.* J Cell Sci, 1999. **112 (Pt 16)**: p. 2725-36.
76. Hausken, Z.E., et al., *Mutational analysis of the A-kinase anchoring protein (AKAP)-binding site on RII. Classification Of side chain determinants for anchoring and isoform selective association with AKAPs.* J Biol Chem, 1996. **271**(46): p. 29016-22.
77. Li, Y. and C.S. Rubin, *Mutagenesis of the regulatory subunit (RII beta) of cAMP-dependent protein kinase II beta reveals hydrophobic amino acids that are essential for RII beta dimerization and/or anchoring RII beta to the cytoskeleton.* J Biol Chem, 1995. **270**(4): p. 1935-44.
78. Newlon, M.G., et al., *The molecular basis for protein kinase A anchoring revealed by solution NMR.* Nat Struct Biol, 1999. **6**(3): p. 222-7.
79. Newlon, M.G., et al., *A novel mechanism of PKA anchoring revealed by solution structures of anchoring complexes.* EMBO J, 2001. **20**(7): p. 1651-62.
80. Alto, N.M., et al., *Bioinformatic design of A-kinase anchoring protein-in silico: a potent and selective peptide antagonist of type II protein kinase A anchoring.* Proc Natl Acad Sci U S A, 2003. **100**(8): p. 4445-50.
81. Gold, M.G., et al., *Molecular basis of AKAP specificity for PKA regulatory subunits.* Mol Cell, 2006. **24**(3): p. 383-95.
82. Kinderman, F.S., et al., *A dynamic mechanism for AKAP binding to RII isoforms of cAMP-dependent protein kinase.* Mol Cell, 2006. **24**(3): p. 397-408.
83. Burns, L.L., et al., *Isoform specific differences in binding of a dual-specificity A-kinase anchoring protein to type I and type II regulatory subunits of PKA.* Biochemistry, 2003. **42**(19): p. 5754-63.
84. Carlson, C.R., et al., *Delineation of type I protein kinase A-selective signaling events using an RI anchoring disruptor.* J Biol Chem, 2006. **281**(30): p. 21535-45.
85. Burns-Hamuro, L.L., et al., *Designing isoform-specific peptide disruptors of protein kinase A localization.* Proc Natl Acad Sci U S A, 2003. **100**(7): p. 4072-7.
86. Banky, P., et al., *Related protein-protein interaction modules present drastically different surface topographies despite a conserved helical platform.* J Mol Biol, 2003. **330**(5): p. 1117-29.

87. Buday, L. and P. Tompa, *Functional classification of scaffold proteins and related molecules.* FEBS J, 2010. **277**(21): p. 4348-55.
88. Alexa, A., J. Varga, and A. Remenyi, *Scaffolds are 'active' regulators of signaling modules.* FEBS J, 2010. **277**(21): p. 4376-82.
89. Zeke, A., et al., *Scaffolds: interaction platforms for cellular signalling circuits.* Trends Cell Biol, 2009. **19**(8): p. 364-74.
90. Brummer, T., C. Schmitz-Peiffer, and R.J. Daly, *Docking proteins.* FEBS J, 2010. **277**(21): p. 4356-69.
91. Logue, J.S. and J.D. Scott, *Organizing signal transduction through A-kinase anchoring proteins (AKAPs).* FEBS J, 2010. **277**(21): p. 4370-5.
92. Wong, W. and J.D. Scott, *AKAP signalling complexes: focal points in space and time.* Nat Rev Mol Cell Biol, 2004. **5**(12): p. 959-70.
93. Pidoux, G. and K. Tasken, *Specificity and spatial dynamics of protein kinase A signaling organized by A-kinase-anchoring proteins.* J Mol Endocrinol, 2010. **44**(5): p. 271-84.
94. Theurkauf, W.E. and R.B. Vallee, *Molecular characterization of the cAMP-dependent protein kinase bound to microtubule-associated protein 2.* J Biol Chem, 1982. **257**(6): p. 3284-90.
95. Vallee, R.B., M.J. DiBartolomeis, and W.E. Theurkauf, *A protein kinase bound to the projection portion of MAP 2 (microtubule-associated protein 2).* J Cell Biol, 1981. **90**(3): p. 568-76.
96. Bregman, D.B., N. Bhattacharyya, and C.S. Rubin, *High affinity binding protein for the regulatory subunit of cAMP-dependent protein kinase II-B. Cloning, characterization, and expression of cDNAs for rat brain P150.* J Biol Chem, 1989. **264**(8): p. 4648-56.
97. Bregman, D.B., A.H. Hirsch, and C.S. Rubin, *Molecular characterization of bovine brain P75, a high affinity binding protein for the regulatory subunit of cAMP-dependent protein kinase II beta.* J Biol Chem, 1991. **266**(11): p. 7207-13.
98. Angelo, R. and C.S. Rubin, *Molecular characterization of an anchor protein (AKAPCE) that binds the RI subunit (RCE) of type I protein kinase A from Caenorhabditis elegans.* J Biol Chem, 1998. **273**(23): p. 14633-43.
99. Kussel-Andermann, P., et al., *Unconventional myosin VIIA is a novel A-kinase-anchoring protein.* J Biol Chem, 2000. **275**(38): p. 29654-9.
100. Miki, K. and E.M. Eddy, *Identification of tethering domains for protein kinase A type Ialpha regulatory subunits on sperm fibrous sheath protein FSC1.* J Biol Chem, 1998. **273**(51): p. 34384-90.
101. Huang, L.J., et al., *Identification of a novel protein kinase A anchoring protein that binds both type I and type II regulatory subunits.* J Biol Chem, 1997. **272**(12): p. 8057-64.
102. Huang, L.J., et al., *D-AKAP2, a novel protein kinase A anchoring protein with a putative RGS domain.* Proc Natl Acad Sci U S A, 1997. **94**(21): p. 11184-9.
103. Skroblin, P., et al., *Mechanisms of protein kinase a anchoring.* Int Rev Cell Mol Biol, 2010. **283**: p. 235-330.
104. Lohmann, S.M., et al., *High-affinity binding of the regulatory subunit (RII) of cAMP-dependent protein kinase to microtubule-associated and other cellular proteins.* Proc Natl Acad Sci U S A, 1984. **81**(21): p. 6723-7.
105. Zhang, J., et al., *Genetically encoded reporters of protein kinase A activity reveal impact of substrate tethering.* Proc Natl Acad Sci U S A, 2001. **98**(26): p. 14997-5002.
106. Fink, M.A., et al., *AKAP-mediated targeting of protein kinase a regulates contractility in cardiac myocytes.* Circ Res, 2001. **88**(3): p. 291-7.
107. Rosenmund, C., et al., *Anchoring of protein kinase A is required for modulation of AMPA/kainate receptors on hippocampal neurons.* Nature, 1994. **368**(6474): p. 853-6.
108. Hundsrucker, C., et al., *High-affinity AKAP7delta-protein kinase A interaction yields novel protein kinase A-anchoring disruptor peptides.* Biochem J, 2006. **396**(2): p. 297-306.
109. Brown, R.L., et al., *AKAP7gamma is a nuclear RI-binding AKAP.* Biochem Biophys Res Commun, 2003. **306**(2): p. 394-401.

110. Gray, P.C., et al., *Identification of a 15-kDa cAMP-dependent protein kinase-anchoring protein associated with skeletal muscle L-type calcium channels.* J Biol Chem, 1997. **272**(10): p. 6297-302.
111. Gray, P.C., et al., *Primary structure and function of an A kinase anchoring protein associated with calcium channels.* Neuron, 1998. **20**(5): p. 1017-26.
112. Hirsch, A.H., et al., *Cloning and expression of an intron-less gene for AKAP 75, an anchor protein for the regulatory subunit of cAMP-dependent protein kinase II beta.* J Biol Chem, 1992. **267**(4): p. 2131-4.
113. Fraser, I.D., et al., *A novel lipid-anchored A-kinase Anchoring Protein facilitates cAMP-responsive membrane events.* EMBO J, 1998. **17**(8): p. 2261-72.
114. Cantrell, A.R., et al., *Dopaminergic modulation of voltage-gated Na+ current in rat hippocampal neurons requires anchoring of cAMP-dependent protein kinase.* J Neurosci, 1999. **19**(17): p. RC21.
115. Tibbs, V.C., et al., *AKAP15 anchors cAMP-dependent protein kinase to brain sodium channels.* J Biol Chem, 1998. **273**(40): p. 25783-8.
116. Hulme, J.T., et al., *Beta-adrenergic regulation requires direct anchoring of PKA to cardiac CaV1.2 channels via a leucine zipper interaction with A kinase-anchoring protein 15.* Proc Natl Acad Sci U S A, 2003. **100**(22): p. 13093-8.
117. Trotter, K.W., et al., *Alternative splicing regulates the subcellular localization of A-kinase anchoring protein 18 isoforms.* J Cell Biol, 1999. **147**(7): p. 1481-92.
118. Henn, V., et al., *Identification of a novel A-kinase anchoring protein 18 isoform and evidence for its role in the vasopressin-induced aquaporin-2 shuttle in renal principal cells.* J Biol Chem, 2004. **279**(25): p. 26654-65.
119. King, L.S., D. Kozono, and P. Agre, *From structure to disease: the evolving tale of aquaporin biology.* Nat Rev Mol Cell Biol, 2004. **5**(9): p. 687-98.
120. Klussmann, E., et al., *Protein kinase A anchoring proteins are required for vasopressin-mediated translocation of aquaporin-2 into cell membranes of renal principal cells.* J Biol Chem, 1999. **274**(8): p. 4934-8.
121. McSorley, T., et al., *Spatial organisation of AKAP18 and PDE4 isoforms in renal collecting duct principal cells.* Eur J Cell Biol, 2006. **85**(7): p. 673-8.
122. Stefan, E., et al., *Compartmentalization of cAMP-dependent signaling by phosphodiesterase-4D is involved in the regulation of vasopressin-mediated water reabsorption in renal principal cells.* J Am Soc Nephrol, 2007. **18**(1): p. 199-212.
123. Hoffmann, R., et al., *cAMP-specific phosphodiesterase HSPDE4D3 mutants which mimic activation and changes in rolipram inhibition triggered by protein kinase A phosphorylation of Ser-54: generation of a molecular model.* Biochem J, 1998. **333 (Pt 1)**: p. 139-49.
124. Lygren, B., et al., *AKAP complex regulates Ca2+ re-uptake into heart sarcoplasmic reticulum.* EMBO Rep, 2007. **8**(11): p. 1061-7.
125. Szentesi, P., et al., *Sarcoplasmic reticulum Ca2+ refilling controls recovery from Ca2+-induced Ca2+ release refractoriness in heart muscle.* Circ Res, 2004. **95**(8): p. 807-13.
126. Traaseth, N.J., et al., *Structural and dynamic basis of phospholamban and sarcolipin inhibition of Ca(2+)-ATPase.* Biochemistry, 2008. **47**(1): p. 3-13.
127. Metcalfe, E.E., et al., *(1)H/(15)N heteronuclear NMR spectroscopy shows four dynamic domains for phospholamban reconstituted in dodecylphosphocholine micelles.* Biophys J, 2004. **87**(2): p. 1205-14.
128. MacLennan, D.H. and E.G. Kranias, *Phospholamban: a crucial regulator of cardiac contractility.* Nat Rev Mol Cell Biol, 2003. **4**(7): p. 566-77.
129. Rossman, K.L., C.J. Der, and J. Sondek, *GEF means go: turning on RHO GTPases with guanine nucleotide-exchange factors.* Nat Rev Mol Cell Biol, 2005. **6**(2): p. 167-80.
130. Diviani, D., J. Soderling, and J.D. Scott, *AKAP-Lbc anchors protein kinase A and nucleates Galpha 12-selective Rho-mediated stress fiber formation.* J Biol Chem, 2001. **276**(47): p. 44247-57.
131. Worthylake, D.K., K.L. Rossman, and J. Sondek, *Crystal structure of the DH/PH fragment of Dbs without bound GTPase.* Structure, 2004. **12**(6): p. 1078-86.

132. Soisson, S.M., et al., *Crystal structure of the Dbl and pleckstrin homology domains from the human Son of sevenless protein.* Cell, 1998. **95**(2): p. 259-68.
133. Li, H., et al., *Protein kinase A-anchoring (AKAP) domains in brefeldin A-inhibited guanine nucleotide-exchange protein 2 (BIG2).* Proc Natl Acad Sci U S A, 2003. **100**(4): p. 1627-32.
134. Mouratou, B., et al., *The domain architecture of large guanine nucleotide exchange factors for the small GTP-binding protein Arf.* BMC Genomics, 2005. **6**(1): p. 20.
135. Gold, M.G., et al., *AKAP18 contains a phosphoesterase domain that binds AMP.* J Mol Biol, 2008. **375**(5): p. 1329-43.
136. Coates, J.C., *Armadillo repeat proteins: beyond the animal kingdom.* Trends Cell Biol, 2003. **13**(9): p. 463-71.
137. Renault, L., B. Guibert, and J. Cherfils, *Structural snapshots of the mechanism and inhibition of a guanine nucleotide exchange factor.* Nature, 2003. **426**(6966): p. 525-30.
138. Mossessova, E., J.M. Gulbis, and J. Goldberg, *Structure of the guanine nucleotide exchange factor Sec7 domain of human arno and analysis of the interaction with ARF GTPase.* Cell, 1998. **92**(3): p. 415-23.
139. Huber, A.H., W.J. Nelson, and W.I. Weis, *Three-dimensional structure of the armadillo repeat region of beta-catenin.* Cell, 1997. **90**(5): p. 871-82.
140. Mazumder, R., et al., *Detection of novel members, structure-function analysis and evolutionary classification of the 2H phosphoesterase superfamily.* Nucleic Acids Res, 2002. **30**(23): p. 5229-43.
141. Rehse, P.H. and T.H. Tahirov, *Structure of a putative 2'-5' RNA ligase from Pyrococcus horikoshii.* Acta Crystallogr D Biol Crystallogr, 2005. **61**(Pt 9): p. 1207-12.
142. Kato, M., et al., *Crystal structure of the 2'-5' RNA ligase from Thermus thermophilus HB8.* J Mol Biol, 2003. **329**(5): p. 903-11.
143. Sambrook, J.F.F., E.F. and Maniatis T. , *Molecular Cloning: A Laboratory Manual*1989: Cold Spring Harbor Laboratory Press.
144. Chung, C.T., S.L. Niemela, and R.H. Miller, *One-step preparation of competent Escherichia coli: transformation and storage of bacterial cells in the same solution.* Proc Natl Acad Sci U S A, 1989. **86**(7): p. 2172-5.
145. Laemmli, U.K., *Cleavage of structural proteins during the assembly of the head of bacteriophage T4.* Nature, 1970. **227**(5259): p. 680-5.
146. Gasteiger, E.H., C. Gattiker, A. Duvaud, S. Wilkins, M.R. Appel R.D. and Bairoch, A., *The Proteomics Protocols Handbook*2005: Humana Press.
147. Bradford, M.M., *A rapid and sensitive method for the quantitation of microgram quantities of protein utilizing the principle of protein-dye binding.* Anal Biochem, 1976. **72**: p. 248-54.
148. Lenzen, C., R.H. Cool, and A. Wittinghofer, *Analysis of intrinsic and CDC25-stimulated guanine nucleotide exchange of p21ras-nucleotide complexes by fluorescence measurements.* Methods Enzymol, 1995. **255**: p. 95-109.
149. Kelly, S.M., T.J. Jess, and N.C. Price, *How to study proteins by circular dichroism.* Biochim Biophys Acta, 2005. **1751**(2): p. 119-39.
150. Greenfield, N.J., *Using circular dichroism spectra to estimate protein secondary structure.* Nat Protoc, 2006. **1**(6): p. 2876-90.
151. Niesen, F.H., H. Berglund, and M. Vedadi, *The use of differential scanning fluorimetry to detect ligand interactions that promote protein stability.* Nat Protoc, 2007. **2**(9): p. 2212-21.
152. Pierce, M.M., C.S. Raman, and B.T. Nall, *Isothermal titration calorimetry of protein-protein interactions.* Methods, 1999. **19**(2): p. 213-21.
153. Slotboom, D.J., et al., *Static light scattering to characterize membrane proteins in detergent solution.* Methods, 2008. **46**(2): p. 73-82.
154. Goddard, T.D., Kneller, D.G., *Sparky 3.* University of California, San Francisco, CA, 1989.
155. Garman, E.F. and R.L. Owen, *Cryocooling and radiation damage in macromolecular crystallography.* Acta Crystallogr D Biol Crystallogr, 2006. **62**(Pt 1): p. 32-47.
156. Leslie, A.G., *The integration of macromolecular diffraction data.* Acta Crystallogr D Biol Crystallogr, 2006. **62**(Pt 1): p. 48-57.

157. Kabsch, W., *Automatic processing of rotation diffraction data from crystals of initially unknown symmetry and cell constants.* J Appl Cryst, 1993.
158. Otwinowski, Z., Minor, W., *Processing of x-ray diffraction data collected in oscillation mode.* Methods in Enzymology (Macromolecular Crystallography, Part A), 1997. **276**: p. 307-326.
159. Navaza, J., *AMoRe: an automated package for molecular replacement.* Acta Crystallogr D Biol Crystallogr, 1994.
160. McCoy, A.J., *Solving structures of protein complexes by molecular replacement with Phaser.* Acta Crystallogr D Biol Crystallogr, 2007. **63**(Pt 1): p. 32-41.
161. Murshudov, G.N., A.A. Vagin, and E.J. Dodson, *Refinement of macromolecular structures by the maximum-likelihood method.* Acta Crystallogr D Biol Crystallogr, 1997. **53**(Pt 3): p. 240-55.
162. *The CCP4 suite: programs for protein crystallography.* Acta Crystallogr D Biol Crystallogr, 1994. **50**(Pt 5): p. 760-3.
163. Vagin, A.T., A, *Molrep: an automated program for molecular replacement.* J Appl Cryst, 1997.
164. Cole, C., J.D. Barber, and G.J. Barton, *The Jpred 3 secondary structure prediction server.* Nucleic Acids Res, 2008. **36**(Web Server issue): p. W197-201.
165. Li, X., et al., *Predicting Protein Disorder for N-, C-, and Internal Regions.* Genome Inform Ser Workshop Genome Inform, 1999. **10**: p. 30-40.
166. Cooper, D.R., et al., *Protein crystallization by surface entropy reduction: optimization of the SER strategy.* Acta Crystallogr D Biol Crystallogr, 2007. **63**(Pt 5): p. 636-45.
167. Huai, Q., J. Colicelli, and H. Ke, *The crystal structure of AMP-bound PDE4 suggests a mechanism for phosphodiesterase catalysis.* Biochemistry, 2003. **42**(45): p. 13220-6.
168. Emsley, P., et al., *Features and development of Coot.* Acta Crystallogr D Biol Crystallogr, 2010. **66**(Pt 4): p. 486-501.
169. Conti, E., et al., *Crystallographic analysis of the recognition of a nuclear localization signal by the nuclear import factor karyopherin alpha.* Cell, 1998. **94**(2): p. 193-204.
170. Fushimi, K., S. Sasaki, and F. Marumo, *Phosphorylation of serine 256 is required for cAMP-dependent regulatory exocytosis of the aquaporin-2 water channel.* J Biol Chem, 1997. **272**(23): p. 14800-4.
171. Derewenda, Z.S., *Application of protein engineering to enhance crystallizability and improve crystal properties.* Acta Crystallogr D Biol Crystallogr, 2010. **66**(Pt 5): p. 604-15.
172. Campbell, J.W., et al., *X-ray diffraction studies on enzymes in the glycolytic pathway.* Cold Spring Harb Symp Quant Biol, 1972. **36**: p. 165-70.
173. Kendrew, J.C., et al., *The species specificity of myoglobin.* Nature, 1954. **174**(4438): p. 946-9.
174. Briant, D.J., et al., *Rapid identification of linear protein domain binding motifs using peptide SPOT arrays.* Methods Mol Biol, 2009. **570**: p. 175-85.
175. Gravel, M., et al., *2',3'-Cyclic nucleotide 3'-phosphodiesterase: a novel RNA-binding protein that inhibits protein synthesis.* J Neurosci Res, 2009. **87**(5): p. 1069-79.
176. Jamali, T., et al., *Nuclear pore complex biochemistry and biophysics of nucleocytoplasmic transport in health and disease.* Int Rev Cell Mol Biol, 2011. **287**: p. 233-86.
177. Fuller, M.D., et al., *Molecular mechanism of calcium channel regulation in the fight-or-flight response.* Sci Signal, 2010. **3**(141): p. ra70.
178. Chen, L., et al., *Mutation of an A-kinase-anchoring protein causes long-QT syndrome.* Proc Natl Acad Sci U S A, 2007. **104**(52): p. 20990-5.
179. Gassanov, N., et al., *Arginine vasopressin (AVP) and treatment with arginine vasopressin receptor antagonists (vaptans) in congestive heart failure, liver cirrhosis and syndrome of inappropriate antidiuretic hormone secretion (SIADH).* Eur J Clin Pharmacol, 2011. **67**(4): p. 333-46.
180. Lygren, B. and K. Tasken, *The potential use of AKAP18delta as a drug target in heart failure patients.* Expert Opin Biol Ther, 2008. **8**(8): p. 1099-108.
181. Christian, F., et al., *Small molecule AKAP/PKA interaction disruptors that activate PKA interfere with compartmentalized cAMP signaling in cardiac myocytes.* J Biol Chem, 2011.

182. Rupp, B., *Biomolecular Crystallography*2010: Garland Science.
183. Drenth, J., *Principles of Protein X-Ray Crystallography*. Vol. 3rd edition. 2007: Springer Science and Business Media LLC.
184. Chenna, R., et al., *Multiple sequence alignment with the Clustal series of programs.* Nucleic Acids Res, 2003. **31**(13): p. 3497-500.

8 Acknowledgment

This work would not have been possible without the help of many people. I am very glad that I spend most of the time of my PhD thesis in Oliver Daumke's laboratory at the Max-Delbrück-Centrum in Berlin-Buch, where everybody is helping each other.

I would like to thank Udo Heinemann for being my doctor father. I really enjoyed the joined group seminars with the scientific discussions, but I also appreciate very much the close cooperation between the Heinemann group and the Daumke group. Whether one searches for scientific advice, laboratory instruments, or any other help, it was always found in your group. It was also very supportive to have the possibility to use the great PSF facility for crystallization (many thanks especially to Yvette Roske and Anja Schütz).

Many thanks to Enno Klussmann who initialized the project I was working on and contributed with his expertise on signal transduction and physiological questions. Many thanks as well to Walter Rosenthal for supporting the project.

When I started my PhD thesis, my knowledge on protein expression and purification was only very basic. Many thanks to Katja Fälber who taught me all the principles about expression and purification of even very complicated proteins in *E. coli* and who also helped me to find my way through the jungle of biophysical methods.

I would like to thank Oli Daumke, of course, who not only accepted me to work in his laboratory from my second PhD year on, but who also supported my project not only financially, but with scientific discussions, tips and tricks, and last but not least with never-ending optimism. Thank you very much that you are always ready to jump up from your desk to run to the lab and give practical advice.

I would also like to thank Bernd Reif. In his laboratory I worked during the first year of my PhD thesis. As the coordinator of the Leibniz Graduate School of Molecular Biophysics, he helped us and made it possible that we as the students could organize mini-symposia and a retreat, where we heard many exciting scientific talks and spoke to scientists from different fields of research.

Many thanks also to Uwe Müller and his group at the BESSY for excellent support.

I definitely have to thank all my colleagues from AG Daumke, AG Heinemann, AG Klussmann, and AG Reif for the great working atmosphere. Whenever I was searching for something, may it be an advice or a shaker flask, I found help from all of you. Thank you very much!

My dear PhD colleagues from the Daumke lab: I would not have been able to write my PhD thesis without you. It was a great to work with you; working with friends is the best that can happen to you. I learnt much, much more, than what is written down in this work…last but not least opening a beer bottle with a lighter. Thank you for scientific discussions in the middle of the

night, support and tons of fun. Chris Fröhlich, Claudio Shah, David Schwefel, Janko Brand, Song Gao, Rosana Pinho, Ulrike ("Ulli") Maschke, we shared our PhD time: this will always bind us together.

Andy Mainz and Jana Bröcker, I think you are my doctor brother and sister.

Sabine Werner, Marion Papst, Dennis Schulz, and Sabine Kraft: thank you very much for excellent technical assistance and support! Whatever was required, you found it or made it. Auf Euch ist Verlass!

I would also like to especially thank Oli Daumke, Stephen Marino, David Schwefel, Florian Mayr, and Andy Mainz for critically reading and correcting my PhD thesis. And, Stephen, thousand thanks for your great support!

Many thanks to all the other colleagues from MDC and FMP who made this time unforgettable.

There are also my friends outside of the MDC and FMP, of course, who had to be patient with me and who supported me in every way. Thank you very much!

My parents and my sister I would like to thank for their love and support in any situation.

Thousand thanks to Nicolaj Mahlstedt, who is always there for me. Your love is the best support.